Universitat
de les Illes Balears

Doctoral Thesis
2021

THERMOHALINE VARIABILITY AND MIXING DYNAMICS IN THE WESTERN MEDITERRANEAN DEEP WATERS WITHIN THE WESTERN MEDITERRANEAN TRANSITION

Olav Safo Piñeiro Rodríguez

Doctoral Thesis
2021

Doctoral Programme in Physics

THERMOHALINE VARIABILITY AND MIXING DYNAMICS IN THE WESTERN MEDITERRANEAN DEEP WATERS WITHIN THE WESTERN MEDITERRANEAN TRANSITION

Olav Safo Piñeiro Rodríguez

Thesis Supervisor: Dr. Rosa Balbín Chamorro
Thesis Supervisor: Dr. César González-Pola Muñiz
Thesis Supervisor: Dr. Pedro Joaquín Vélez Belchí
Thesis Tutor: Dr. Damià Gomis Bosch

Doctor by the Universitat de les Illes Balears

Universitat de les Illes Balears

Dr. Rosa Balbín Chamorro, of the *Instituto Español de Oceanografía*
Dr. César González-Pola Muñiz, of the *Instituto Español de Oceanografía*
Dr. Pedro Joaquín Vélez Belchí, of the *Instituto Español de Oceanografía*
Olav Safo Piñeiro Rodríguez

DECLARE:

That the thesis titled *'Thermohaline variability and mixing dynamics in the Western Mediterranean deep waters within the Western Mediterranean Transition'*, presented by Olav Safo Piñeiro Rodríguez to obtain a doctoral degree, has been completed under the supervision of Dr. Rosa Balbín Chamorro, Dr. César González-Pola Muñiz and Dr. Pedro Joaquín Vélez Belchí, and meets the requirements to opt for an International Doctorate.

For all intents and purposes, we hereby sign this document.

Signatures

Palma, March 2021.

A mi familia y a Ro.

Agradecimientos

A lo largo de mi tesis doctoral pensé en muchas ocasiones en esta sección. Me he sentido tantas veces afortunado y agradecido en estos años que supuse que escribirla sería una tarea fácil. Sin embargo, ahora que he puesto el punto final a esta tesis y he de hacerlo, me veo abrumado al darme cuenta realmente de la cantidad de gente que me he cruzado durante este periodo y que ha hecho que creciese tanto profesional como personalmente. Espero no olvidarme de nadie. Si lo hago es, sin duda, fruto de las prisas finales.

Una tesis doctoral es un camino largo y difícil de recorrer. La travesía está llena de obstáculos y retos que muchas veces hacen que te sientas perdido. Si he conseguido recorrer este camino y llegar entero al final, ha sido, sin lugar a dudas, gracias a mis directores: Rosa Balbín, César González-Pola y Pedro Vélez. Por ello, en primer lugar, me gustaría agradecerles profundamente todo su esfuerzo, confianza, dedicación y enseñanzas. Muchas gracias por apoyarme y atenderme siempre, incluso en días y a horas que se escapan de lo sensato. Gracias a vosotros he aprendido mucho, no solo de ciencia, y me he sentido un doctorando muy afortunado.

Junto a ellos, he tenido también la suerte de trabajar con otras personas que han contribuido enormemente a cincelar lo que aquí se presenta y que figuran como coautores de los trabajos de esta tesis: Julio Fernández, Alberto Naveira, Ricardo Sánchez, Pere Puig y Jordi Salat. Gracias a todos por responder tan amablemente a mis incansables dudas, por ayudarme y hacer que aprendiese tanto. A su vez, quiero agradecer a todas aquellas personas que no figuran en la lista de coautores, pero cuyo incesante trabajo durante muchos años ha sido crítico para que esta tesis haya visto la luz. Especialmente a José Luis López-Jurado, Mariano Serra, Juan Antonio Jiménez, Rocío Santiago, Vicenç Moltó, Melissa Martín, Verónica Caínzos y, en general, a todo el personal científico y tripulaciones de los buques del IEO que han participado en las campañas RADMED y en las del proyecto ATHAPOC. También a todo el personal del Centro Oceanográfico de Baleares, con los que he compartido todos estos años. Ha sido un auténtico placer trabajar con todos vosotros.

A lo largo de mi tesis doctoral he tenido la fortuna de poder moverme de aquí para allá, dentro y fuera de España. He asistido a congresos, cursos, simposios y he participado en varias campañas oceanográficas. El viaje que más he repetido ha sido a Asturias, al centro del IEO en Gijón, a trabajar bajo la dirección de César González-Pola, con la inestimable ayuda de Julio Fernández. Muchas gracias, de nuevo, por toda vuestra dedicación y el apoyo que siempre me habéis dado. Igualmente, me gustaría agradecerle a todas las personas del IEO de Gijón que tan amablemente me acogieron desde el primer día y, cómo no, a Rocío Graña, quien siempre supo cómo animarme y motivarme. Gracias.

Además de mis visitas al IEO de Gijón, tuve la oportunidad de hacer una estancia de investigación en el National Oceanography Center de Southampton (NOCS), en Reino Unido. Por ello, me gustaría expresar, otra vez, mi agradecimiento a Alberto Naveira, quien me tutorizó durante ese periodo y con el que he tenido el privilegio de continuar trabajando desde entonces. Así mismo, a Harry Bryden, quien desde el principio se interesó por la investigación que llevábamos a cabo y contribuyó activamente en la valoración y discusión de los resultados, originando nuevas preguntas y líneas de investigación que, espero, se puedan explorar en un futuro. El tiempo que pasé en el NOCS no habría sido igual sin la acogida que me brindó la gente que trabajaba allí, especialmente Gwyn Evans, Alessandro Silvano y Carl Spingys, quienes supieron hacerme sentir bienvenido tanto dentro como fuera del trabajo. Muchas gracias.

Entre idas y venidas, he conocido a mucha gente con la que he compartido horas de trabajo, risas y fiestas: Vero, Lara, Cati, Melissa, Vic, Ale, Merlu, Sergio, Quique, Albert, Javi, Vero (Canaria), Andrea, Javi (Canario), Vicenç, Fran, Miguel y Laura; así como largas horas surfeando en el siempre inconsistente Mediterráneo: Lucas, Mati, Tommy y Seba. Muchas gracias a todos por estar siempre ahí y hacer que mi tiempo en la isla haya sido (y sea) tan bueno.

Gracias Laura y Alex por vuestra ayuda con el catalán y los entresijos de LaTeX durante los últimos momentos de la escritura de esta tesis.

A mi grupo de amigos de siempre, la mayoría lejos de casa (como buenos gallegos): Fran, Jorge, Jacobo, Manuel, B y Puñal; gracias por vuestro constante apoyo y ánimos desde la distancia, los momentos difíciles hubieran sido mucho peores sin vosotros.

A toda mi familia, la que está y la que se ha ido, gracias por vuestro apoyo incondicional en todo lo que he llevado a cabo. Siento no poder estar más con vosotros. A mi tío, siempre preocupado por mi futuro, por su apoyo para que consiguiese llegar hasta aquí. A mi madre, por ser un ejemplo de lucha para mi hermano y para mí, por saber motivarnos como nadie para que alcancemos nuestras metas y por su constante esfuerzo en entender a qué me dedico. A mi hermano, por hacer que siempre me sienta tan orgulloso de él. A mis abuelos, por hacerme sentir continuamente tan arropado. A todos y a cada uno, muchísimas gracias.

Finalmente, mi más sincero agradecimiento es para la persona que ha vivido más de cerca los altos y los bajos, las idas y venidas y, sobre todo, las ausencias físicas y mentales durante todos estos años. Gracias Ro, por recorrer este camino conmigo y hacerlo infinitamente más agradable. Sin querer, tú también has acabado haciendo una tesis doctoral.

Abstract

During winter 2005, a large production of anomalous dense waters triggered the formation of a complex deep thermohaline structure, which led to a basin-scale abrupt shift in the historical evolution of the Western Mediterranean characteristics. This new situation, termed the Western Mediterranean Transition (WMT), has been traced since its formation by the *'Instituto Español de Oceanografía'* throughout a regularly sampled deep hydrographic station located in the north-eastern continental slope of Minorca Island. From this long-term hydrographic time series, the thermohaline evolution of the WMT signal between 2005 and 2017 is analyzed in this doctoral thesis. By means of a 1-D diffusion numerical model that includes parameterizations of double-diffusive mixing phenomena, the diffusive evolution of the WMT structure was reproduced and the contribution to the heat and salt budgets of the deep waters in terms of ventilation due to lateral advection of dense waters and downward diffusive transference from the intermediate layers was evaluated. Results show distinct stages in the deep waters evolution, dominated by permanent diapycnal mixing and interannual water renewals. Overall, the deep layers of the Western Mediterranean underwent remarkable heat and salt gains during this period, mostly due to the production of deep waters during the 2005-2006 and 2011-2013 periods. Heat uptake rate within the WMT was higher than estimations for the intermediate layers of the global ocean. The analysis of the long-term evolution highlighted the rapid consumption of near-bottom signatures of the hydrographic structure of the WMT during its initial stages. By permitting vertical variation of the background mixing coefficient in the 1-D model and including a localized heat and salt source term to represent the lateral advection of dense waters from the formation area, the observed evolution was successfully reproduced. The results robustly indicate that not only the densest levels, but almost the whole portion of the deep waters disturbed by the WMT structure off Minorca, was subjected to persistent, enhanced turbulent mixing during the 2005-2007 period, well above previous regional estimates and common values of the deep Western Mediterranean interior. The regional continental slope was regarded as a plausible source of the intensified deep mixing diagnosed by the modeling approach necessary to reproduce the observations during the considered period. By means of novel, extensive oceanographic observations gathered in recent years, the occurrence of bottom-generated small-scale turbulence over the continental slope of Minorca is evidenced during intensification periods of the along-slope deep boundary current. The observations are compatible with a deep-ocean boundary mixing mechanism recently documented in the Southern Ocean, which promotes enhanced diapycnal mixing rates over the topography and lateral exchange of near-boundary well-mixed waters and stratified interior waters. This doctoral thesis complements and advances our knowledge on the WMT climatic event, its temporal evolution, the large-scale effects of the distinct mixing regimes operating throughout the water column off Minorca, the contribution of vertical diffusive and lateral advective heat-salt transports to the deep budgets, and provides insights into the unexplored regional deep mixing environment.

Resumen

Durante el invierno de 2005, una gran producción de aguas densas anómalas desencadenó la formación de una compleja estructura termohalina profunda que causó un cambio abrupto en la evolución histórica de las características del Mediterráneo occidental. Esta nueva situación, denominada la Transición del Mediterráneo Occidental (WMT por sus siglas en inglés), ha sido monitorizada desde su formación por el Instituto Español de Oceanografía a través de una estación hidrográfica profunda visitada regularmente, localizada en el talud continental nororiental de la isla de Menorca. En esta tesis doctoral, a partir de esta serie temporal hidrográfica de larga duración, se analiza la evolución termohalina de la señal de la WMT entre 2005 y 2017. Por medio de un modelo numérico unidimensional de difusión que incluye parametrizaciones de fenómenos de mezcla doble-difusiva, se reprodujo la evolución difusiva de la estructura de la WMT y se evaluó la contribución al contenido de calor y sal de las aguas profundas en términos de ventilación por advección lateral de aguas densas y de transferencia difusiva desde las capas intermedias. Los resultados muestran distintos estadios en la evolución de las aguas profundas, dominados por constante mezcla diapicna y renovaciones de agua interanuales. En general, las capas profundas del Mediterráneo occidental sufrieron importantes ganancias de calor y sal durante este periodo, debido principalmente a la producción de aguas profundas durante los periodos 2005-2006 y 2011-2013. La tasa de absorción de calor durante la WMT excede las estimaciones para las capas intermedias del océano global. El análisis de la evolución a largo plazo remarcó la rápida erosión de firmas termohalinas de la parte más profunda de la estructura hidrográfica de la WMT durante sus estadios iniciales. Permitiendo que el coeficiente de mezcla variase verticalmente en el modelo unidimensional e incluyendo un término fuente localizado de calor y sal para representar la advección lateral de aguas densas desde la zona de formación, se reprodujo satisfactoriamente la evolución observada. Los resultados indican robustamente que no solo los niveles más densos, si no que casi toda la columna de agua ocupada por la estructura de la WMT frente a Menorca estuvo sujeta a mezcla turbulenta intensificada y persistente durante el periodo 2005-2007, muy por encima de las estimaciones regionales realizadas anteriormente y de los valores comunes en el interior del Mediterráneo occidental profundo. El talud continental de Menorca fue considerado una fuente plausible de la mezcla intensificada necesaria para reproducir las observaciones con el modelo durante el periodo contemplado. Por medio de nuevas y exhaustivas observaciones oceanográficas obtenidas en años recientes, se evidenció el desarrollo de turbulencia de pequeña escala originada sobre el fondo del talud continental de Menorca durante periodos de intensificación de la corriente de contorno profunda a lo largo del talud. Las observaciones son compatibles con un mecanismo de mezcla de contorno, recientemente documentado en el océano Antártico, que favorece tasas elevadas de mezcla diapicna sobre la topografía e intercambio lateral entre aguas bien mezcladas cercanas al talud y aguas interiores estratificadas. Esta tesis doctoral complementa y avanza nuestro conocimiento del evento climático de la WMT,

su evolución temporal, los efectos de larga escala de los diferentes regímenes de mezcla que operan a lo largo de la columna de agua frente a Menorca, la contribución de los transportes por difusión vertical y advección lateral al balance de calor y sal en las profundidades y aporta información sobre el ambiente de mezcla profunda inexplorado en la región.

Resum

Al llarg de l'hivern de 2005, una gran producció d'aigües denses anòmales va desencadenar la formació d'una complexa estructura termohalina profunda que va causar un canvi abrupte en l'evolució històrica de les característiques del Mediterrani occidental. Aquesta nova situació, denominada la Transició del Mediterrani Occidental (WMT per les seves sigles en anglès), ha sigut monitorada des de la seva formació per l'Institut Espanyol d'Oceanografia a través d'una estació hidrogràfica profunda regularment visitada i localitzada en el talús continental nord-oriental de l'illa de Menorca. En aquesta tesi doctoral, a partir d'aquesta sèrie temporal hidrogràfica de llarga durada, s'analitza l'evolució termohalina del senyal de la WMT entre 2005 i 2017. Mitjançant un model numèric unidimensional de difusió que inclou parametritzacions de fenòmens de barreja doble-difusiva, es va reproduir l'evolució difusiva de l'estructura de la WMT i es va avaluar la contribució al contingut de calor i sal de les aigües profundes en termes de ventilació per advecció lateral d'aigües denses i de transferència difusiva des de les capes intermèdies. Els resultats mostren diferents estadis en l'evolució de les aigües profundes, dominats per una barreja diapicna constant i renovacions d'aigua interanuals. En general, les capes profundes del Mediterrani occidental van sofrir importants guanys de calor i sal durant aquest període, degut principalment a la producció d'aigües profundes durant els períodes 2005-2006 i 2011-2013. La taxa d'absorció de calor durant la WMT excedeix les estimacions per a les capes intermèdies de l'oceà global. L'anàlisi de l'evolució de llarg termini va remarcar la ràpida erosió de les firmes termohalinas prop del fons de l'estructura hidrogràfica de la WMT durant els seus estadis inicials. Permetent que el coeficient de barreja varies verticalment en el model unidimensional i incloent un terme font localitzat de calor i sal per representar l'advecció lateral d'aigües denses des de la zona de formació, es va reproduir satisfactòriament l'evolució observada. Els resultats indiquen robustament que no només els nivells més densos, sinó que quasi tota la columna d'aigua ocupada per l'estructura de la WMT enfront de Menorca va estar subjecta a barreja turbulenta intensificada i persistent durant el període 2005-2007, molt per sobre de les estimacions regionals realitzades anteriorment i dels valors comuns en l'interior del Mediterrani occidental profund. El talús continental de Menorca va ser considerat una font plausible de la barreja intensificada necessària per reproduir les observacions amb el model durant el període contemplat. Mitjançant noves i exhaustives observacions oceanogràfiques obtingudes en anys recents, es va posar en evidència el desenvolupament de turbulència de petita escala originada sobre el fons del talús continental de Menorca durant períodes d'intensificació del corrent de contorn profund al llarg del talús. Les observacions són compatibles amb un mecanisme de barreja de contorn, recentment documentat en l'oceà Antàrtic, que promou taxes elevades de barreja diapicna sobre la topografia i intercanvi lateral entre aigües ben barrejades properes al talús i aigües interiors estratificades. Aquesta tesi doctoral complementa i avança en el nostre coneixement de l'esdeveniment climàtic de la WMT, la seva evolució temporal, els

efectes de llarga escala dels diferents règims de barreja que operen al llarg de la columna d'aigua enfront de Menorca, la contribució dels transports per difusió vertical i advecció lateral al balanç de calor i sal en les profunditats i aporta informació sobre l'inexplorat ambient de barreja profunda en la regió.

Funding

This doctoral thesis has been funded by the predoctoral FPI fellowship (BES-2015-074316) from the Spanish Ministry of Science and Innovation (MICINN), co-funded by the European Social Fund. It has been conducted in the framework of the ATHAPOC project (*'estudio de la Anomalía TermoHalina en las Aguas Profundas del mediterráneo occidental y su relación con las Oscilaciones Climáticas'*; CTM2014-54374-R), funded by *Plan Nacional I+D+I* from the Spanish Ministry of Economy and Competitiveness (MINECO). The research carried out in this thesis has receive financial support from the RADMED project (*'series tempoRAles de Datos oceanográficos del MEDiterráneo'*), funded by the *'Instituto Español de Oceanografía'* (IEO). A three-month predoctoral research stay at the National Oceanography Centre, University of Southampton (NOCS) – Southampton, UK –, was funded by the predoctoral FPI fellowship and the ATHAPOC project.

Publications

The three chapters containing the original contributions that constitute the core of this doctoral thesis (Chapters 3 to 5) consist of three scientific manuscripts for publication in peer-reviewed international, indexed journals. Two of them have already been published (Chapters 3 to 4) and the last one is almost ready for submission at the time of writing these lines (Chapter 5). Each chapter is structured as a research article with its own abstract, introduction, materials and methodology, results, discussion and conclusions sections.

Piñeiro, S., González-Pola, C., Fernández-Díaz, J. M., and Balbin, R. (2019). Thermohaline evolution of the Western Mediterranean deep waters since 2005: diffusive stages and interannual renewal injections. *Journal of Geophysical Research: Oceans*, 124 (12), 8747–8766. https://doi.org/10.1029/2019JC015094.

Piñeiro, S., González-Pola, C., Fernández-Díaz, J. M., Naveira-Garabato, A. C., Sánchez-Leal, R., Puig, P., Salat, J. and Balbin, R. (2021). Persistent, depth-intensified mixing during the Western Mediterranean Transition's initial stages. *Journal of Geophysical Research: Oceans*, 126 (2), e2020JC016535. https://doi.org/10.1029/2020JC016535.

Piñeiro, S., Naveira-Garabato, A. C., González-Pola, C., Sánchez-Leal, R., Puig, P., and Balbin, R. Boundary mixing of the Western Mediterranean deep waters. In preparation.

Contents

Chapter 1

General introduction

1.1 The Mediterranean Sea

The Mediterranean Sea is a semi-enclosed mid-latitude sea that extends between 30° − 46° N and °6 W −° 36 E (Figure 1.1). It is located between the Eurasian and African continents and has a restricted natural connection with the Atlantic Ocean and the Black Sea through the Strait of Gibraltar (∼ 300 meters depth) and the Dardanelles (∼ 100 meters depth), respectively (it is also marginally connected to the Red Sea through the artificial Suez Canal). The Mediterranean Sea has a mean depth of ∼ 1500 meters and a maximum depth of ∼ 5000. It is divided in two main basins separated by the Strait of Sicily (∼ 400 meters deep): the Western Mediterranean (WMED) and the Eastern Mediterranean (EMED). Both basins are, in turn, divided in other several sub-basins or regional seas. The WMED is divided in the Alboran Sea, the Algerian sub-basin, the Balearic Sea, the Liguro-Provençal sub-basin and the Tyrrhenian sub-basin. The EMED is divided in the Ionian sub-basin, the Adriatic Sea, the Levantine sub-basin and the Aegean Sea.

The Mediterranean Sea is a concentration basin, where freshwater loss due to evaporation exceeds inputs from precipitation and river runoff (Bethoux 1979, Tsimplis et al. 2006). The Mediterranean large-scale circulation is primarily forced by such a negative freshwater budget and by surface heat losses, which set a basin-scale anti-estuarine circulation. Relative fresh surface Atlantic Water (AW) entering the Mediterranean through the narrow (∼ 13 kilometers) and shallow Strait of Gibraltar is converted in saltier-denser waters that flow back into the Atlantic Ocean by overflowing the Gibraltar sill at depth (Bryden et al. 1994, Tsimplis & Bryden 2000).

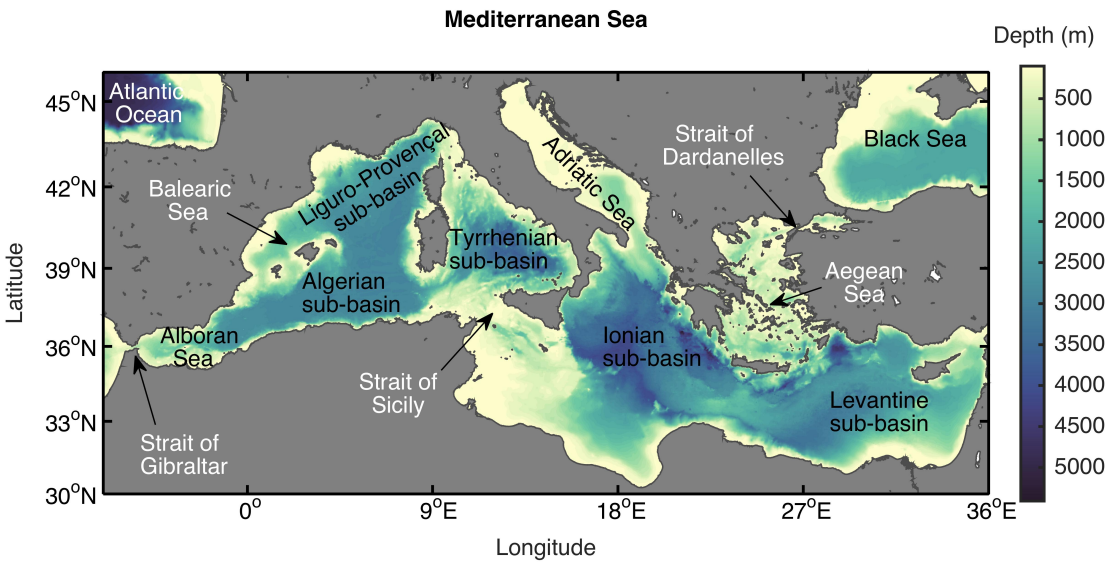

Figure 1.1. Bathymetric map of the Mediterranean Sea. Its several sub-basins, regional seas and main straits are indicated.

This basin-scale circulation connecting both main basins of the Mediterranean is therefore, an open thermohaline circulation cell driven mostly by the exceeding evaporation. Two additional closed thermohaline cells can be found in the WMED and the EMED analogous to the global conveyor belt (Malanotte-Rizzoli et al. 2014). These overturning cells are driven by dense-water formation processes in particular northern areas of the Mediterranean where strong heat fluxes toward the atmosphere occur (Millot & Taupier-Letage 2005). This, along with its dimensions and its mid-latitude location, make the Mediterranean Sea a region of special interest to investigate oceanographic processes that occur in the global ocean at much larger scales and in regions of limited access to observational surveys. Its importance also lies in its land-locked nature – surrounded by continental masses – and its relative reduced size, as it is strongly influenced by atmospheric warming and changes in the freshwater balance, and can respond fast to climate shifts (Schroeder et al. 2017). Furthermore, it is a source of salty and warm waters to the Atlantic Ocean, thus changes in its characteristics could impact the global thermohaline circulation (Bethoux et al. 1999, Ivanovic et al. 2014, Lozier & Stewart 2008, Reid 1979). Consequently, it has been referred to as a miniature ocean and a laboratory basin for oceanographic and climatic studies (Bethoux et al. 1999).

The Mediterranean Sea can be described as a three-layer system formed by surface, intermediate and deep water masses, which can be identified by their temperature and salinity signatures but also by other biogeochemical properties. Such water masses interact between them and with the atmosphere (at surface) and form the large-scale thermohaline circulation of the basin. Their regional properties, circulation paths and specific interactions are intricately influenced by superimposed processes occurring at smaller spatio-temporal scales, and also by the intrinsic large-scale internal variability and changes in the external forcing. Many questions still remain unresolved (Malanotte-Rizzoli et al. 2014), such as the spatio-temporal variability of the large-scale circulation or the role of the mesoscale field in the water-mass transport. The overall features of the main water masses and their large-scale circulation may be described as follows. In this description, the features of the WMED basin and the Western Mediterranean Deep Water (WMDW), the main deep water mass present in this basin, are emphasized. The thermohaline variability of this deep water mass during the last decades is the subject of this doctoral thesis.

1.1.1 Surface layer

The surface layer ($0 - 200$ meters) of the Mediterranean Sea is occupied by waters strongly influenced by the Atlantic inflow. The incoming relatively fresh AW crossing the Strait of Gibraltar progresses eastward following the mean cyclonic circulation of the basin (Figure 1.2a). It flows along the coast of both sub-basins, strongly affected by large-scale gyres, fronts and an energetic eddy field. AW gradually becomes warmer and saltier by mixing with the resident waters and by sea-air exchanges (Millot & Taupier-Letage 2005), being progressively transformed. When it reaches the Levantine sub-basin, it is notably saltier-denser and sinks via winter heat loss and strong evaporation, becoming partly transformed into Levantine Intermediate Water (LIW; see Section 1.1.2; Kubin et al. 2019).

When the inflowing AW reaches the entrance of the Strait of Sicily, a vein progresses northward through the Tyrrhenian sub-basin, describing an anticlockwise circuit, and continues flowing northward into the Ligurian Sea. Then, it flows southwestward along the northern continental slope of

the Liguro-Pronvençal sub-basin (the so-called Northern Current; Millot & Taupier-Letage 2005) and proceeds along the continental slope of the Iberian Peninsula toward the Algerian sub-basin, closing the cyclonic circulation of the WMED. A branch of this current forms the North Balearic Current, which flows eastward along the northern continental slope of the Balearic Archipelago. In the southern part of the basin, the mean circulation pattern is dominated by the Alboran gyres (Millot 1999), the unstable Algerian Current (Send et al. 1999) that flows eastward and by large-scale gyres (Testor et al. 2005), which also affect the circulation at deeper levels.

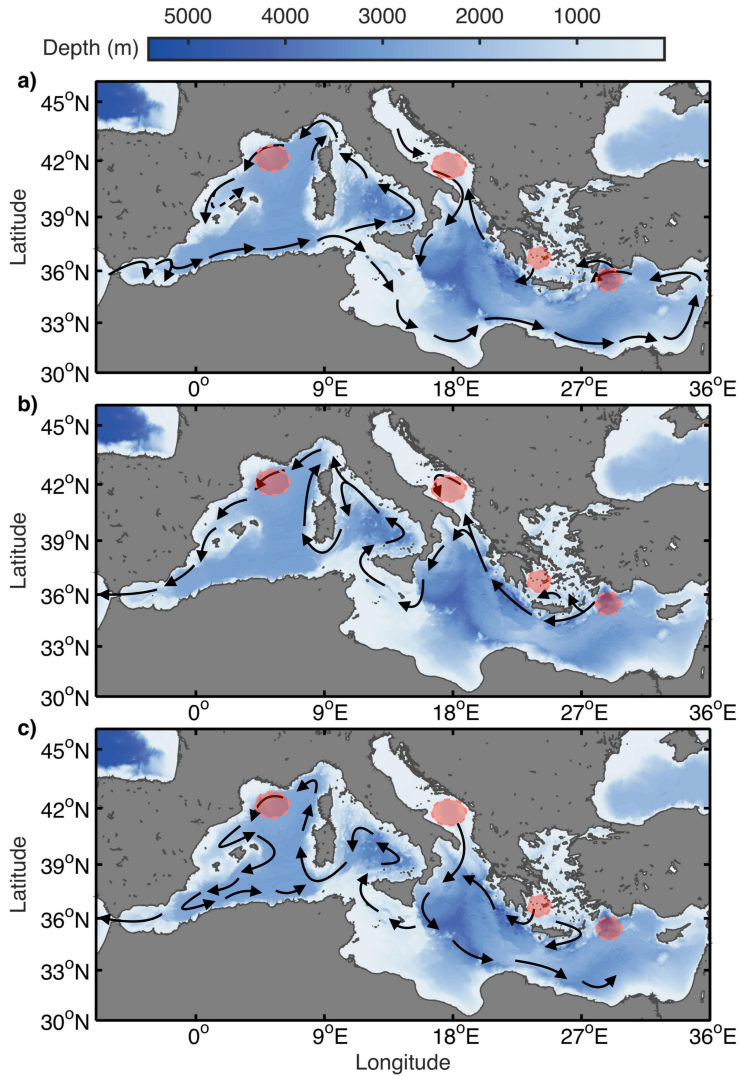

Figure 1.2. Main circulation paths in the Mediterranean Sea of (a) AW, (b) LIW, (c) WMDW, TDW and EMDW as depicted in Schroeder et al. (2012), following Millot & Taupier-Letage (2005). The reader is referred to Schroeder et al. (2012) for a complete description of the circulation features including seasonal, interannual and secondary/recirculation paths. Orange areas indicate the main dense-water formation sites. Dashed arrow in (a) denotes the North Balearic Current.

1.1.2 Intermediate layer

The intermediate layer ($\sim 200 - 1000$ meters) is occupied by water masses located at intermediate depths (as the name suggests), which have lost contact with the atmosphere-sea interaction region. The main intermediate water mass is the LIW, which is formed in the Levantine sub-basin. Its core is located at $\sim 200 - 600$ meters throughout the basin and is characterized by a prominent subsurface salinity maximum and a relative temperature maximum. As it progresses westward from its formation area in the EMED, following the basin-scale cyclonic circuit (Figure 1.2b), the LIW properties are progressively eroded, becoming less warm, salty and oxygenated (in the WMED it can be clearly identify by a dissolved oxygen minimum; Balbín et al. 2014, Manca et al. 2004). This water mass is a reservoir of large amounts of heat and salt, preconditions the deep-water formation areas for dense-water production (Wu & Haines 1996), and is a major contributor to the Mediterranean waters that outflow the Strait of Gibraltar at depth and enter the Atlantic Ocean. After crossing the Strait of Sicily at depth, the LIW mainly circulates following the mean cyclonic circulation along the continental margins, constrained by the bathymetry (Send et al. 1999, Millot & Taupier-Letage 2005). The LIW eventually reaches the northwestern part of the WMED where deep-intermediate water production occurs (see Section 1.1.3), playing an important role in the properties of the newly-formed dense waters produced in the region (Grignon et al. 2010). Other intermediate water masses also contribute to the Sicily Strait outflow such as the Cretan Intermediate Water (CIW; Schroeder et al. 2017), which is sporadically formed in the Cretan Sea.

Intermediate waters are also formed in the WMED, such as the Western Intermediate Water (WIW; Salat & Font 1987), which is produced during winter by off-shore convection in the northwestern part of the basin and over the continental shelf of the region (Juza et al. 2013), but also over a large geographical area along the Spanish Mediterranean continental margin during exceptionally severe winters (Vargas-Yáñez et al. 2012). It is located above the LIW levels (~ 200 meters) and is characterized by a local thermal minimum (Juza et al. 2019).

All these water masses contribute to the properties of the Mediterranean waters that eventually exit the basin into the Atlantic Ocean (Schroeder et al. 2012). Those intermediate waters that do not get through the straits of Sicily and Gibraltar remain recirculating in both sub-basins (Malanotte-Rizzoli et al. 2014).

1.1.3 Deep layer

The deep layer of the Mediterranean Sea is occupied by dense water masses located beneath ~ 1000 meters. Such waters are formed in particular regions of the basin: the Adriatic Sea, the Aegean Sea and the Gulf of Lion (GoL; Millot & Taupier-Letage 2005, Tsimplis et al. 2006); where atmospheric forcing and oceanographic conditions enable strong buoyancy losses.

In the eastern basin, the deep layer is mainly occupied by the Eastern Mediterranean Deep Water (EMDW), primarily formed in Adriatic Sea (Bergamasco & Malanotte-Rizzoli 2010). In the 1980-1990s, the main deep-water source shifted to the Aegean and large amounts of salty-warm, dense deep waters were produced, abruptly changing the thermohaline structure and circulation of the EMED. This event is termed the Eastern Mediterranean Transient (EMT; Lascaratos et al. 1999, Malanotte-Rizzoli et al. 1999). Along with the intermediate waters of eastern origin, upper

parts of the EMDW can overflow the Strait of Sicily (Schroeder et al. 2012). The EMT induced changes in the deep and intermediate layers of the EMED that triggered variations in the heat and salt content of the waters that flow toward the WMED, propagating westward the EMT signal (Gasparini et al. 2005).

In the WMED, the deep layer is occupied by the WMDW and the Tyrrhenian Deep Water (TDW). The WMDW is colder-fresher than the LIW and is formed intermittently in specific winters in the GoL area by excess cooling and evaporation under the action of dry and cold continental winds. Deep-water production is mainly preconditioned by the regional cyclonic circulation and the presence of salty surface and intermediate waters (see Section 1.2). Another deep water mass of the WMED is the TDW, which is formed in the Tyrrhenian sub-basin by mixing of relative old WMDW with waters that overflow the Sicily Channel (Send et al. 1999), not influenced by direct sea-air exchanges. This deep water mass flows back into the Algerian sub-basin and spreads throughout the western basin interior. It is located above the more recently formed WMDW and is warmer than waters found at those levels (Send & Testor 2017). The TDW has also been suggested to be originated by local dense-water formation processes within the Tyrrhenian sub-basin (Fuda et al. 2002).

The deep waters of the Mediterranean follow a general deep cyclonic circuit constrained by the deep bathymetry of each basin, mainly following deep boundary currents and being dispersed into the basins interior by mesoscale structures (Figure 1.2c). The upper part of the WMED deep waters can eventually reach the Alboran Sea and cross the Strait of Gibraltar at depth (García-Lafuente et al. 2009, Kinder & Bryden 1990, Stommel et al. 1973). Along with the intermediate waters (mainly LIW), they form the bulk of the Mediterranean waters that flow into the Atlantic Ocean (Mediterranean Outflow Water; MOW).

1.2 The Western Mediterranean Deep Water

The WMDW is formed in winter at inter-annual scales in the northwestern part of the WMED, mainly in the GoL area, by open-ocean deep convection (Marshall & Schott 1999, MEDOC Group 1970), but also over a larger area during exceptional winters (Smith et al. 2008). This region is characterized by a regional cyclonic circulation which induces a doming of the isopycnals, partly related to the horizontal density field and the local dominant wind forcing (Somot et al. 2018). During winter, northerly cold and dry winds (Tramontane and Mistral) blow over the region enhancing evaporation and cooling, causing surface layers to become unstable. Inside the cyclonic gyre, the uplift of isopycnals favours winter vertical mixing between the AW and the LIW, producing further reduction of the vertical stability. During harsh winters, intense surface bouyancy loss can trigger vertical mixing to reach the deep waters and even the seafloor, transferring heat and salt from the LIW toward the deep layers and forming the WMDW. In early spring, restratification of the water column and spreading of the newly-formed WMDW occur (Herrmann et al. 2008). The ventilated WMDW exits the formation area incorporated into the boundary current and also transported away by mesoscale and submesoscale eddies, spreading throughout the basin following the general deep cyclonic circulation pattern (Herrmann et al. 2008, Send et al. 1996, Send & Testor 2017, Send et al. 1996, Testor & Gascard 2003, 2006).

In addition to the deep ventilation by the open-ocean convection process, distinct dense waters can be formed over the continental shelf of the region (Canals et al. 2006, Durrieu De Madron et al. 2005). Coastal waters can become denser than the surrounding waters under the influence of the winter dry and cold winds and sink, eventually cascading along the continental shelf edge and submarine canyons up to their equilibrium depth and exporting shelf and slope sediment particles toward the ocean interior (Puig et al. 2008, 2013). If buoyancy losses are large enough, cascading waters can reach the deep levels (even the bottom) and contribute to the ventilation of the deep waters and the final characteristics of the WMDW formed off-shore (Durrieu de Madron et al. 2013, Puig et al. 2009). Deep dense shelf-water cascading is a sporadic process with a strong inter-annual variability.

Deep-water formation processes redistribute heat and salt from the upper and intermediate layers into the deep WMED. Therefore, they are an important driver modulating the deep-ocean storage of the heat absorbed from the atmosphere. The deep layers of the WMED have been subjected to long-term warming and salinification trends during the last century (see for instance Borghini et al. 2014, Vargas-Yáñez et al. 2010, 2017). However, as described below, a regime shift in the historical evolution of the WMDW thermohaline characteristics was initiated in the first decade of the 21st century.

1.3 The Western Mediterranean Transition

During the severe winter of 2005, a massive production of anomalous dense waters in the northwestern part of the WMED drastically modified the historical stratification and smooth salinification and warming trends of the WMED deep waters. This event set the beginning of a period of enhanced thermohaline variability that extends to the present day, termed the Western Mediterranean Transition (WMT; Font et al. 2009, Schroeder et al. 2016).

The anomalous dense waters formed in 2005 created an unprecedented thick, complex thermohaline structure in the deep layers with an associated hook-shaped signature in the deep θ-S diagrams. Such a structure was formed by the contribution of a salty-warm deep water mass produced by open-ocean deep convection (new WMDW; nWMDW) and a colder-fresher and denser bottom water mass originated by deep cascading (cWMDW; Canals et al. 2006, Font et al. 2007, Puig et al. 2009). The large injection of new deep waters uplifted the isopycnals hundreds of meters throughout the basin (Schroeder et al. 2008) and created a sharp thermohaline interface between the resident WMDW (old WMDW; oWMDW) and the new deep waters located below (see notations in Figure 1.3, following Salat et al. 2006).

The thermohaline anomaly spread rapidly throughout the basin and in less than a year, the WMT hydrographic signature was present in the Liguro-Provençal sub-basin, the Balearic Sea, the Algerian sub-basin and even in the entrance of the Alboran Sea (López-Jurado et al. 2005, Schroeder et al. 2008). Since the onset of the WMT, additional major productions of salty-warm anomalous new deep waters have occurred intermittently (Durrieu de Madron et al. 2013, Fuda et al. 2009, Houpert et al. 2016, Puig et al. 2013, Schroeder et al. 2008, 2010, Smith et al. 2008, Somot et al. 2018, Zunino et al. 2012, Waldman et al. 2016), progressively adding heat and salt into the deep WMED and enhancing the complexity of the deep stratification established by the WMT original structure. Eventually, the WMT signature has effectively propagated eastward

and westward into the Tyrrhenian sub-basin and the Alboran Sea (Schroeder et al. 2016), and its influence has been detected also within the Strait of Gibraltar (Naranjo et al. 2017, Sammartino et al. 2018), raising questions about its potential impact on the characteristics of the Mediterranean outflow.

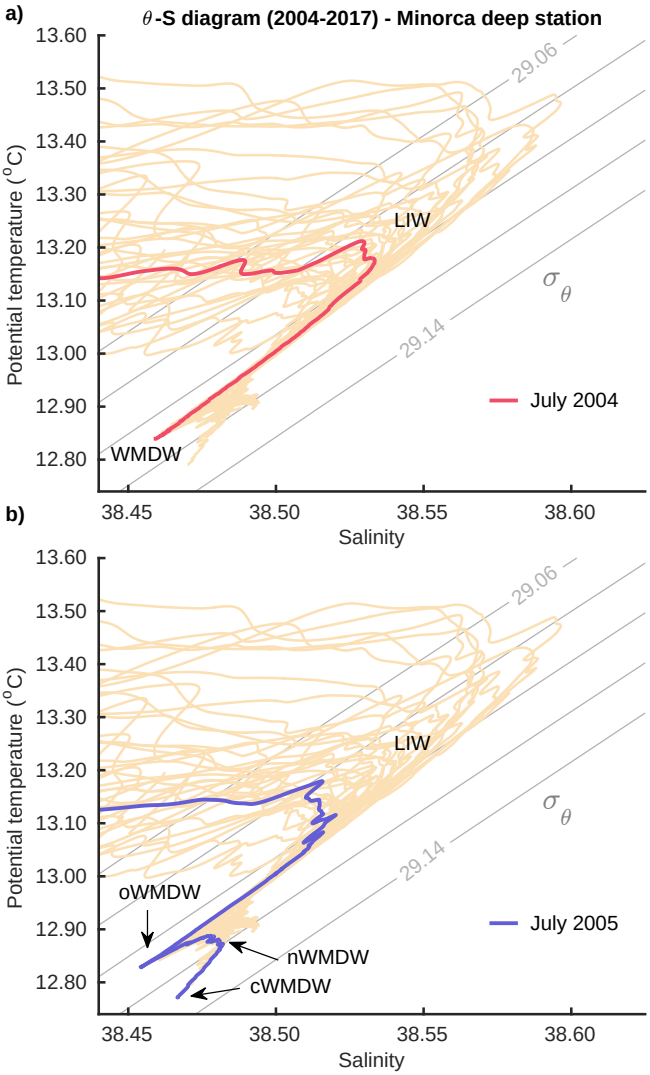

Figure 1.3. (a) θ-S diagram of the intermediate and deep layers between July 2004 and February 2017 in the Minorca deep station (NE Balearic Archipelago) of the RADMED program (see Sections 2.2 and 2.2.1). July 2004 profile is highlighted in red. The levels of the the LIW and WMDW cores are also indicated. (b) Same as (a) but highlighting the July 2005 profile in purple, in which the WMT structure was observed for the first time in this hydrographic station. The three waters masses that formed the complex hydrographic structure are indicated: the old WMDW (oWMDW; WMDW in (a)), the new WMDW (nWMDW) and the cascading-origin bottom waters (cWMDW). Gray lines denote isopycnal levels (σ_θ) every 0.02 kg m^{-3}.

The causes of the onset of the WMT have been attributed to a contribution of different atmospheric and oceanographic factors (Schroeder et al. 2010), such as the remarkably cold and dry winter of 2005 with persistent and strong northerly winds (Font et al. 2007, López-Jurado et al. 2005), the progressive heat and salt increment in the intermediate layers as a result of the westward propagation of the EMT influence (Schroeder et al. 2006, 2010); and the absence of deep convective processes in the GoL area in the previous decade, which enabled accumulation of heat and salt in the region (Herrmann et al. 2010). Changes in the regional circulation pattern during winter 2005 were also suggested to have play a role (Salat et al. 2009).

This doctoral thesis is focused on the study of the thermohaline variability of the WMED deep waters within the WMT period and the deep mixing dynamics that can be inferred from the evolution of such a stratified structure that emerged in the deep WMED, where background mechanical mixing is expected to be modest compared to the global oceanic regions and other thermohaline mixing processes may be relevant (Bryden, Schroeder, Sparnocchia, Borghini & Vetrano 2014).

1.4 Aims of the thesis

This doctoral thesis aims to complement and advance our current knowledge about the WMT climatic event and mixing dynamics in the deep WMED. Throughout this work, several aspects of the long-term thermohaline variability of the deep layers of the WMED within the WMT period are analyzed. The present research is based on observational datasets gathered by the *'Instituto Español de Oceanografía'* (IEO) in the continental slope of Minorca Island (Balearic Archipelago) over the last 16 years, in the framework of systematic monitoring programs and projects. Such oceanographic time series provide a comprehensive view of the long-term, deep hydrographic changes that occurred within the WMT and the regional dynamics. As is often the case in the course of a doctoral thesis, each study conducted to answer a number of specific scientific questions also remarks peculiarities or generates further questions that motivate subsequent investigations. The studies included in this thesis (Chapter 3 to 5) are the result of this natural development of any research.

Specifically, the aims of this doctoral thesis are:

- To analyze the WMT long-term thermohaline evolution between 2005 and 2017 in terms of irregular deep-water renewals and permanent vertical diffusive mixing in order to disentangle the contribution of both processes to the deep heat and salt budgets.
- To study the observed peculiar evolution of the deep hydrographic structure during the initial stages of the WMT (2005-2007) off Minorca Island, which is plausibly indicative of a combination of lateral advection of warm and salty deep waters and depth-intensified turbulent mixing.
- To investigate the occurrence of regional deep boundary mixing over the continental slope of Minorca Island by means of novel, extensive observations gathered in recent years in the region.

As stated before, the first two studies (Chapters 3 to 4) have been published in peer-reviewed international scientific journals and the last one (Chapter 5) is under preparation for publication. The complete reference to the published article is indicated in the corresponding chapter. The contents of the chapters are similar to the published manuscripts, albeit with some modifications to maintain coherence throughout the thesis structure. The oceanographic datasets that constitute the basis of this doctoral thesis are presented in Chapter 2. The main results of this thesis, along with final considerations and future perspectives are discussed in Chapter 6. Conclusions are gathered in Chapter 7.

Chapter 2

General methodology

This chapter provides an overview of the observational datasets used in this doctoral thesis and the environmental monitoring programs and platforms that gather and maintain such oceanographic time series. The particular methodology followed to conduct each of the studies that constitute the core of the doctoral thesis is presented within the specific chapter.

2.1 Long-term oceanographic records

The ocean is subjected to strong natural variability as a result of the intricate interaction of processes that occur at different spatial and temporal scales. As part of the climatic system, the chaotic variability of the ocean is also intrinsically influenced by the dynamics of the atmosphere, and the precise connection between processes occurring in – and affecting – both physical systems is not always well understood. Therefore, solid development of knowledge on processes occurring at different variability scales in the ocean is paramount in establishing our ability to predict future ocean and climate conditions, as well as the consequent potential impacts on ecosystems, which is a matter of pressing importance in a context of global climate change. Accordingly, it is of crucial importance to have sufficiently long time series of oceanographic data with a broad spatial coverage to enable us to study natural ocean variability and disentangle anthropogenic forcing. Large-scale shifts such as the WMT may be related to natural ocean-variability modes or may be a consequence of the unsteady conditions in the climate system. Elucidating its forcing, observing its evolution and studying the connection of the distinct physical processes that modulate it, cannot be accomplish without extensive quality oceanographic time series.

In recent decades, there has been an international effort, both scientific and technological, to maintain and promote the establishment of global networks of oceanographic observatories and regional observing systems, as well as the maintenance and standardization of historical long-term monitoring programs and databases in order to obtain homogeneous and quality oceanographic records with a global coverage. In this regard, the IEO has been investing in the development and maintenance of oceanographic observing systems for more than three decades. This scientific institution created an oceanographic monitoring system consisting of several distinct projects that currently collect systematic ship-based hydrographic and biogeochemical data over the Spanish continental margins and off-shore territorial waters at semi-annually, seasonal and even monthly frequency. This monitoring system also supports the Spanish contribution to the international Argo program (see Tel et al. (2016) for a comprehensive description of the Spanish Institute of Oceanography Observing System – IEOOS – and all its components). IEOOS' long-term monitoring records were initiated in the Atlantic region by the RADIALES project (Valdés et al. 2002), and were lately created independently in the Mediterranean margin of the Iberian Peninsula (López-Jurado et al. 2015), and other areas such as the Gulf of Cadiz and the Canary Islands, as a consequence of the prolonged effort and attempt to maintain oceanic observatories over time.

2.2 The RADMED monitoring program

In the WMED, several monitoring programs and observatories operate (Tintoré et al. 2019) such as, for instance, the MOOSE (Mediterranean Ocean Observing System on the Environment; Coppola et al. 2019), the SOCIB observing network (Balearic Islands Coastal Ocean Observing and Forecasting System; Tintoré et al. 2013), the Med-SHIP program (Mediterranean Sea Ship-based Hydrographic Investigations Programme; Schroeder et al. 2015), the HYDROCHANGES network (Schroeder et al. 2013) or the DYFAMED site (Dynamics of atmospheric fluxes in the Mediterranean Sea; Marty 2002). The contribution to the IEOOS in this region is the RADMED monitoring program (*'series tempoRAles de Datos oceanográficos del MEDiterráneo'*, also known simply as *'RADiales del MEDiterráneo'*; López-Jurado et al. 2015), which was established in 2007 as an

integration of previous monitoring projects of the IEO, such as ECOMALAGA, ECOMURCIA, CIRBAL and CANALES.

The RADMED program is currently constituted by a series of aligned oceanographic stations (i.e. sections) located across the continental margin of the Iberian Peninsula and the Balearic Archipelago (Figure 2.1). Throughout these sections, hydrographic, chemical and biological data in coastal, shelf and deep waters are gathered at a seasonal frequency. The geographic distribution of the sections responds to the aim of monitor regions where distinct large-scale oceanographic conditions are expected such as the Alboran Sea, the eastern continental shelf of the Iberian Peninsula or the Balearic Islands. These are also important regions to monitor water exchanges and associated heat and salt transports within the WMED (see for instance Vargas-Yáñez et al. 2020).

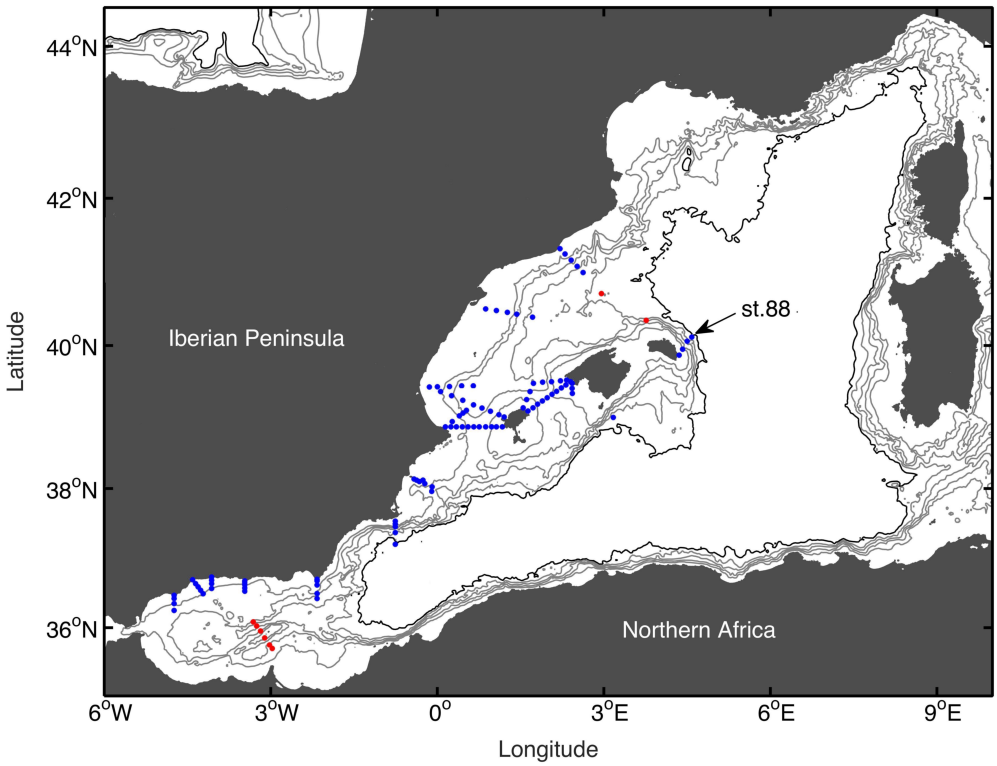

Figure 2.1. Geographical distribution of the RADMED monitoring program sampling stations (blue dots). Red dots refer to the new hydrographic stations included in the sampling strategy after the ATHAPOC project (see Section 2.3). The location of the Minorca deep station (station 88; Section 2.2.1) is indicated by an arrow. Light gray lines denote isobaths of 200 and from 500 to 2500 with a 500-meter interval in order to emphasize the extension of the deep pool.

Thermohaline data are gathered throughout the water column at each station commonly by means of a SBE 911plus CTD (conductivity-temperature-depth) – occasionally SBE 25 or

SBE19plus – installed on a SBE 32 carousel water sampler. Instrument calibration and cast processing are performed following standard protocols and routines, as described in López-Jurado et al. (2015).

The RADMED stations are integrated into the Mediterranean Operational Network for the Global Observing System (MonGOOS). All CTD data of the seasonal surveys are incorporated into the Pan-European Infrastructure for Ocean and Marine Data Management (SeaDataNet; see Tel et al. (2016) for data management protocols) and are also available at standard depth levels at the IBAMar regional database (Aparicio-González et al. 2015).

2.2.1 The Minorca deep station

The Minorca deep station (station 88; Figure 2.1), also called the Mahón deep station, is one of the deep hydrographic stations located along the Mediterranean continental slope of the Iberian Peninsula that are seasonally occupied by the RADMED monitoring program (along with the deep stations off Cape Palos, Barcelona and Cabrera Island) and occasionally, by other supporting projects. It is the most off-shore station of a hydrographic section located across the northeastern continental shelf and slope of Minorca Island (the easternmost island of the Balearic Archipelago). Since it is located in the outer continental slope (40° 10.00' N, 04° 34.96' E), where the bathymetry reaches a depth of roughly $\sim$ 2540 meters deep, it provides a detailed picture of the different water masses present in the WMED from surface to the deep layers, and enables us to study the long-term thermohaline variability of the deep waters. This station, located outside the typical dense-water formation area, is also a privileged site since the continental slope of the Balearic Islands is the preferential advective pathway of the newly-formed dense waters toward the Algerian sub-basin (Beuvier et al. 2012, Durrieu de Madron et al. 2013).

The Minorca deep station was first sampled in 2001, prior to the implementation of the RADMED program, and it was established in 2005 as a deep-water observatory to track the evolution of the WMED hydrographic structure following the detection of the WMT structure in summer of 2005 (López-Jurado et al. 2005). After 15 years of monitoring and 45 seasonal occupations (2005-2020), it is the station with the most comprehensive deep hydrographic time series available in the RADMED database and a valuable tool to study the thermohaline changes in the WMED deep waters induced by WMT onset event and successive injections of dense waters up to present. This record constitutes the main observational basis of the present doctoral thesis, along with the ATHAPOC mooring and oceanographic section (Sections 2.3.1 and 2.3.2).

2.3 The ATHAPOC project

The ATHAPOC (*'estudio de la Anomalía TermoHalina en las Aguas Profundas del mediterráneo occidental y su relación con las Oscilaciones Climáticas'*) project (2015-2018), funded by *Plan Nacional I+D+I* (CTM2014-54374-R) from the Spanish Ministry of Economy and Competitiveness (MINECO), was conceived with the aim of complementing and advancing our knowledge of the impact on the regional hydrography due to the dense-water formation processes in the northwestern part of the WMED and, particularly, of the changes induced after the onset the the WMT, documented through the RADMED program.

Additionally, in order to improve our observing capacity, several new stations were included in the RADMED sampling strategy in relevant locations for the monitoring of the deep waters, such as the Alboran Island, the northwestern continental slope of Minorca Island and an additional deep station between the Catalan continental slope and the Balearic Archipelago (see red dots in Figure 2.1). To complement the long-term variability of the deep waters recorded in the Minorca deep station and to obtain insight on local dynamics, a fully instrumented deep mooring line was installed in the outer northeastern continental slope of Minorca (the ATHAPOC mooring) and a high-resolution cross-slope oceanographic section was conducted on a semi-annual basis (the ATHAPOC section).

2.3.1 The ATHAPOC mooring

The ATHAPOC mooring consisted of a fully instrumented moored line (Figure 2.2) installed on the outer part of the northeastern flank of the continental slope of Minorca (40° 9.64' N, 04° 36.87' E. Figure 2.3) that remained in the water during two periods: September 2015-April 2016 and February 2017-August 2018. The instruments included in the original design, their nominal depths and sampling rates were:

- Eight CTDs (SeaBird MicroCat SBE37) at 200, 400, 1000, 1300, 1600, 1900, 2250 and 2500 meters (sampling rate of 10 minutes)
- Five single-point current meters (Nortek Aquadopp) at 200, 400, 1000, 1600 and 2500 meters (sampling rate of 30 minutes)
- Seven temperature sensors (SeaBird SBE56) at 150, 300, 500, 600, 700, 850, 1150, 1450 meters (sampling rate of 10 minutes)
- Two Sediment traps (PPS3 Technicap) at 200 and 2510 meters (sampling rate 8-16 days)

Some instruments of the original configuration of the mooring line were changed during maintenance operations in order to accommodate emerging scientific necessities or removed due to instrumental issues. In the second period (February 2017-August 2018), a Seapoint turbidimeter was included at 2500 meters with a sampling rate of 5 minutes (changed to 1 minute from November 2017 onward).

The moored instrumentation was regularly calibrated by means of shipborne CTD casts encompassing the deployment periods conducted in a nearby station. When the ATHAPOC mooring was not installed (April 2016-February 2017), the calibration station continued to be regularly visited in order to obtain reference values.

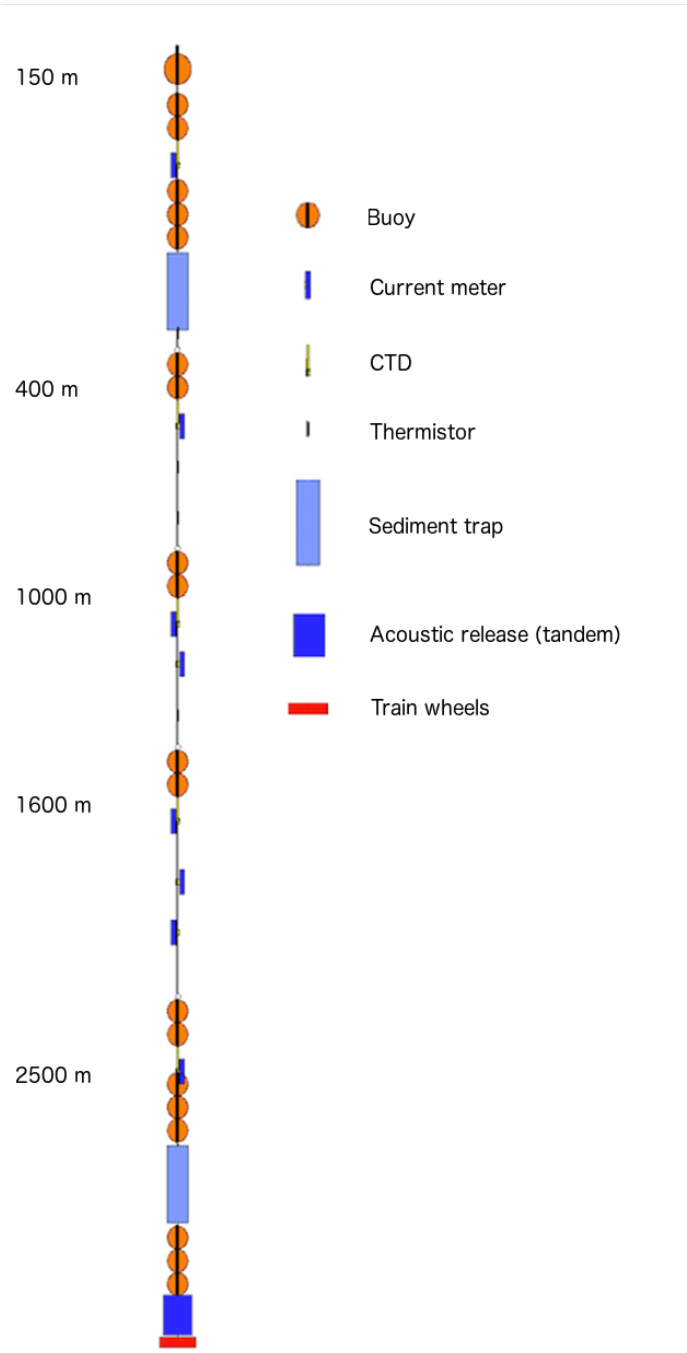

Figure 2.2. Schematic of the original configuration of the ATHAPOC mooring line.

In August 2018, the ATHAPOC mooring was removed from the water and a much shorter and simpler moored line was installed (HC-IEO-M mooring). This mooring was equipped with a single-point Nortek Aquadopp current meter, a SeaBird MicroCat SBE37 and a Seapoint turbidimeter located at 2500 meters depth, programmed with the same sampling rates as those specified for the ATHAPOC mooring. The HC-IEO-M mooring was removed from the water in October 2019 for maintenance and is currently (2021) deployed. Along with a similar mooring line located in the Ibiza Channel, the HC-IEO-M mooring is integrated within the HYDROCHANGES network (Schroeder et al. 2013). Both moorings are regularly maintained and calibrated with CTD casts in the framework of the RADMED monitoring program.

2.3.2 The ATHAPOC oceanographic section

Besides the ATHAPOC mooring, a high-resolution cross-slope oceanographic section was designed within the ATHAPOC project, which covered the entire bathymetric range of the northeastern continental slope of Minorca Island beneath 800 meters (Figure 2.3). This section was occupied in November 2017, February 2018, August 2018, February 2019, October 2019, and January 2020. Between November 2017 and February 2019, the ATHAPOC section involved 11 oceanographic stations that spanned 25 km off-shore (40° 2.28' N, 04° 25.00' E – 40° 10.92' N, 04° 38.58' E). In October 2019, two additional stations were incorporated, increasing the spatial resolution of the section and extending the observations to more than 28 km off-shore (40° 2.28' N, 04° 25.00' E – 40° 12.00' N, 04° 40.20' E). In addition to hydrographic measurements, LADCP (Lowered Acoustic Doppler Current Profiler) measurements were obtained from August 2018 onward. All CTD-LADCP casts were obtained, processed and calibrated following standard protocols.

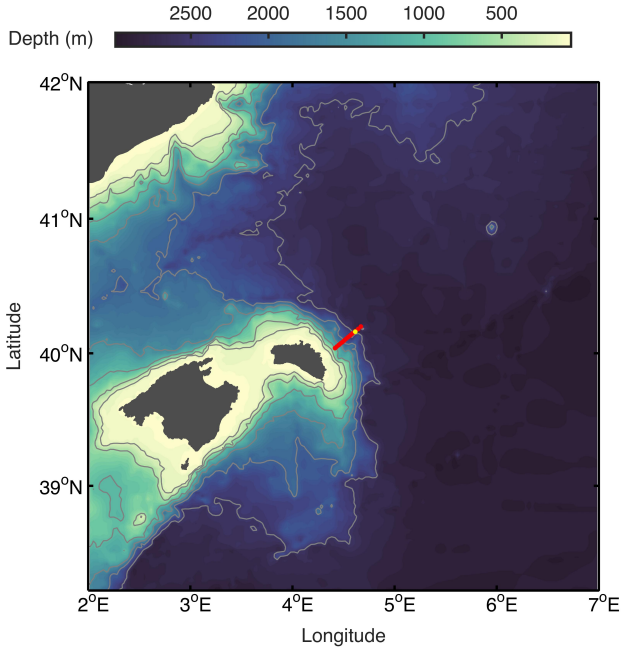

Figure 2.3. Bathymetric map around the northeastern part of the Balearic Archipelago, and location of the ATHAPOC mooring (yellow dot) and the ATHAPOC cross-slope high-resolution oceanographic section (red dots).

Chapter 3

Thermohaline evolution of the Western Mediterranean deep waters since 2005: diffusive stages and interannual renewal injections

---

This chapter has been published as:

Piñeiro, S., González-Pola, C., Fernández-Díaz, J. M., and Balbin, R. (2019). Thermohaline evolution of the Western Mediterranean deep waters since 2005: diffusive stages and interannual renewal injections. *Journal of Geophysical Research: Oceans*, 124 (12), 8747–8766. https://doi.org/10.1029/2019JC015094.

Within this chapter, two animations (Movie S1 and Movie S2) are referred to as supplementary information. These files can be accessed at: https://doi.org/10.1029/2019JC015094.

Keypoints

- Western Mediterranean deep layers were monitored in detail during the WMT at a key site near Minorca
- Evolution of the layered structure is analysed in terms of double-diffusive mixing and ventilation
- Large heat and salt uptake of the deep Western Mediterranean was dominated by irregular renewals

Abstract

A large production of anomalous dense water in the northwestern Mediterranean Sea during winter 2005 led to a widespread abrupt shift in WMED deep waters characteristics. This new configuration, the so-called WMT, involved a complex thermohaline structure that was tracked over time through a deep hydrographic station located NE of Minorca Island, sampled 37 times between 2004 and 2017. In this study, the thermohaline evolution of the WMT signal is analysed in detail. Using a 1-D diffusion model sensitive to double-diffusive mixing phenomena, the contribution to the heat and salt budgets of the deep WMED in terms of ventilation and diffusive transference from the intermediate layers above is disentangled. Results show distinct stages in the evolution of the deep waters, driven by background diffusion and intermittent injections of new waters. The progression of a multi-layered structure in the deep ocean is well represented through existing parameterizations of salt fingering and diffusive layering processes, and makes it possible to infer an independent estimate of regional background diffusivity consistent with current knowledge. Overall, the deep layers of the Western Mediterranean underwent substantial warming (0.059 °C) and salt increase (0.021) between 2004 and 2017, mostly dominated by injections of dense waters in the 2005–2006 and 2011–2013 periods. Thus, within the WMT period, heat uptake rate in the deep WMED was substantially higher than that of the intermediate levels in the global ocean.

3.1 Introduction

Ocean ventilation is a fundamental piece in Earth's heat redistribution dynamics and hydrological cycle. Winter buoyancy loss of surface waters in dense-water formation areas is the main mechanism driving the ventilation of the ocean interior and modulating heat storage below the permanent thermocline. For this reason, areas prone to deep convection activity are hot spots for the study of ocean circulation and climate (Marshall & Schott 1999, Winton et al. 2013).

The northwestern Mediterranean Sea is one of the few active dense-water formation areas outside the polar regions (MEDOC Group 1970). In this area, the WMDW is formed during some winters (see Section 1.2). As described in the introductory chapter, the historical evolution of the characteristics of this deep water mass was drastically disrupted in winter of 2005, due to the large production of anomalous dense water that led to the formation of the WMT (Section 1.3; Font et al. 2007, López-Jurado et al. 2005, Salat et al. 2007, Schroeder et al. 2006, 2016).

Since its formation, the evolution of the WMT has been tracked and studied directly or indirectly by different projects and monitoring programs, from the formation area in the GoL to the Algerian basin (e.g., Durrieu de Madron et al. 2013, Houpert et al. 2016, Puig et al. 2013, Schroeder et al. 2009, 2013, 2016, Waldman et al. 2016). Several projects carried out by the IEO and grouped nowadays under the RADMED monitoring program (see Section 2.2) have been gathering hydrographic data on a seasonal basis along the Spanish Mediterranean coast since the late 1990s. The deep stations included in this program provide a detailed picture of the evolution of the WMT along the eastern continental slope of the Iberian Peninsula, midway between the WMDW origin at the GoL and the Alboran Sea.

In this chapter, the thermohaline evolution of the WMT signal, its fade and subsequent deep-water renewal variability are analysed in detail using hydrographic data from the Minorca deep station of the RADMED program. A 1-D diffusion model sensitive to double-diffusive mixing phenomena is used in order to obtain the theoretical diffusive evolution of the θ-S profiles. This numerical approach enables us to disentangle the contribution to the heat and salt budgets of the deep WMED in terms of ventilation due to the advection of dense waters injected in the formation area and the diffusive transfer of heat and salt from the intermediate layers above.

The chapter is organized as follows. The dataset is presented in Section 3.2. In Section 3.3, the processing applied to the hydrographic data is explained and the diffusion model scheme is described in detail. In Section 3.4, the obtained results are exposed; and subsequently discussed in Section 3.5. Lastly, final conclusions and considerations are presented in Section 3.6.

3.2 Dataset

In this study, we use hydrographic data between 2004 and 2017 from the Minorca deep station (Fig. 3.1a), occupied 37 times during that period (Fig. 3.1b). This time series offers a comprehensive view of the temporal variability of the thermohaline changes induced by the WMT and the subsequent intermittent injections of dense waters in the formation region (Fig. 3.1c).

The thermohaline signature of the different water masses present below 300 dbar in the WMED is easily identifiable in the θ-S diagram (Fig. 3.1c). The warm and salty LIW core is located between 300 and 600 dbar, followed by a transition region with a smooth stratification where salinity (S) and potential temperature (θ) decrease with depth toward the WMDW core at the bottom of the basin. The complex thermohaline structure that emerged in winter 2005 modified this classical vertical structure and created the distinctive hook-shaped θ-S profile in the deep waters shown in Section 1.3, due to the appearance of the saltier and warmer nWMDW beneath the oWMDW, and the fresher and colder cWMDW at the bottom (see notations in Fig. 3.1c; López-Jurado et al. 2005, Puig et al. 2009, Schroeder et al. 2006, Salat et al. 2007). Even though thermohaline anomalies in the deep layers of the WMED have been observed previously (as bottom increments of θ and S or even complete hook-like features; Bethoux & Tailliez 1994, Bethoux et al. 2002, Lacombe et al. 1985, Salat et al. 2009, Puig et al. 2013), the large input of dense water in 2005 created an unprecedented structure hundreds of metres thick that triggered a large uplift of the isopycnals over the whole basin (Schroeder et al. 2008), causing the appearance of an interface between the oWMDW and the nWMDW at about 1000 dbar above the bottom (clearly identifiable in Fig. 3.1c).

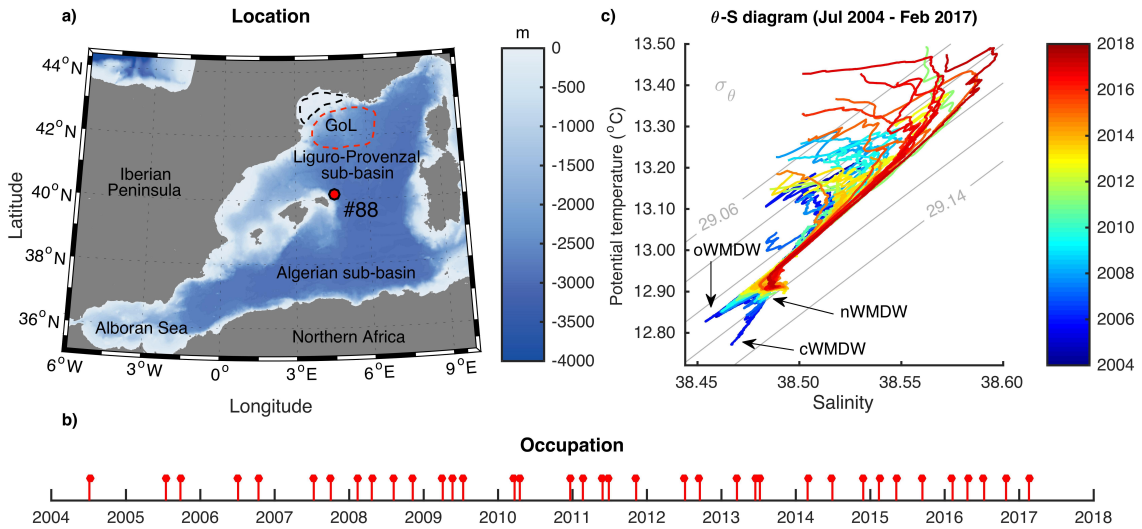

Figure 3.1. (a) Location of the RADMED #88 deep station (red dot). Red dashed line shows the open-ocean deep water formation area and the black dashed line shows the cascading-origin dense waters formation area as stated in Houpert et al. (2016). (b) Occupation from 2004 to 2017. (c) θ-S diagram from 300 dbar to the bottom from July 2004 to February 2017. Gray lines denote isopycnal levels (σ_θ) every 0.02 kg m^{-3}.

3.3 Methodology

This study focuses on the relative role of diffusion versus advection of dense waters in the long-term thermohaline evolution of the deep waters at the Minorca station during the WMT period. To address the issue, the output of the theoretical diffusive evolution of the water column from a 1-D model, is compared with the actual 12-year hydrographic time series. Divergences between observations and the model are then attributed to lateral advection of ventilated dense waters from the formation area in the GoL. This approach treats local observed profiles as the result of decoupled advection and diffusion, which is an approximation of a much more complex 3-D process in which the advected water column mixes vertically while spreading, strongly conditioned by background shear. The idealised 1-D diffusive evolution requires assumptions regarding diffusive coefficients values and its vertical structure that have to be based on current knowledge of ocean mixing processes while being consistent with the local observed evolution. The limitations of what the 1-D model can represent, i.e. spatial heterogeneity in mixing and spreading cannot be taken into account, should be kept in mind when discussing the outcomes.

Since raw hydrographic time series have a noisy character, a necessary first step is to construct a smoothed version of the hydrographic evolution. Then, a brief description of the diffusive processes expected in the deep waters of the WMED within the WMT configuration is provided, followed by a description of the procedure for the numerical treatment of such a diffusion process.

3.3.1 Smoothed evolution of the hydrography

Pre-processing of the raw hydrographic record is required to obtain a smooth evolution of the WMT structure. Filtering of natural noise due to mesoscale or higher frequency processes is not straightforward, since the vertical and temporal scales are not comparable and time series are not evenly sampled. While different approaches could be followed, this specific study only required a reasonable smooth temporal variation of the hydrographic structure to be achieved, therefore a simple approach was applied as described below.

Discarding the surface layer (0-300 dbar), the 37 θ-S profiles were first stabilized to remove small scale density inversions using the algorithm described in Barker & McDougall (2017) and included in the TEOS-10 software (IOC et al. 2010). Then a digital filter with a 50-dbar window was applied to remove small-scale structures below such a range. Since 5 profiles did not reach the bottom (see Section 3.4), the vertical structure of the closest profile (in time) was used to interpolate the time-series matrix. Finally, a Locally Estimated Scatterplot Smoothing (LOESS; Seifert & Gasser 2004) was used as a smoother for the temporal variation of θ and S, making it possible to obtain continuous time series at each pressure level encompassing the period between 15 July, 2005 and 12 February, 2017 (Section 3.4). A fortnightly series of profiles was then extracted. Vertical stability of the interpolated profiles was carefully examined to verify that there were no spurious density inversions larger than the instrument resolution (10^{-4} $\mathrm{kg\,m^{-3}}$) due to the data treatment. Further checks indicated that the LOESS smoother applied here is similar to a 3rd order Butterworth digital filter (Emery & Thomson 2001) with a cut-off frequency of 12-18 months, adequate to remove intra-annual noise and to maintain the signal of inter-annual injections of dense waters. The LOESS approach was preferred since it is less sensitive to outliers, mainly present in the interface region.

A comparison between the smoothed and original profiles can be observed in Movie S1 in the supporting information (https://doi.org/10.1029/2019JC015094). Root-mean-square deviation between raw and smoothed time series can be considered as indicative of the intrinsic noise of the dataset. Hereafter this smoothed time series will be considered as the observational record.

3.3.2 Turbulent diffusion and double-diffusive mixing parameterization

In the absence of ventilation, the water column structure generated by the WMT should evolve by diapycnal mixing, mostly accomplished by transient turbulent motions induced by dynamical instabilities such as internal wave breaking or current shear (Klymak & Nash 2009). By analogy with molecular fluxes, turbulent fluxes of heat and salt are commonly parameterized by Fickian diffusion. Thus, following Fick's Second Law, vertical (z) temporal (t) diffusive evolution of the thermohaline properties (c) of the water column in Minorca can be straightforwardly estimated in terms of the tracer gradient and an eddy diffusion coefficient (K_c; Klymak & Nash 2009). In one dimension:

$$\frac{\partial c}{\partial t} = \frac{\partial}{\partial z}\left(K_c(z)\frac{\partial c}{\partial z}\right). \tag{3.1}$$

General circulation models usually approach diapycnal mixing assuming same depth-dependent K_c for both scalars (S and θ; e.g. Jayne 2009). However, under certain thermohaline configurations of the water column (both θ and S decreasing or increasing with depth) asymmetries may arise between θ and S diffusion coefficients due to the difference in heat and salt molecular diffusivity. This so-called double-diffusive mixing (Kelley et al. 2003, Radko 2013, Schmitt 2009) can become of great importance if turbulence is not strong because it may greatly vary both K_θ and K_S and transfer heat and salt unequally.

During the WMT, the vertical thermohaline structure in the Minorca deep station appears to be favourable for both forms of double-diffusion: salt fingering (warmer salty waters over colder and fresher ones) and diffusive layering (cold and relatively fresh waters over warmer and saltier ones) (Bryden, Schroeder, Borghini, Vetrano & Sparnocchia 2014). The warm and salty LIW overlying the fresher and colder WMDW is a permanent feature of the basin, causing salt fingering instabilities to be operating transporting salt downward more efficiently than heat. Its main fine-scale signature, the thermohaline staircases (Schmitt 1994), has been observed repeatedly in this region and seems to be an ubiquitous feature throughout the Algerian and Tyrrhenian sub-basins (Bryden, Schroeder, Borghini, Vetrano & Sparnocchia 2014, Bryden, Schroeder, Sparnocchia, Borghini & Vetrano 2014, Durante et al. 2019, Johannessen & Lee 1974, Zodiatis & Gasparini 1996). Additionally, the injection of anomalous warm and salty dense waters during the WMT created a transition region between the oWMDW and the nWMDW prone to diffusive layering, known to transfer heat upward more efficiently than salt. Similarly, the deepest region of the water column, between the nWMDW and the cWMDW, became a region prone to salt fingering.

In order to identify where double-diffusive mixing processes are operating in the water column, the reference parameter is the local density ratio $R_\rho = (\alpha T_z)/(\beta S_z)$ (Turner 1973), where T_z and S_z are the vertical gradients of temperature and salinity and α and β are the thermal expansion and haline contraction coefficients of seawater, respectively. Under static stability, the condition for double diffusion is $R_\rho > 0$ and its intensity depends, besides R_ρ value, on the Lewis number ($\tau = \kappa_T/\kappa_S$), where κ_T and κ_S are the molecular diffusivities of heat and salt. Salt fingering is active when $1 < R_\rho < \tau \approx 100$, whereas diffusive layering requires $1 > R_\rho > \tau^{-1} \approx 0.01$ (Kelley et al. 2003, Schmitt 2009).

Both forms of double diffusion are more active and have a major impact on diapycnal mixing when R_ρ approaches one (Schmitt 1994). In this study, large-scale K_θ and K_S under these mixing regimes are estimated following R_ρ-dependent parameterizations used in Zhang et al. (1998) and Zhang & Schmitt (2000), which evaluate diffusivities as a separate contribution of double-diffusive mixing added to constant background mixing. Accordingly, for the salt fingering regime:

$$K_S = \frac{K^*}{1 + (R_\rho/R_c)^n} + K^\infty \text{ and } K_\theta = \frac{0.7K^*}{R_\rho[1 + (R_\rho/R_c)^n]} + K^\infty, \tag{3.2}$$

where $K^* = 2 \times 10^{-4}\ \mathrm{m^2\,s^{-1}}$ is the maximum salt finger diffusivity, $R_c = 1.6$ is the critical density ratio above which salt-finger-driven diffusivities decrease abruptly, $n = 6$ controls the drop of K_θ and K_S regarding the increment of R_ρ, and K^∞ is the constant diapycnal diffusivity due to background mixing related to intermittent dynamical instabilities and not to double diffusion.

For the diffusive layering regime, Zhang et al. (1998) parameterize K_θ and K_S according to the empirical formulations of Kelley (1984, 1990) but with minor modifications to address both forms

of double diffusion and to represent the effects of background turbulence:

$$K_\theta = CR_a^{1/3}\kappa_T + K^\infty \text{ and } K_S = R_F R_\rho (K_\theta - K^\infty) + K^\infty, \tag{3.3}$$

where

$$C = 0.0032 \exp(4.8{R_\rho}^{0.72}),$$

$$R_a = 0.25 \times 10^9 R_\rho^{-1.1},$$

$$R_F = \frac{1/R_\rho + 1.4(1/R_\rho - 1)^{3/2}}{1 + 14(1/R_\rho - 1)^{3/2}}$$

and

$$\kappa_T = 1.4 \times 10^{-7}\ \mathrm{m^2\,s^{-1}}.$$

For regions where the water column is doubly stable for both S and θ (no double diffusion), a classical turbulence parameterization is adopted to represent the background mixing induced by transient dynamical instabilities:

$$K_\theta = K_S = K^\infty. \tag{3.4}$$

It should be noted that the general vertical structure of the WMED is prone to double-diffusive regimes and the doubly stable portions of the water column are a minority and, generally, transient.

The same parameters as used in Zhang & Schmitt (2000) are adopted here. As opposed to Zhang et al. (1998), who discard double-diffusion in the deep layers, no constraint to the double-diffusion activity is applied. Indeed, regions prone to both forms of double diffusion can be found in the deep waters of the Mediterranean (Meccia et al. 2016, Onken 2003).

$K_{S,\theta}(z)$ values (both under double-diffusive regimes and not) can be found in the literature inferred from analytical studies or derived from field observations (e.g. Kunze & Toole 1997, Ledwell et al. 1993, 1998, 2000, Polzin 1997, Schmitt et al. 2005, Schmitt & Ledwell 2001, Schmitt et al. 2005, St. Laurent & Schmitt 1999, St. Laurent et al. 2001, Toole et al. 1994). As described below, specific periods where the evolution of the profiles is consistent with pure diffusion were used here to estimate an optimal K^∞ local value.

3.3.3 Numerical integration of the diffusion equation

The basis of this study was the comparison between the actual evolution of the deep ocean hydrography and what would be caused by pure diffusion alone. Therefore, it was necessary to integrate the diffusion equation numerically given some boundary conditions and a $K_{S,\theta}(z)$ parameterization, i.e. it was necessary to set up a simple 1-D diffusion model. The setting was as follows:

The vertical coordinate (z) was discretized regularly on a vertical grid of n points and height H, with a resolution of $\delta z = H/n$. At each time step (δt), mixing regimes throughout the water column were identified by means of the Turner angle (Ruddick 1983) and K_θ and K_S profiles were estimated following the R_ρ-dependent parameterizations previously described (Sec. 3.3.2).

The one-dimensional diffusion equation (3.1) was solved numerically for both θ and S using a Crank-Nicolson scheme (second-order implicit; Crank & Nicolson 1947), with $\delta t = 2.4$ hours and $\delta z = 10$ metres (chosen to secure numerical stability while allowing quick runs). The domain ranged from 800 dbar, well below the influence of the LIW core fluctuations, to 2420 dbar. Simulations started with an observed profile from the smoothed set.

Density is used here as a diagnosis variable. Since evolution of θ and S is considered independently, it is in principle possible to create spurious density inversions invalidating the simple diffusion scheme. Finally, this was not the case in any of the simulations so no convective adjustment scheme for unstable stratification regions was required.

To close the scheme, two boundary conditions were set. At the seafloor it is assumed that there is no flux (i.e. a Neumann condition $\partial c/\partial z = 0$ at $z = H$). This is obvious for salinity and can be arguable for temperature due to geothermal heating, as discussed below.

Conditions at the upper boundary of the domain were set by the θ and S values and their vertical gradient at the thermo-halocline, inferred from the observed profiles below the LIW core. These values change over time, modulating the heat and salt fluxes toward deeper layers. To include this time varying boundary condition, an assimilation scheme was applied that replaced, at each δt, the upper domain of the profile with a combination of the simulated profile and the observed profile in such a way that the top of the simulation matched the observations, imposing continuity in the profile and its gradient (Fig. 3.2). The assimilation was performed above an isopycnal level slightly lighter than the bottom limit of the oWMDW, ensuring that the heat and salt fluxes transferred by downward diffusion into the WMT structure were modulated by the actual hydrographic record but never altering the anomaly. An isopycnal level was preferred rather than a fixed isobaric level because it integrates changes in the vertical position of the structures due to heave effects (Bindoff & McDougall 1994). Further details concerning the numerical assimilation can be found in the Appendix A. Movie S2 in the supporting information (https://doi.org/10.1029/2019JC015094) illustrates the process.

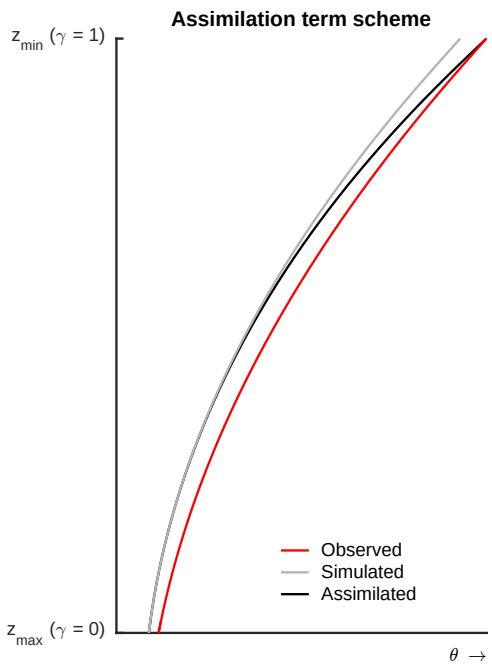

Figure 3.2. Assimilation term scheme used in the 1-D diffusion model. Two θ profiles are shown: the simulated one (gray) and the one inferred from the observations (red) at that particular moment of the time series. The resulting profile (black) is a combination of both. z_{min} refers to the upper limit of the domain (800 dbar) and z_{max} to the assimilation limit, which in turn corresponds to the pressure of the heaviest isopycnal that always remains above the oWMDW-nWMDW interface. For further details on nomenclature and formulation, the reader is referred to the Appendix A.

3.3.4 K^{∞} local estimation

Due to the nearly seasonal frequency sampling, it is possible to look for periods within the overall 12 years when the thermohaline evolution had a clear purely diffusive behaviour. An estimate of K^{∞} can be inferred from such periods. In order to identify these, certain criteria were followed: (i) no appearance of new isopycnals at the bottom, (ii) no large doming of isopycnals in the time series that could indicate lateral advection at intermediate depths, (iii) θ-S profile maxima and minima erosion over the period and (iv) no bibliographic evidence of deep convection in the formation area within the period.

Over the periods identified as diffusive, θ and S differences between the model and the observations were computed. Since both variables were measured simultaneously and had different ranges of variation in the water column, the error of the two measurements can be normalized by dividing each measure (c_i) by the standard deviation (σ_c) after subtracting the mean ($\bar{c}$), i.e. $Z(c)_i = (c_i - \bar{c})/\sigma_c$. Therefore, a combined normalized root-mean-square error (RMSE) can be defined:

$$\mathrm{RMSE}_{\theta S}^{nor} = \sqrt{\frac{1}{2}\left(\frac{1}{n}\sum\left(Z(\theta)_{mod} - Z(\theta)_{obs}\right)^2 + \frac{1}{n}\sum\left(Z(S)_{mod} - Z(S)_{obs}\right)^2\right)}. \tag{3.5}$$

A locally estimated optimum K^{∞} can be obtained by minimizing $\mathrm{RMSE}_{\theta S}^{nor}$ from an exhaustive inspection of K^{∞} over realistic ranges in the simulations of markedly diffusive periods.

3.4 Results

3.4.1 θ-S shape evolution

The local thermohaline evolution of the deep waters in Minorca is roughly governed by continuous diffusive mixing and water renewals by irregular inputs. Considering the shape of the θ-S diagrams in the deep layers (Fig. 3.3), it can be noticed that since the event that gave rise to the WMT, different waters with specific signatures were injected at inter-annual scales. Advection of these new waters to Minorca caused an enhancement of the thermohaline gradients and the appearance of new structures in the θ-S plane that distorted the initial signature of the WMT.

Three main stages in the evolution of the deep waters can be distinguished from the hydrographic data: first, a hook-shaped stage from July 2005 to presumably December 2010 (since the CTD did not reach the bottom depth) corresponding to the appearance of the initial WMT structure and the consequent interface between the oWMDW and the nWMDW at about 1200 dbar. Within this period, after winter 2006, the production of deep water seems absent or not relevant for the evolution of the new deep waters, which appear to be dominated by diffusive mixing processes. The cascading waters and the θ-S maximum associated with the nWMDW were progressively eroded. In 2009, a small disturbance appeared at the bottom and established the beginnings of the second stage, defined by a more complex m-shaped θ-S structure, ranging from 2010 to 2014. Several major deep-water formation events occurred within this period (see Section 3.5.1). From November 2014 to February 2017, without evidence or report of large-scale convective events, the θ-S profile turned into an V-shape, defining the third stage.

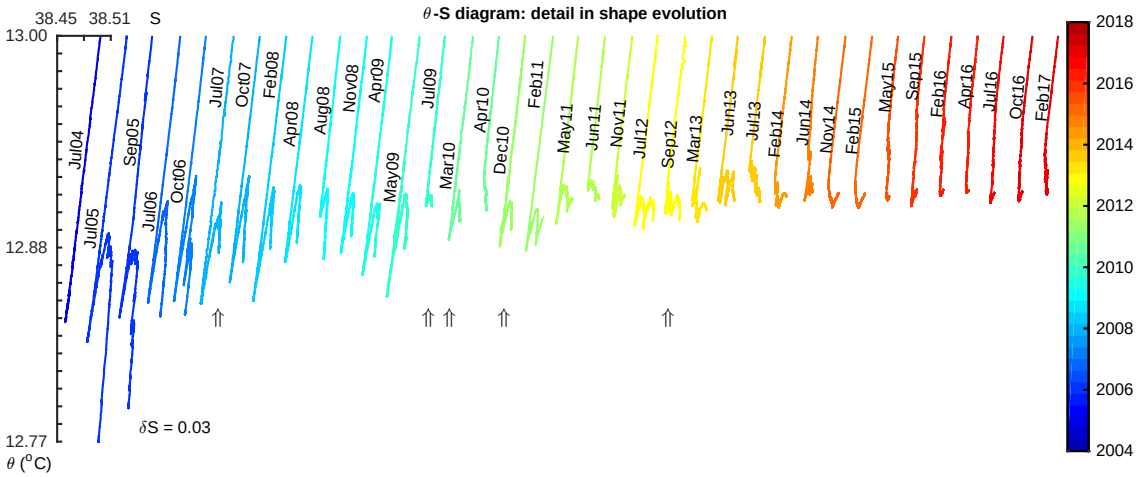

Figure 3.3. Detail in shape evolution of the θ-S diagram below the LIW core in Minorca. Axes refer to the 2004 profile. Subsequent profiles are shifted in time by δS. Arrows indicate the profiles that did not reach the bottom depth.

3.4.2 Best estimate of K^{∞}

Figure 3.4 shows contours of the smoothed observational records where short-term and small-scale variations were filtered (see also supporting information at https://doi.org/10.1029/2019JC015094). A key portion of the water column is the oWMDW-nWMDW interface created by the WMT, clearly visible in the contours as a salinity minimum starting around 1200 dbar (Fig. 3.4a). This interface remains traceable until around mid-2014, when the structure of the deep waters is strongly eroded. By inspection, the $\sigma_\theta = 29.1088\ \mathrm{kg\,m^{-3}}$ isopycnal (white dashed line in Fig. 3.4) was selected as the reference level closest to the oWMDW-nWMDW interface, since it always remained above it throughout the entire time series. This isopycnal was taken as the limit of assimilation in the simulations and the maximum pressure reached was 1280 dbar. This pressure was later used as a reference to compute changes in the heat and salt budgets of the deep waters within the WMT.

Potential density anomaly (σ_θ) contour corroborates what was anticipated by the analysis of the θ-S profiles shape, showing the occurrence of new density levels at the bottom and a generalized uplift of the isopycnals in the whole water column in the two periods characterized by the presence of anomalous structures below 1000 dbar, 2005–2006 and 2009–2013 (Fig. 3.4c). Within the *a priori* diffusive periods inferred from the observed profiles (Fig. 3.3), the hook-shaped stage after 2006 and the V-shaped stage, two periods that met the criteria established in Section 3.3.4 were selected to infer a local estimate of K^{∞}: the first one, from 15 February, 2008 to 26 December, 2008 (315 days); and the second one, between 6 September, 2015 and 2 July, 2016 (300 days). Both periods, highlighted in Figure 3.4, include four observed profiles each.

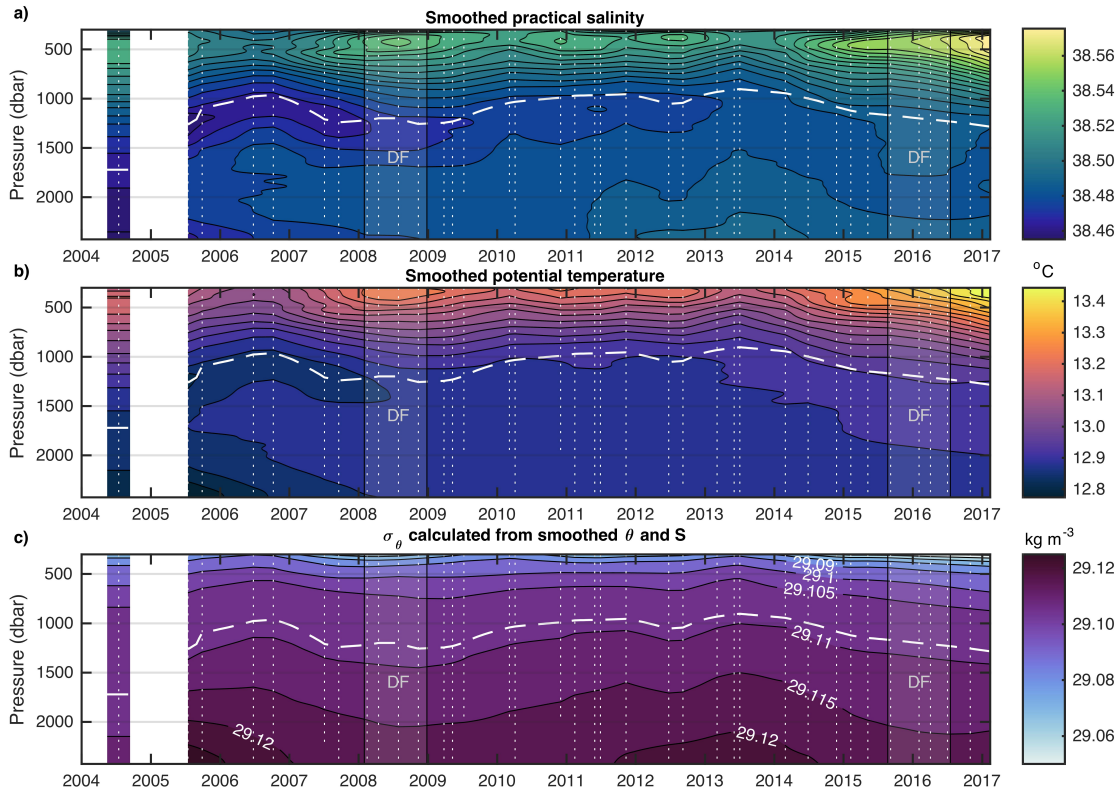

Figure 3.4. (a) Smoothed S, (b) θ and (c) σ_θ evolution between July 2005 and February 2017 in Minorca from 300 dbar to 2420 dbar. July 2004 profile is included for reference. The white dashed line indicates 29.1088 $\mathrm{kg\,m^{-3}}$ isopycnal pressure. Highlighted boxes delimitate the diffusive periods (DF) where local K^∞ was estimated. Vertical white dotted lines indicate the date of each CTD cast and their maximum pressure reached.

Since the periods have substantially similar time intervals, giving equal weight to both, the $\mathrm{RMSE}^{nor}_{\theta S}$ were combined and a minimum in $K^\infty = 4.25 \times 10^{-4}\ \mathrm{m^2\,s^{-1}}$ was obtained (Fig. 3.5). This value minimizes the differences between the simulations of both periods and the observational record. Roughly speaking, $K^\infty \in (3.5\ \times 10^{-4}\ \mathrm{m^2\,s^{-1}}, 5.5 \times 10^{-4}\ \mathrm{m^2\,s^{-1}})$ is consistent with the observed evolution of the purely diffusive stages. Taking the combined optimized K^∞, specific simulations for each period yield maximum θ differences of 10^{-3} °C and $< 10^{-3}$ for S.

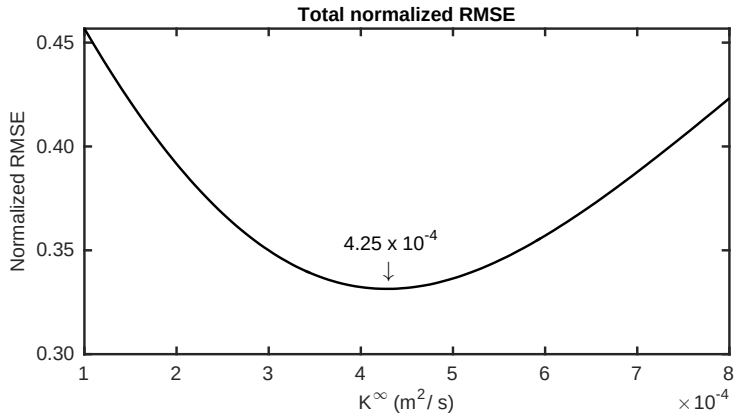

Figure 3.5. Total normalized RMSE for the two diffusive periods between the simulations and the observational record for simulations with $K^{\infty} \in (1 \times 10^{-4}\ \mathrm{m^2\,s^{-1}}, 8 \times 10^{-4}\ \mathrm{m^2\,s^{-1}})$.

3.4.3 The 2005-2017 simulations. Long-term single runs

In order to evaluate what the degradation of the WMT structure would be like if only diffusion were present, two 12-year simulations were carried out using 15 July, 2005 as the initial profile (i.e. the profile in which the anomaly was observed for the first time). Every 15 days an output profile was obtained from the simulation, enabling a comparison with the fortnightly observational record. In the first simulation, the assimilation term was not included, i.e. the initial θ and S values at the upper boundary (800 dbar) were kept constant, thus allowing the thermo-halocline below to evolve freely by diffusion. The second simulation included the assimilation term up to the indicated 29.1088 isopycnal pressure, forcing the thermo-halocline to evolve toward observations (see Fig. 3.6 and Movie S2 in the supporting information at https://doi.org/10.1029/2019JC015094). As indicated, the inclusion of assimilation modulates the downward transference of heat and salt from intermediate layers by taking into account their actual evolution.

In both simulations, the initial Turner angle profiles show a complex interleaved succession of mixing regimes throughout the water column derived from the WMT structure. As expected, mixing near the bottom in the transition region between the cWMDW and the nWMDW core presents salt finger activity of moderate intensity ($Tu \approx 69°$) with some enhancement of diffusive coefficients from background values (up to $K_\theta \approx 4.3 \times 10^{-4}\ \mathrm{m^2\,s^{-1}}$ and $K_S \approx 4.5 \times 10^{-4}\ \mathrm{m^2\,s^{-1}}$), thus salt is transported downward more efficiently than heat. In the transition region between the nWMDW core and its interface with the oWMDW, diffusive layering is operating ($Tu \approx -81°$) transporting heat upward more efficiently than salt ($K_\theta \approx 4.4 \times 10^{-4}\ \mathrm{m^2\,s^{-1}}$ and $K_S \approx 4.3 \times 10^{-4}\ \mathrm{m^2\,s^{-1}}$). Above the interface, at the base of the thermo-halocline, the mixing regime returns to salt finger activity that is much stronger than at the deepest levels ($Tu \approx 87°$), yielding values up to $K_\theta \approx 5.4 \times 10^{-4}\ \mathrm{m^2\,s^{-1}}$ and $K_S \approx 6 \times 10^{-4}\ \mathrm{m^2\,s^{-1}}$ (Fig. 3.6d and Fig. 3.6e).

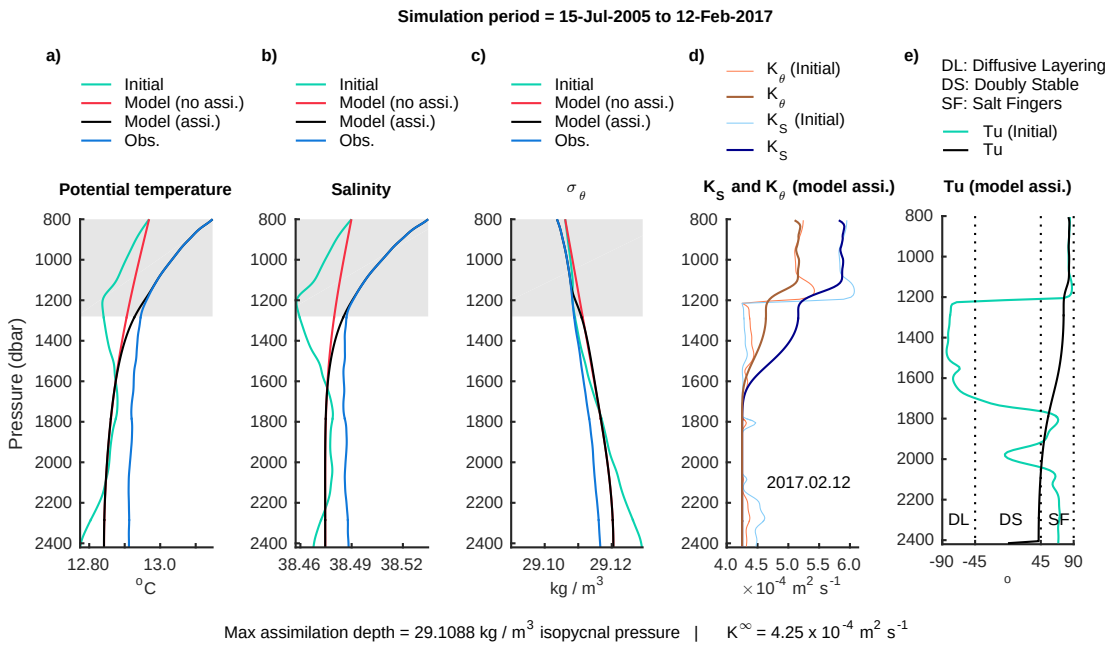

Figure 3.6. (a) θ profile evolution between July 2005 and February 2017 (800–2420 dbar). Initial profile (turquoise line) and observed (blue line), simulated without assimilation (red line) and simulated with assimilation (black line) profiles in February 2017. (b) Same as (a) but for S. (c) Same as (a) and (b) but for σ_θ. Shaded areas indicate the maximum assimilation pressure range during the simulation. (d) K_θ (brown line) and K_S (dark blue line) simulated profiles with assimilation in February 2017. K_θ (thin orange line) and K_S (thin light blue line) profiles corresponds to the July 2005 initial profile. (e) Turner angle profile in February 2017 simulated with assimilation (black line) and July 2005 initial profile (turquoise line). Dotted vertical lines delimit the three mixing regimes (see Ruddick 1983). To observe the complete simulation the reader is referred to Movie S2 in the supporting information at https://doi.org/10.1029/2019JC015094.

As the structures erode, transitions between the different water masses are subjected to weaker gradients and hence the intensity of double-diffusion below the interface decreases. By mid-2008, the transition region above nWMDW core reverses its θ gradient, halting diffusive layering. By the end of 2011, regions prone to double diffusion below 1600 dbar are no longer detected. As the profiles evolve and the WMT degrades, the influence of the salt fingers of the thermo-halocline deepens until reaching a maximum at about 1700 dbar by the end of the simulation. Strictly speaking, in 2017 there are areas prone to salt fingers down to 2000 dbar but salinity gradients are so weak that salt fingering instabilities cannot develop to effectively influence the eddy diffusion coefficients (Fig. 3.6d and Fig. 3.6e).

Differences between simulations (with and without assimilation) are subtle at the interface and the water masses beneath are degraded in the same fashion (Fig. 3.6). By 2011 only a cold-haline tongue is perceptible in the deepest part of the θ-S diagram as a remnant of the WMT (see Movie S2 in the supporting information at https://doi.org/10.1029/2019JC015094). At the end of the simulation in 2017 the WMT signature is barely perceptible; its erosion is practically complete (Fig. 3.6 and Fig. 3.7a).

After 12 years of simulation, a comparison between the modeled diffusive evolution and the observational record highlights a large deficit of heat and salt in the deep waters (Fig. 3.6a,b and Fig. 3.7). The origin of this deficit is irremediably water renewal, i.e. lateral advection. To evaluate the relative contribution of both terms (diffusive transference from the intermediate layers and lateral advection) to the evolution of heat (QC) and salt contents (SC) in the deep layers, budgets were calculated for the simulated time series and for the observed profiles below 1280 dbar (Fig. 3.7b and Fig. 3.7c).

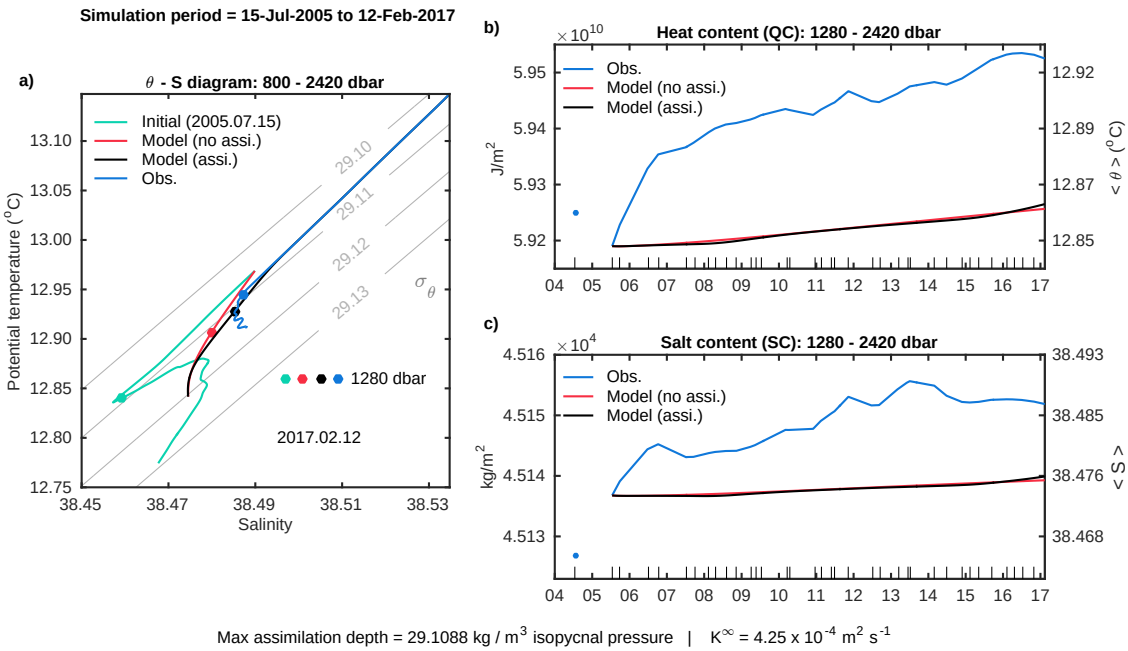

Figure 3.7. (a) θ-S diagram evolution between July 2005 and February 2017 (800–2420 dbar); initial profile (turquoise line) and modeled with assimilation (black line), modeled without assimilation (red line) and observed (blue line) profiles in February 2017. Dots indicate the maximum assimilation pressure (1280 dbar). Gray lines denote isopycnal levels (σ_θ). (b) QC evolution between July 2005 and February 2017 (1280–2420 dbar) in the model with assimilation (black line), in the model without assimilation (red line) and in the observed profiles (blue line). (c) Same as (b) but for SC. QC and SC in 2004 (1280-2420 dbar) are included in (b) and (c) for reference (blue dot). Thin vertical lines on the x-axis in (b) and (c) indicate the date of the CTD casts. Corresponding $<\theta>$ and $<S>$ changes of the layer were obtained as $\overline{\theta} = QC/(\overline{\rho}\overline{C_p}V)$ and $\overline{S} = SC/(\overline{\rho}V)$. $\overline{C_p} = 3926\ \mathrm{J\,kg^{-1}\,°C^{-1}}$, $\overline{\rho} = 1029\ \mathrm{kg\,m^{-3}}$ and $V = 1140\ \mathrm{m^3}$.

On the whole, QC and SC in the deep layers evolved similarly in both simulations (with and without assimilation), with slight differences due to the thermo-halocline assimilation. As the gradients of the deep regions weakened, transfer of heat and salt through the thermo-halocline expanded the extension of the salt fingering influence. Therefore, after 2008, as the thermohaline structure of the WMT faded from the θ-S diagram, QS and SC began to increase more rapidly (Fig. 3.7b and Fig. 3.7c)

QC and SC below 1280 dbar calculated from the observed profiles showed that, after the 2005–2006 large increase, the deep layers continued to gain heat and salt in a fairly progressive manner over time, showing swings attributed to injections of differentiated advected waters. Between 2005 and 2017, θ and S of the deep layers (below 1280 dbar) rose by 0.073°C and 0.013, respectively. This represents an increase in the QC and SC of 3.35×10^8 J m^{-2} and 15.10 kg m^{-2}. Heat uptake of this portion of the water column within the period was $\dot{Q} = 0.92$ W m^{-2}. The diffusive heat transfer from the thermo-halocline as estimated from the model runs was $\dot{Q} = 0.21$ W m^{-2}, i.e. 22%, leaving 78% to lateral advection. In the case of salt, 3.13 kg m^{-2} was transferred from the intermediate layers between 2005 and 2017, representing 21% of the observed increments. An estimate of the relative contribution of background diffusion and double diffusion to $\dot{Q}$ and $\dot{S}$ can be inferred from specific model runs evaluating separately both terms. If double diffusion is discarded, downward heat and salt fluxes are reduced by 8% and 21% respectively for the whole period. The greatest advective contribution of heat and salt occurred in the first years after the onset of the anomaly. Around half of the QC and SC was injected between 2005 and 2006. After such a period, the relative importance of the diffusive transference through the thermo-halocline to the heat and salt budgets of the deep layers increased to around 40%.

3.4.4 The 2005-2017 simulations. Re-starting runs by observations

In order to evaluate the inter-annual evolution of heat and salt advection, short-term simulations were carried out starting on the dates when the station was occupied (i.e. starting on the actual profiles that determine the smoothed fortnightly time series). After evolving by diffusion to the next actual observed profile, differences in QC and SC were estimated (Fig. 3.8) and grouped annually to obtain the time series of advected heat and salt budgets (Fig. 3.9). Due to the irregular sampling frequency, it was not possible to specify when advected water actually arrived between years and it was assumed a smooth progression between consecutive occupations. Root-mean-square error between the QC ($\mathrm{RMSE}_{QC} = 2.29 \times 10^7$ J m^{-2}) and SC ($\mathrm{RMSE}_{SC} = 2.5$ kg m^{-2}) computed from the smoothed time series and the actual observations may be considered an intrinsic error estimate for the observational record in terms of annually advected heat and salt and are included in Figure 3.9 as error bars (in gray) for reference.

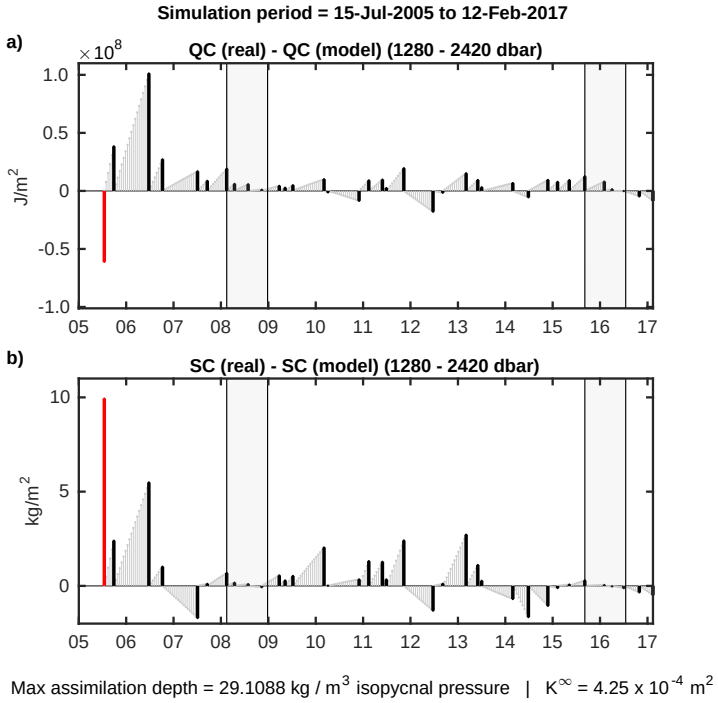

Figure 3.8. (a) QC differences between the observations and the model 2005–2017 (1280-2420 dbar) (gray bars). (b) SC differences between the observations and the model 2005–2017 (1280-2420 dbar) (gray bars). Black bars are the differences between the observations and the model at model runs re-start. The red bars in 2005 include the differences between 2004 and 2005. Highlighted boxes delimit the periods in which K^{∞} was estimated.

As expected, the best fit between observed and modeled heat-salt evolution is found in the periods previously regarded as diffusive and chosen to infer K^{∞} (highlited boxes in Figure. 3.8), especially in the case of salt. It is worth noting that the first markedly diffusive period starts on 15 February, 2008; and over 60% of annual heat advection in 2008 (Fig. 3.9b) occurred prior to this date.

To assess the changes caused by the advection of ventilated waters in the density structure, the average σ_θ and the potential energy deficit (Planque et al. 2006, de Boer et al. 2008) of the layer were computed, as well as the σ_θ at 2240 dbar (Fig. 3.9a).

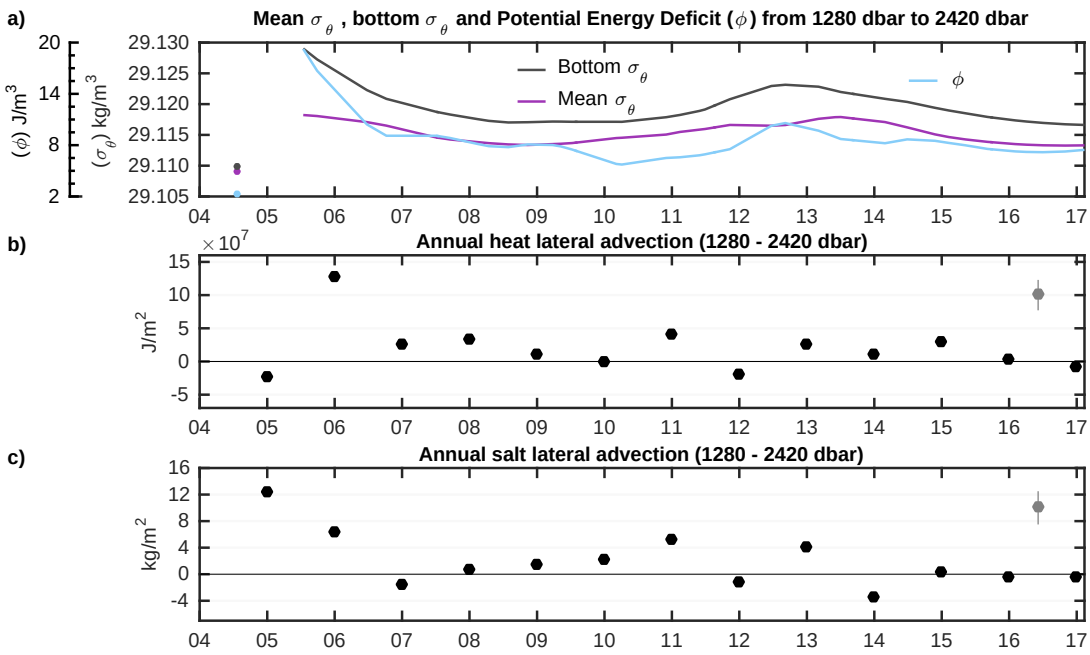

Figure 3.9. (a) Mean σ_θ (purple line), bottom σ_θ (black line) and potential energy deficit (ϕ) (blue line) evolution in the observed profiles 2005–2017 (1280-2420 dbar). 2004 values are included (purple, black and blue dots). (b) Annual heat lateral advection evolution 2005–2017 (1280-2420 dbar). (c) Annual salt lateral advection evolution 2005–2017 (1280-2420 dbar). Error bars are included in (b) and (c) (upper right corner, in gray) for reference (see Section 3.4.4).

3.5 Discussion

The existence of the Minorca hydrographic station regularly occupied since the WMT formation enables a detailed view of the evolution of the anomaly at a key site that complements our current knowledge of this event. The signature of yearly renewals of deep waters in the basin and their relevance in terms of heat and salt content evolution is discussed in this section. Moreover, we address how the formation and free evolution of a multi-layered structure with a sharp interface provides insights into the mixing behaviour of the deep waters.

3.5.1 Interannual contribution of lateral advection versus vertical diffusion

Assessment of diffusive heat and salt fluxes through the thermo-halocline provided by the model enables us to infer the contribution to the QC and SC of the deep waters due to lateral advection. These contributions provide information on the characteristics of the newly formed deep water

along its passage across the NE of Minorca toward the Algerian basin. In practice, if any of the locally observed properties (salt or heat) diverge from what would be consistent with purely diffusive evolution, advection of new waters should be present. Lack of such divergence may be assumed as indicative of the absence of advection, although strictly speaking this is not certain since arrival of waters with the same hydrographic signature would yield no signal. Estimates of deep-water formation rate and properties can be found in the bibliography from observational data and models. This enables us to understand the tracking of changes as seen at the Minorca station. The sequence is as follows.

From the inventory of annual heat and salt advective component (Fig. 3.9b and Fig. 3.9c), it was observed that the onset of the WMT in winter 2005 entailed the largest advective contribution to the salt content of the deep layers on record. In contrast, despite the nWMDW being markedly warmer than oWMDW, heat content below 1280 dbar was reduced in 2005 due to the presence of very cold cascading-origin waters (Canals et al. 2006, Font et al. 2007). The water column above the newly created interface also cooled due to the generalized uplift of the oWMDW (López-Jurado et al. 2005, Zunino et al. 2012). The cold-fresh cascading waters signature progressively vanished within a year, likely due to the combination of its erosion due to mixing and its continued advection toward the deepest part of the basin. The following year, 2006, nWMDW was again created and the formation area extended to the Ligurian Sea (Smith et al. 2008, Schroeder et al. 2008, Zunino et al. 2012, Somot et al. 2018) but cascading events were much less prominent (Fuda et al. 2009, Puig et al. 2013). Large amounts of heat and salt were incorporated into the water column in 2006 (Fig. 3.9b and Fig. 3.9c) in agreement with observations at the DYFAMED site (Schroeder et al. 2010).

No deep convective events were reported in the MEDOC formation area in the two following years, 2007 and 2008 (Houpert et al. 2016, Puig et al. 2013, Schroeder et al. 2013). Local balances at Minorca suggest salt loss in 2007 (below estimated uncertainty) and heat gain in 2007 and 2008, in the latter mostly gathered at the beginning of the year. We interpret this outcome as the progressive rearrangement of the water column after the two convective years 2005–2006. 2007–2008 evolution implied a reduction in density, i.e. consistent with leakage of denser (colder) water toward deeper areas of the basin.

In 2009 and 2010 deep-water formation events were reported in the GoL (Fuda et al. 2009, Houpert et al. 2016, Schroeder et al. 2013) as well as minor cascading events (Puig et al. 2013). The hindcast simulation of Somot et al. (2018) identified 2009 as strongly convective, but small advective contributions were detected off Minorca, especially in terms of salt (Fig. 3.9b and Fig. 3.9c). New thermohaline structures in the deep layers emerged in the GoL region in 2010 (Houpert et al. 2016, Puig et al. 2013) and by 2011 the signature in the Minorca station was prominent.

From 2011 to 2013, moderate to intense deep-water formation events were reported in the GoL (Durrieu de Madron et al. 2013, Houpert et al. 2016, Schroeder et al. 2013, Puig et al. 2013, Waldman et al. 2016). The record at Minorca shows that within the period 2011–2013 almost as much salt as in 2005 was incorporated into the deep layers. The 2012 case, a remarkably cold winter in the Mediterranean (Chiggiato et al. 2016, Durrieu de Madron et al. 2013, Houpert et al. 2016, Somot et al. 2018), is notable since it is the only one showing cooling+freshening signature. The newly formed WMDW along with the dense cascading water formed that year occupied the deepest part of the basin underlying the resident deep waters (Durrieu de Madron et al. 2013) thus causing the complete development of the m-shape in the θ-S diagram characteristic of the

2011–2013 convective period. Accordingly, 2012 shows a bottom density maximum and an increase in stratification of the deep layers that reflect the dense cascading signal and the appearance of such a complex structure. In 2013, an intense deep water formation event occurred again (Houpert et al. 2016, Waldman et al. 2016), but no cascading signal was detected. This event was subject of detailed observational and modeling studies presented in *Journal of Geophysical Research-Oceans* and *Journal of Geophysical Resarch-Atmospheres* special issues (Conan et al. 2018). After this period no further convective events were reported except for one of minor intensity in 2015 (Durrieu de Madron et al. 2017).

The years following 2013 revealed salt loss (2014) and heat gain (mostly 2015). This sequence partially resembles the post-convection stages after the WMT onset in 2005, despite the very different water column structures emerging after both events. A year with extreme cascading (2005 and 2012) was followed by a year with large deep convection but weaker or absent cascading (2006 and 2013). A year later, salt loss was observed (2007 and 2014) and further gain of heat followed next (early 2008 and 2015). Density dropped smoothly throughout the process (2005–2008; 2012–2015). The overall sequence is consistent with the arrival of signatures of newly formed waters at timescales within a year or less, followed by a more complex transient stage which involves further leakage of denser portions of the water column. The salinity drop in both cases – 2007 and 2014 – is mostly driven by sinking of the salinity minimum at the oWMDW-nWMDW interface. The last years of the series – 2016 and 2017 – showed a stable water configuration consistent with further diffusive erosion of the remnants of the structures.

Continuous tracking of changes at the Minorca station provides a complementary record that, being consistent with current knowledge of deep-water formation events, adds insights regarding transient post-convective stages and propagation timescales across the basin. Overall balance indicates that $\approx 80\%$ of the heat and salt injected into the water column disturbed by the WMT anomaly came from ventilation. It is worth noting that warming and salting through the thermo-halocline is not a process that ought to occur at a homogeneous rate across the basin. Indeed, studies of the diffusive evolution of the WMT anomaly in the Algerian basin (Bryden, Schroeder, Borghini, Vetrano & Sparnocchia 2014, Borghini et al. 2014) suggest that downward heat-salt fluxes along the local higher-gradient thermo-halocline may be comparable to episodic large injections of dense waters, i.e. diffusion would be much relevant than at our site. Neither are diffusive downward heat-salt fluxes homogeneous over time: saltier-warmer intermediate layers (LIW levels) since mid-2013 at the Minorca site yielded an increase in gradients of the thermo-halocline and consequently in downward heat-salt fluxes (Fig. 3.4a,b and Fig. 3.7b,c). These observations are consistent with the progressive increment of θ and S of the LIW overflowing the Sicily Channel since 2011 reported by Schroeder et al. (2017) and are of special interest since it may have important implications for the preconditioning of the water column in the GoL and therefore, for the new dense water formation.

3.5.2 Bulk changes in the deep Western Mediterranean: heat, salt and density

In a steady state ocean basin the downward diffusive transfer of heat and salt from the intermediate layers should be balanced by its removal through ventilation of the deep layers. The global ocean is currently out of equilibrium, gaining heat progressively for decades due to global warming (Cheng et al. 2019). During the early 21st century, the WMED has been markedly out of equilibrium, with

the injection of ventilated waters adding heat and salt to the deep layers (rather than removing them) at a much higher rate than the continuous diffusive transfer.

Robust warming and salinification trends in the WMED deep waters have been reported for the twentieth century (e.g. Vargas-Yáñez et al. 2010) and diverse explanations of such trends have been discussed including atmospheric patterns (Rixen et al. 2005), modified properties of the AW entering through the Strait of Gibraltar (Millot 2007) and changes in fresh water inputs due to river damming (Rohling & Bryden 1992). Trends of around 0.002 $^{\circ}\mathrm{C\,yr^{-1}}$ for temperature and 0.001 $\mathrm{yr^{-1}}$ for salinity in the deep layers of the WMDW for the 1950–2000 period are accepted estimates (Vargas-Yáñez et al. 2009). When the WMT is added to the long-term series, temperature trends double (0.004 $^{\circ}\mathrm{C\,yr^{-1}}$ (below 600 dbar), Vargas-Yáñez et al. 2017).

Although we rely on a single site time series, our trends are aligned with those of the overall WMED. Between 2004 and 2017 θ and S in the deep layers (1280–2420 dbar) off Minorca increased 0.059 °C and 0.021, respectively, from which 0.022 °C and 0.015 occurred during 2004–2006 through the onset of the WMT. This abrupt rise added the equivalent of previous decadal increments in just two years. Linear trends for the 2007–2017 period (i.e. after the event) are similar to the long-term background salt-increase (0.001 $\mathrm{yr^{-1}}$) but still higher for warming (0.003 $^{\circ}\mathrm{C\,yr^{-1}}$).

Therefore, the effect of the WMT on the bulk changes of temperature and salinity of the deep WMED is outstanding. Translated into energy uptake, the 1280–2420 dbar layer in Minorca warming rate of $\dot{Q} = 0.92\ \mathrm{W\,m^{-2}}$ (2005–2017) is more than two times that of the global intermediate ocean in the same period (0.4 $\mathrm{W\,m^{-2}}$, 700-2000 dbar, 2005–2016, Von Schuckmann et al. 2018). Such warming rate of the deep layers in the Western Mediterranean is even higher than the $\dot{Q} \lesssim 0.7\ \mathrm{W\,m^{-2}}$ estimated for the upper 2000 dbar in the global ocean in recent decades (Cheng et al. 2019, Von Schuckmann et al. 2018), indicating the relevance of the WMT as a case study of heat transfer into the deep ocean.

We have not considered so far the possible effect of geothermal heating on the evolution of the deep waters structure, however it is known to have a non-negligible contribution. Estimates of heat fluxes through the lithosphere in the WMED basin range between $\dot{Q} \approx 0.05\ \mathrm{W\,m^{-2}}$ (Hofmann & Morales Maqueda 2009) and $\dot{Q} \approx 0.1\ \mathrm{W\,m^{-2}}$ (Davies & Davies 2010), with slightly higher values for the more geothermally active Tyrrhenian basin. Mean geothermal flux for the Algero-Provencal basin taken in Ferron et al. (2017) is $\dot{Q} \approx 0.1\ \mathrm{W\,m^{-2}}$. This is about half of our estimation of downward diffusive heat flux during the 2005–2017 period. Geothermal heating was not included explicitly in the diffusion model since it is irregular in space and intermittent, so the inclusion of a fixed flux boundary condition at the seafloor would be arguable. Whatever the case, geothermal heating could account for up to 50% of the heat diffused from the intermediate layers into the deep waters. This extra heat coming across the seafloor should be removed from the budget assigned to lateral advection, i.e. roughly speaking $\dot{Q}$ would be shared as 0.6, 0.2 and 0.1 $\mathrm{W\,m^{-2}}$ for advection of ventilated waters, diffusion from the thermo-halocline and geothermal heating respectively.

In addition to heat and salt increments, substantial changes were recorded in the density structure and stratification of the deep waters off Minorca. The onset of the WMT caused an increase in the potential density of the deep layers in just one year, inducing a strong stratification beneath the base of the thermo-halocline (Fig. 3.3 and Fig. 3.9a). After 2005, stratification was rapidly reduced to increase again with the arrival of new convective waters in the 2011-2013 period. Over the last years, deep-water density stabilized above 2004 values. Deep waters therefore show a quick stratification increase after major deep-water production events, followed by smooth stratification

erosion afterward. Density and stratification of the deep waters play a major role in the formation rates of new deep waters, since they set the threshold for upper ocean densification. Deep water density levels higher than those pre-2005 hinder further deep-convection events. On the other hand, large periods when deep-water formation is absent will lighten the deep waters. Model projections suggest that the density of the deep waters formed in the WMED during the 21st century may be drastically reduced under a climate change scenario, leading to a sharp reduction in the formation rate of deep waters that penetrate below 1000 metres and consequently a weakening of the deep thermohaline circulation (Somot et al. 2006). Additionally, the recurrence of anomalous atmospheric patterns such as that of the extreme winter of 2005 is expected to increase due to global warming (Somavilla et al. 2016), so it seems likely that renewal of the deep WMED may be driven in the future by abrupt step-like shifts like the event that gave rise to the WMT.

3.5.3 Diffusive mixing of the WMT structure

Diffusive mixing was not dominant in the evolution of bulk QC and SC of the deep layers in Minorca, but it is a decisive agent in the overall evolution. Besides being the main driver in non-convective periods, its action erodes the transient signals by homogenizing the water column, thus causing stratification to decrease relatively quickly. Simulations indicate that the signature of the extraordinary injection of 2005, without considering subsequent convective events, would need only 15 years to completely fade from the θ-S plane due to diffusive mixing.

The creation of the anomalous structure of 2005, showing distinct layers prone to the development of salt-fingering and diffusive layering, enabled us to run specific simulations based on state-of-the-art parameterizations and to infer a best guess of the general background turbulent diffusion coefficient due to processes not related to double-diffusion phenomena (K^{∞}). The obtained value of $K^{\infty} = 4.25 \times 10^{-4}$ m^2 s^{-1} is an order of magnitude higher than those representative of the ocean interior (Zhang et al. 1998, Thorpe 2007) but comparable to those typical of the abyssal ocean, especially in areas near seamounts or steep continental slopes (Waterhouse et al. 2014). Previous observational studies in the Mediterranean showed large spatial variability ranging from $0.1 - 1 \times 10^{-4}$ m^2 s^{-1} for the deep waters in the abyssal plain between Sardinia and the Balearic Islands and much greater variability in certain areas such as the Ligurian Sea ($1 - 3 \times 10^{-4}$ m^2 s^{-1}), especially over the continental slope (Ferron et al. 2017). Cuypers et al. (2012) obtained estimated eddy diffusivity values ranging from $0.1 - 10 \times 10^{-4}$ m^2 s^{-1} in the WMED basin below 1500 dbar. Local K^{∞} is estimated here from two periods, with four observations each, in which the thermohaline evolution is consistent with small or negligible advective contributions. Nevertheless, as stated before, diffusion and advection are not decoupled in the actual 3-D ocean. The implicit premise is that within each of these periods, the water column is homogeneous within the spatial advective scale. Since this is an arguable assumption, our K^{∞} should be understood as a regional average which is in agreement with the upper limit of current estimates but is not necessarily as reliable as those emerging from specific ocean-mixing studies.

Treatment of double-diffusion processes considers specific terms to be added to an independent background K^{∞}. Using parameterizations from Zhang et al. (1998) and Zhang & Schmitt (2000), we found a satisfactory representation of the succession of mixing regimes and the asymmetries created in the mixing efficiency of heat and salt. Maximum transfer occurs at the base of the thermo-halocline, where the greatest salt fingering activity was detected. Mean $K_S = 5.8 \times$

10^{-4} $m^2\,s^{-1}$ derived in the thermo-halocline is similar to that estimated by Bryden, Schroeder, Borghini, Vetrano & Sparnocchia (2014) and Bryden, Schroeder, Sparnocchia, Borghini & Vetrano (2014) from profiles in the Algerian basin at the same water column levels, although our mean $K_\theta = 5.2 \times 10^{-4}$ $m^2\,s^{-1}$ is slightly higher.

An interesting feature within the WMT is the oWMDW-nWMDW interface at the base of the thermo-halocline since it allows us to follow the spatio-temporal evolution of the anomaly (Schroeder et al. 2008, 2016) and to study the convergent effects of two different mixing phenomena. Upward fluxes due to diffusive layering below the interface supplement the downward transference of salt and heat due to the salt fingers above, causing an increase in θ and S over time (Bryden, Schroeder, Borghini, Vetrano & Sparnocchia 2014). It is well known that diffusive layering is less effective than salt fingers in transferring heat and salt but the magnitude of the diffusive fluxes depends to a large extent on thermohaline gradients. Model runs indicate that for our WMT onset configuration the relative contribution of the diffusive layering to the evolution of salt in the interface during the first year of the anomaly represents up to 30%. By the end of 2008, diffusive layering was no longer operating effectively in the oWMDW-nWMDW region.

3.6 Conclusions

The onset of the WMT in 2005 created an unprecedented multi-layered hydrographic structure in the deep ocean. The existence of a repeated hydrographic station, sampling this structure at seasonal frequency, enabled its evolution to be tracked for over 10 years until its almost complete erosion. The thermohaline evolution of the deep waters was understood as the combination of background diffusive mixing and intermittent advective renewals. Following this approach, a 1-D diffusion model sensitive to double-diffusion was set up in order to reproduce the hydrographic record. The exercise enabled us to show the large-scale specificities of double diffusion using current parametrizations of salt fingering and diffusive layering processes, to infer a regional background diffusivity value, and to describe the properties of the newly formed waters midway along their track from the formation area to the deepest part of the basin.

Two convective periods (2005–2006 and 2011–2013) account for most of the heat and salt gain of the deep water. Remarkably, heat uptake in the deep layers in the early 21st century period exceeds the estimated warming rate of the upper 2000 dbar in the global ocean in the same period. After 12 years of evolution, the WMT hydrographic signature had been effectively eroded by the combined effect of the successive injections of dense waters and the diffusive mixing of their properties, yielding markedly warmer, saltier and slightly denser deep water than that present in the profiles prior to 2005. This may have a substantial impact on WMDW ventilation since the newly formed deep waters currently need to overcome a higher density threshold in order to penetrate to the deepest levels.

This study complements current knowledge of the WMT climatic event, as well as giving new insights into the mixing dynamics in the WMED interior. The dataset and results presented here can be a useful tool to validate numerical simulations of deep-water formation. The importance of maintaining and expanding deep-water observatories such as the RADMED deep station in Minorca under a global change scenario should be highlighted. Finally, it is worth stressing the unique opportunity afforded by the formation of a well-defined interface in the deep ocean so as to understand the diffusive evolution in the ocean interior.

Acknowledgments

This work was supported by the ATHAPOC project (CTM2014-54374-R), funded by *Plan Nacional I+D+I* and by the RADMED project, funded by the IEO. S. Piñeiro acknowledges the pre-doctoral FPI Fellowship (BES-2015-074316) support from the Spanish Ministry of Science, Innovation and Universities (MICINN), co-funded by the European Social Fund. The authors would like to thank the fieldwork and effort made by all the personnel involved in the RADMED surveys and especially M. Serra and J. L. López-Jurado. The authors are very grateful to the entire ATHAPOC group for their fruitful comments during the development of this work. Some of the instruments used during the cruises were made available by the Balearic Islands Coastal Observing and Forecasting System (ICTS-SOCIB); the Mediterranean Institute for Advanced Studies (IMEDEA CSIC-UIB) and the University of the Balearic Islands (UIB). The DoWEX experiment (https://doi.org/10.17600/12450170), part of the MERMEX program, and the BLUEFIN TUNA project, an ICTS-SOCIB and IEO joint research initiative, occupied the Minorca deep station in support of the RADMED monitoring program in 2012 and 2014, respectively. All the CTD casts used in this work can be accessed upon request at the SeaDataNet repository (www.seadatanet.org).

Chapter 4

Persistent, depth-intensified mixing during the Western Mediterranean Transition's initial stages

---

This chapter has been published as:

Piñeiro, S., González-Pola, C., Fernández-Díaz, J. M., Naveira-Garabato, A. C., Sánchez-Leal, R., Puig, P., Salat, J., and Balbin, R. (2021). Persistent, depth-intensified mixing during the Western Mediterranean Transition's initial stages. *Journal of Geophysical Research: Oceans*, 126 (2), e2020JC016535. https://doi.org/10.1029/2020JC016535.

Within this chapter, an animation (Movie S1) is referred to as supplementary information. This file can be accessed at: https://doi.org/10.1029/2020JC016535.

Keypoints

- A rapid erosion of bottom water thermohaline signatures was observed off Minorca Island during the WMT's initial stages
- Local evolution of the WMT deep hydrographic structure during 2005-2007 is consistent with persistent intense mixing
- Evidence that intense mixing occurs at the continental slope and mixed waters are exported offshore is found

Abstract

Major deep-convection activity in the northwestern Mediterranean during winter 2005 triggered the formation of a complex anomalous deep-water structure that substantially modified the properties of the WMED deep layers. Since then, evolution of this thermohaline structure, the so-called WMT, has been traced through a regularly sampled hydrographic deep station located on the outer continental slope of Minorca Island. A rapid erosion of the WMT's near-bottom thermohaline signal was observed during 2005-2007. The plausible interpretation of this as local bottom-intensified mixing motivates this study. Here, the evolution of the WMT structure through 2005-2007 is reproduced by means of a 1-D diffusion model including double-diffusive mixing that allows vertical variation of the background mixing coefficient and includes a source term to represent the lateral advection of deep-water injections from the convection area. Using an optimization algorithm, a best guess for the depth-dependent background mixing coefficient is obtained for the study period. WMT evolution during its initial stages is satisfactorily reproduced using this simple conceptual model, indicating that strong depth-intensified mixing ($K^{\infty}(z) \approx 22 \times 10^{-4}$ m^2 s^{-1}; $z \gtrapprox 1400$ dbar) is a valid explanation for the observations. Extensive hydrographic and current observations gathered over the continental slope of Minorca during winter 2018, the first deep-convective winter intensively sampled in the region, provide evidence of topography-localized enhanced mixing concurrent with newly-formed dense waters flowing along-slope toward the Algerian sub-basin. This transport-related boundary mixing mechanism is suggested to be a plausible source of the water-mass transformations observed during the initial stages of the WMT off Minorca.

4.1 Introduction

Since winter of 2005, the original WMT signal has been eroded by diffusive mixing and subsequent instances of deep-water renewal, resulting in a denser, warmer, saltier and more stratified deep water (relative to that present before 2005) that currently (as of 2021) fills the deepest layers of the WMED. The long-term thermohaline evolution of the deep layers during the WMT was tracked by means of a seasonally occupied deep hydrographic station located in the outer continental slope of Minorca Island (Figure 4.1), analysed in detail by Piñeiro et al. (2019) (Chapter 3). This comprehensive dataset enabled the study of deep-ocean mixing dynamics and their impact on the large-scale thermohaline evolution of the regional water masses. A remarkable feature of the WMT hydrographic structure evolution shown by Piñeiro et al. (2019) (Chapter 3) was the rapid

erosion of the cWMDW-nWMDW portion of the water column during 2005-2007, concurrent with a prominent increase in the θ-S maximum associated with the nWMDW core (Figure 4.2).

During the winter of 2006 (the following winter after the WMT onset), the deep-water formation area of the WMED was extended to the Ligurian Sea (Smith et al. 2008), and anomalous dense waters were formed again (Schroeder et al. 2008) with a much less relevant contribution of cascading waters (Fuda et al. 2009, Puig et al. 2013, Schroeder et al. 2013). No deep convection was reported in the two following winters (2007-2008; Houpert et al. 2016, Puig et al. 2013, Schroeder et al. 2013, Somot et al. 2018). The observed rapid erosion of the cWMDW-nWMDW water column structure during 2005-2007 may thus be indicative of enhanced near-bottom mixing.

Our goal in this work is to establish whether the observed evolution of the WMT hydrographic structure in the Minorca deep station during 2005-2007 is indeed consistent with increased mixing near the seafloor, combined with the advection of warmer and saltier waters at shallower levels. To evaluate this hypothesis, we set up a 1-D diffusion model including double-diffusive mixing schemes that incorporates (i) a source term to represent the lateral advection of newly-formed dense waters under simple and realistic assumptions, and (ii) a depth-dependent vertical mixing coefficient that can be tuned so the simulated evolution of hydrographic structure may resemble the overall observed evolution.

The outcomes of our analysis are discussed by reference to the local changes in density structure and circulation measured during a much less dramatic, albeit intensively sampled, deep convective period in winter 2018. Since no extensive regional observations during the WMT initial stages are available, these measurements enable us to explore the impinging of newly-formed deep waters on the continental slope of Minorca and deep-ocean mixing dynamics during post-convective periods. The dataset entails two high-resolution CTD sections in the NE flank of the continental slope of Minorca occupied in 2017-2018, and a three current meter mooring deployed in the outer part of the slope during 2015-2018.

The chapter is organized as follows. Datasets used in this study, the 2005-2007 observations and the working hypotheses are presented in Section 4.2. Section 4.3 describes the 1-D diffusion model setup, the spatio-temporal configuration of the advective term, and the mixing coefficient profile optimization procedure. Section 4.4 explicitly presents the configuration of the experiments. In Section 4.5, results are reported, to be subsequently discussed in Section 4.6. Final considerations and conclusions are gathered in Section 4.7.

4.2 Observational record and initial hypotheses

4.2.1 The Minorca time series

Since this study focuses on the thermohaline evolution of the deep waters as observed in the Minorca deep station (red vertical line in Figure 4.1b) during the 2005-2007 period, we consider as our observational record for the study period a subset (15 July 2005 - 06 January 2007) of the fortnightly hydrographic time series used in Piñeiro et al. (2019) (Chapter 3). These time series were constructed by spatio-temporally smoothing of the raw profiles of the Minorca deep station during 2005-2017 in order to filter natural noise and to obtain a reasonably smooth, continuous evolution

of the hydrographic profiles which can be compared with the theoretical evolution obtained from the 1-D model (Chapter 3; see the animation, Movie S1, included as supporting information in Piñeiro et al. (2019) – https://doi.org/10.1029/2019JC015094 – to observe a comparison between smoothed and raw profiles).

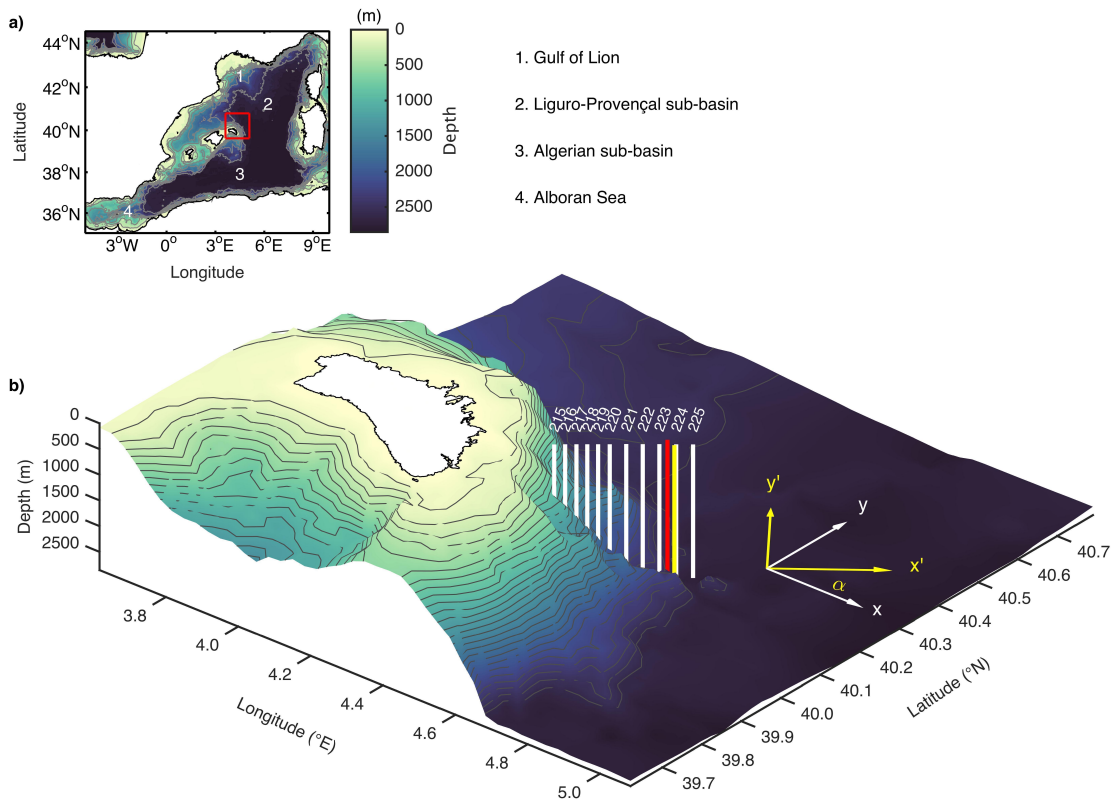

Figure 4.1. (a) Location of the study area (red square). (b) 3D perspective of the bathymetry in the study area and location of the Minorca deep station (vertical red line), the ATHAPOC section stations (vertical whites lines) and the ATHAPOC mooring (yellow vertical line). North-South (y), East-West (x), along-slope (y') and cross-slope (x') axes are included for reference. The x' and y' axes are rotated 38°(α) counterclockwise relative to x and y.

4.2.2 The ATHAPOC CTD section and mooring

Unfortunately, the initial occupations of the Minorca deep station during the WMT onset period did not include extensive regional, synoptic observations. Instead, the cross-slope oceanographic section (white vertical lines in Figure 4.1b) carried out in November 2017 and February 2018 (which was also a deep convective period, but much weaker than that in 2005) under the auspices of the ATHAPOC project (see Section 2.3.2), provides insight into the impact of deep-water formation on the local hydrographic structure across the continental slope, which cannot be obtained from a single hydrographic station such as the Minorca deep station.

Additionally, information on the local circulation patterns of the deep waters over the continental slope of Minorca and changes due to the arrival of newly-formed dense waters in winter 2018 are provided by the ATHAPOC deep mooring (yellow vertical line in Figure 4.1b), equipped with 3 single-point current meters at 1000, 1600 and 2500 dbar (see Section 2.3.1).

4.2.3 Bottom-intensified mixing in 2005-2007: direct evidence and working hypotheses

Visual inspection of the evolution of the deep hydrographic profiles between 2005 and 2007 in the Minorca deep station readily reveals the plausibility of the assumption that motivates this study and generates the working hypotheses.

The remarkable thermohaline structure that emerged in the WMED deep layers as a result of deep convection in the winter of 2005, and its annual evolution during the two following years, is shown in Figure 4.2. Beneath the intermediate layers, occupied by the markedly salty and warm LIW ($300 - 600$ dbar), the smoothly stratified thermo-halocline, within which θ and S decrease with depth, extends toward the fresher and colder oWMDW, which historically occupied the deepest part of the basin. The intrusion of the anomalous WMT dense waters triggered the uplift of the resident deep waters by hundreds of meters and the appearance of the sharp transition around 1200 dbar, between the oWMDW and the new deep waters (the salty-warm nWMDW and the fresher-colder cWMDW at the bottom). Subsequent profiles in Figure 4.2 reveal the above-mentioned (i) increase of the θ-S maxima associated with the nWMDW over the 2005-2007 period, and (ii) the significant cWMDW signal erosion.

The rapid fading of the cascading waters in the θ-S plane is still noticeable up to late 2007. Nevertheless, as argued in Piñeiro et al. (2019) (Chapter 3), observed changes in the water column during 2007 were strongly dominated by large heave of isopycnals (Bindoff & McDougall 1994) throughout the water column, preventing a description based on our conceptual model based on vertical diffusion and a localized source term. Consequently, the analysis period in this study had to be curtailed to before January 2007. This constraint is addressed in detail in the Discussion (Section 4.6.1.3).

As stated before, this study focuses on reproducing the thermohaline evolution of the WMED deep waters during the two years following the onset of the WMT as observed in the Minorca deep station, in order to determine whether the erosion of the cWMDW-nWMDW portion signal may be explained by bottom-intensified mixing.

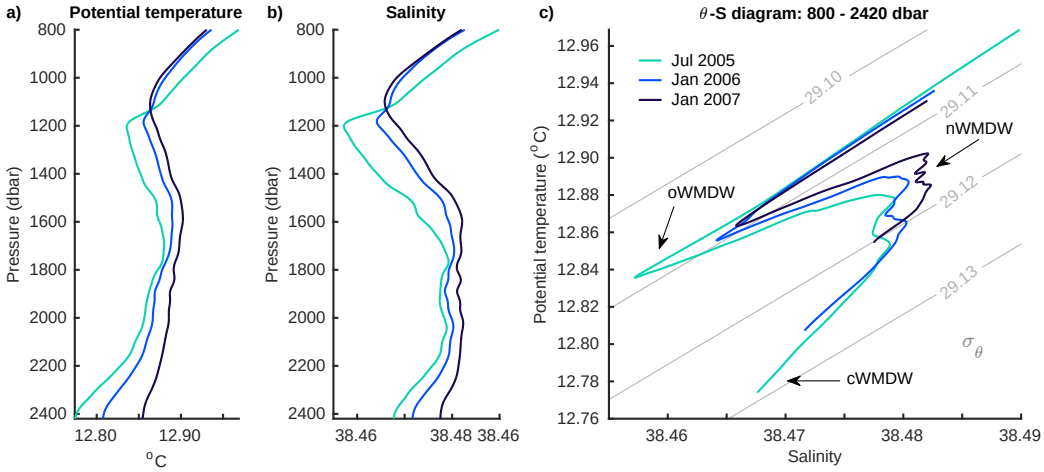

Figure 4.2. (a) Observed θ profile in July 2005 (turquoise line), January 2006 (blue line) and January 2007 (dark blue line) between $800 - 2420$ dbar at the Minorca deep station. (b) Same as (a) but for S. (c) Same as (a) and (b) but for θ-S. Gray lines denote isopycnal levels (σ_θ).

Two hypotheses may be put forward to explain the observed evolution of the cascading waters in the 2005-2007 period:

(I) The erosion of the cWMDW-nWMDW segment simply responds to lateral advection of heat and salt within the nWMDW density class, leading to an increase of vertical thermohaline gradients and, consequently, of the downward fluxes of heat and salt toward the deepest layers. In this scenario, no vertical structure in the mixing coefficient needs to be invoked.

(II) Lateral advection of heat and salt in the nWMDW class fails to reproduce the observations if a constant mixing coefficient is assumed for the entire water column, such that it is mandatory to model thermohaline evolution with a depth-dependent mixing coefficient in order to match the observations. This would indicate that the rapid erosion of the cascading waters could have been effected by the presence of near-bottom turbulent mixing elevated above background levels.

It is important to note that other combinations can be invoked to explain the observed thermohaline evolution. In particular, drainage of the thermohaline structures cannot be dismissed (i.e. cascading waters leaking from the sampling site toward deeper parts of the basin). Since this study relies on a single hydrographic station, a spatial description is not possible. Nevertheless, this issue will be discussed in depth on the basis of the available knowledge of the post-convective response within the basin.

4.3 Methodology

To analyze the observed thermohaline evolution of the water column, the 1-D diffusion model described by Piñeiro et al. (2019) (Chapter 3) is used as the starting point. This model provides a theoretical description of the evolution of the θ-S profiles when subject to diapycnal mixing,

including double-diffusive mixing schemes. To represent the lateral advection of dense waters formed in the winters of 2005 and 2006, a heat-salt source term is added (the design of this advective term is described in Section 4.3.1). Finally, the background turbulent mixing coefficient is allowed to vary with depth ($K^{\infty} \equiv K^{\infty}(z)$), so an optimization algorithm is devised to minimize differences between the simulation and the observations while preserving overall consistency (Section 4.3.3).

4.3.1 Lateral advection of heat and salt

In order to simulate the increases in θ and S within the nWMDW core induced by the 2005-2006 injections, bulk changes of these tracers in the 2005-2007 period are computed beneath the base of the thermo-halocline (1300 dbar). This level is chosen to avoid the oWMDW-nWMDW interface region, which oscillates above $\sim$ 1200 dbar and is strongly influenced by a downward diffusive heat-salt transfer from intermediate layers. The spatio-temporal structure of the advective source is unknown, so assumptions must necessarily be made.

As regards the vertical (z) distribution of lateral advection, the simplest approach would be to distribute the increases in θ and S homogeneously across a layer of the water column. This option is, however, unrealistic, as newly-formed dense waters mix vertically while advected, and also poses computational problems at the boundaries. Since the relative maximum associated with the nWMDW core increases prominently throughout the period, and lacking further information on the shape of the injected anomaly, a Gaussian shape centered at the nWMDW core is a convenient option to represent in a simple fashion the core's erosion as it extends horizontally throughout the basin. With this choice, continuity in the θ-S gradients is then guaranteed. A caveat, which will be addressed below, is that independent injections of heat and salt should not create vertical instabilities, such that further fine-tuning of the source distributions is required.

Assumptions regarding the injection rates of heat and salt into the nWMDW class are also needed. The observational record indicates a smooth increase of θ and S values at the nWMDW core, whereas the physical setting of the process suggests that the two independent convective events in 2005 and 2006 may have provided two distinct advective inputs. Whether the arrival of source waters at the sampling site is actually progressive (i.e. oceanographic processes blur the distinct signatures of the two consecutive deep convection events) or our available observational record is insufficient to disentangle these, cannot be appraised. Therefore, the simplest approach is to add the heat-salt advective column as a decreasing curve throughout the 2005-2007 period, and a more elaborate strategy would be to include the distinct advective pulses (simulating the remnants of the 2005 injection and the following one in 2006) . Both of these approaches are analyzed in the simulations in order to explore the robustness of the $K^{\infty}(z)$ profile optimization.

4.3.2 Diapycnal mixing parameterization

As the discrete intrusions of the newly-formed dense waters in 2005-2006 distorted the original WMT structure observed in July 2005, continuous diapycnal mixing eroded the emergent thermohaline signals and weakened vertical gradients. Turbulent heat-salt fluxes are commonly parameterized following Fick's diffusion equation ($\frac{\partial c}{\partial t} = \frac{\partial}{\partial z}\left(K_c(z)\frac{\partial c}{\partial z}\right)$), which can be used to estimate the vertical evolution of the thermohaline tracers (c) over time (t). The rate of mixing is represented

by the eddy diffusion coefficient ($K_c(z)$; Klymak & Nash 2009), usually assumed to be the same for all scalars (θ and S; e.g. Jayne 2009). Nevertheless, asymmetries between $K_\theta(z)$ and $K_S(z)$ can arise under specific thermohaline configurations of the water column, as a result of the different molecular diffusivities of heat and salt. Portions of the water column prone to developing both forms of these so-called double-diffusive mixing regimes (Kelley et al. 2003, Radko 2013, Schmitt 2009), i.e. salt fingering and diffusive layering, have been identified throughout the WMT structure (Bryden, Schroeder, Borghini, Vetrano & Sparnocchia 2014, Piñeiro et al. 2019, Chapter 3).

Thus, to simulate the evolution of the θ and S profiles effected by diapycnal mixing as the lateral advection of dense waters occurs, the 1-D diffusion model sensitive to double-diffusive mixing phenomena described in Piñeiro et al. (2019) (Chapter 3) was adopted. This model vertically integrates the diffusion equation using $K_c(z)$ parameterizations to represent the asymmetries of vertical heat-salt fluxes under double-diffusive and non-double-diffusive mixing regimes. The setting and treatment of advection-diffusion are summarized below. As stated before, the detailed description of the numerical model is provided by Piñeiro et al. (2019) (Chapter 3).

The spatial domain of the one-dimensional (in z) model is discretized onto a regular vertical grid ranging from depths of 800 to 2420 m with a resolution of $\delta z = 10$ meters. Using the 15 July 2005 θ-S observed profile as initial condition, at each temporal step ($\delta t = 2.4$ h), the corresponding percentage of the advective column of each tracer (c) is added following the different advective evolution rates, and the mixing regimes throughout the water column are identified by means of a Turner angle analysis (Ruddick 1983). The 1-D diffusion equation is then solved numerically for θ and S using a Crank-Nicolson scheme (Crank & Nicolson 1947).

The diffusion model is closed by a Neumann boundary condition at the seafloor ($\partial c/\partial z = 0$ at $z = 2420$ m) and by an assimilation scheme at the upper boundary. This time-varying boundary condition is determined by the observed vertical gradients of θ and S in the thermo-halocline, which in turn modulate changes in the vertical heat-salt fluxes toward the deep layers. Data assimilation operates from the upper limit of the vertical domain up to an isopycnal level (29.1088 kg m^{-3}) close to and above the oWMDW-nWMDW interface selected by visual inspection of the hydrographic time series, in order to avoid altering the WMT structure; therefore, θ-S values in the thermo-halocline relax toward observations at these levels. Beneath this region, θ and S evolve as a combination of the lateral advection of heat and salt and the continuous erosion of the thermohaline structure by diapycnal mixing.

$K_c(z)$ within the model is estimated throughout the water column independently for θ and S, using the parameterizations of Zhang et al. (1998), Zhang & Schmitt (2000), which evaluate the mixing rate as an independent contribution of double diffusion in the regions prone to developing these instabilities ($K_c^{dd}(z)$), and added a constant turbulent background mixing coefficient (K^∞) for the entire water column (i.e. $K_c(z) = \left[K_c^{dd}(z) + K^\infty\right]$). Contributions from salt fingering and diffusive layering regimes are estimated from the thermohaline gradients according to the parameterizations of Schmitt (1981) and Kelley (1984, 1990). Piñeiro et al. (2019) (Chapter 3) inferred a depth-independent $K^\infty = 4.25 \times 10^{-4}$ m^2 s^{-1} from observations between 2005 and 2017. This coefficient was understood as a regional estimate representative of the average background mechanical mixing levels in the water column off Minorca. The novel additions to the model in this study are the source term at the nWMDW core and the optimization scheme to obtain a best guess of $K^\infty(z)$ for the 2005-2007 period.

4.3.3 K^∞ local optimization

Once the inclusion of the advective term is defined in z and t, we may evaluate whether the observed thermohaline evolution is compatible with a bottom intensification of the mixing coefficient, by optimizing a depth-dependent $K^\infty(z)$. We represent a theoretical two-layer structure of $K^\infty(z)$, as might be expected from a bottom intensification of the mixing coefficient, through a hyperbolic-tangent idealized target functional shape. This permits representation of the magnitude, location and steepness of the change in mixing coefficient with depth, i.e.:

$$K^\infty(z) = K_b^\infty + 0.5\, c_1 \left(\tanh\left(\frac{z - c_3}{c_2} \right) + 1 \right), \tag{4.1}$$

where $K_b^\infty = 4.25 \times 10^{-4}\ \mathrm{m^2\,s^{-1}}$ is the constant background mixing coefficient, c_1 is the maximum increment over K_b^∞, c_3 is the center of the hyperbolic tangent, and c_2 refers to the slope at c_3, since it sets the thickness of the transition region between the two layers. The factor of 0.5 forces c_1 to be the maximum increment over K_b^∞.

To find the parameters of the $K^\infty(z)$ profile that minimize differences between the model and the observations, a combined θ-S normalized root-mean-squared error is defined:

$$\mathrm{RMSE}_{\theta S}^{nor} = (1-\eta) \sum_{i=1}^{n} \frac{(\theta_i^{\mathrm{mod}} - \theta_i^{\mathrm{obs}})^2}{s_\theta^2} + \eta \sum_{i=1}^{n} \frac{(S_i^{\mathrm{mod}} - S_i^{\mathrm{obs}})^2}{s_S^2}, \tag{4.2}$$

where n is the number of vertical levels considered, θ_i^{mod} and S_i^{mod} are the simulated θ and S values for each depth (z_i), s_θ and s_S are the respective standard deviations of both tracers in the observations (θ_i^{obs} and S_i^{obs}) for a sample of size n (serving as scaling factors accounting for the different variation ranges of both variables in the water column), and η controls the weight of each tracer in the fitting. Here, θ and S are fitted giving equal weight to both, so $\eta = 0.5$ is adopted.

Then, (4.2) can be minimized numerically by using a Differential Evolution (DE) global optimization algorithm (Feoktistov 2006, Chakraborty 2008) that seeks solutions based on linear combinations of the three hyperbolic function (4.1) parameters. Note that the constant-K^∞ profile is a particular case in equation (4.1) with $c_1 = 0$. Details concerning the algorithm function minimization procedure and the numerical parameters used in this study can be found in the Appendix B.

4.4 Simulations setup

Before presenting the results of the complete simulations, it is necessary to precisely define the model setup of the experiments that address the targeted process. Since model outcomes, results and refined model runs are strongly interrelated, this section shares characteristics between Methodology and Results.

4.4.1 Source water term

Differences in the heat and salt contents below 1300 dbar between July 2005 and January 2007 indicate that as much as 1.648×10^8 J m^{-2} and 7.494 kg m^{-2} were respectively injected in the deep layers as a result of the 2005-2006 convective events. To include these heat and salt inputs in the simulation, θ-S bulk changes are used to construct the advective water column (Figure 4.3a). This is done following a Gaussian-shaped distribution, with most of the heat and salt placed in the vicinity of the nWMDW core around 1800 dbar, whose θ-S maximum increased significantly over the 2005-2007 period. Upper and lower limits of the source term are set at 1400 dbar and 2200 dbar, 400 dbar above and below the nWMDW core and spanning the portion of the water column occupied by this deep water mass while preserving the cWMDW-nWMDW mixing line. Within these water column segments, the remaining heat and salt are allocated following the tails of the Gaussian distribution, i.e. diminishing with increasing vertical distance from the core.

Since the evolution of θ and S is considered separately within the model, assuming a theoretical functional shape for the independent advection of both heat and salt requires the resulting advective column to be stable, so that spurious vertical instabilities are not generated that would prevent the diffusive scheme from correctly solving the tracer evolution. Thus, fitting one of the tracers to a Gaussian curve to generate the advective column implies that the distribution of the remaining tracer is constrained by the equation of state. Whereas 100% of the salt is assigned following a Gaussian curve, only 90% of the heat can be normally distributed without generating density inversions. The remaining heat has to be allocated carefully throughout the advective column in order to ensure that stability is preserved. This is performed by successively adding heat (following a Gaussian-shaped distribution) to specific segments of the advective column, selected and recursively smoothed in such a way so that the column remains statically stable. The ensuing distortion of the heat source term can be observed in Figure 4.3a.

Figure 4.3 shows the observed θ-S profiles in July 2005, January 2007 and the combination of the former plus the advective term that is introduced in the simulation over time. As expected, the source water core ($\theta = 12.950$ °C, $S = 38.494$, $\sigma_\theta = 29.113$ kg m^{-3}) is located on the isopycnal levels on which the nWMDW evolved, forming a mixing triangle between the three deep water masses with small perturbations around the mixing lines.

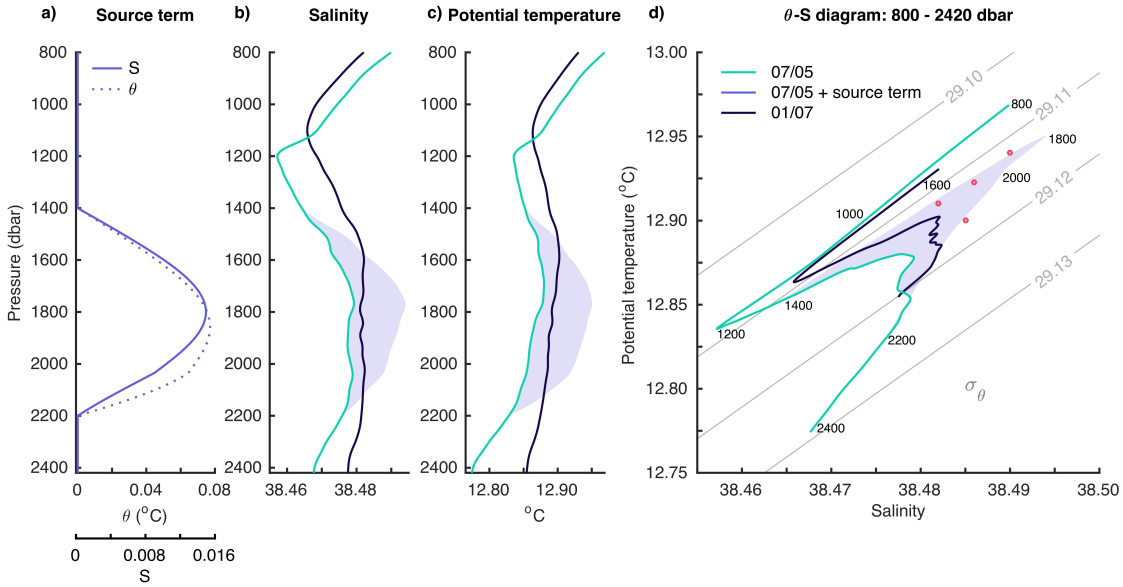

Figure 4.3. (a) S (purple solid line) and θ (purple dotted line) source terms. (b) Observed S profiles in July 2005 (turquoise line), in July 2005 plus the S source term (combined turquoise-shaded purple area), and in January 2007 (dark blue line). (c) Same as (b) but for θ. (d) Same as (b) and (c) but for θ-S. Gray lines denote isopycnal levels (σ_θ). Red dots refer to reported observations of the nWMDW properties in 2006 in the GoL and Ligurian Sea (Smith et al. 2008, Somot et al. 2018, Puig et al. 2013, 2009). Pressure levels corresponding to the July 2005 profile plus the source term profile are included for reference. Note that the source terms are not completely injected at the start of the simulation, but added progressively.

The percentage of the advective column that is included in each δt in the simulation varies over time. Figure 4.4 shows the evolution of the heat-salt input rates under the three assumptions used to represent the arrival of the distinct 2005-2006 injections, which will enable us to test the robustness of the $K^{\infty}(z)$ profile estimation. In all three approaches, a smoothly decreasing curve (Simulation 1) and a double Gaussian shape giving equal weight to each pulse centered on different times (Simulations 2 and 3), lateral advection is restricted to the first year of simulation, adhering to a reasonable spreading time of the newly formed deep waters toward our site. That is, 90% of the heat and salt input is already included in the model by mid-summer 2006, so that the thermohaline evolution of the water column after that time is affected mainly by diffusive mixing processes.

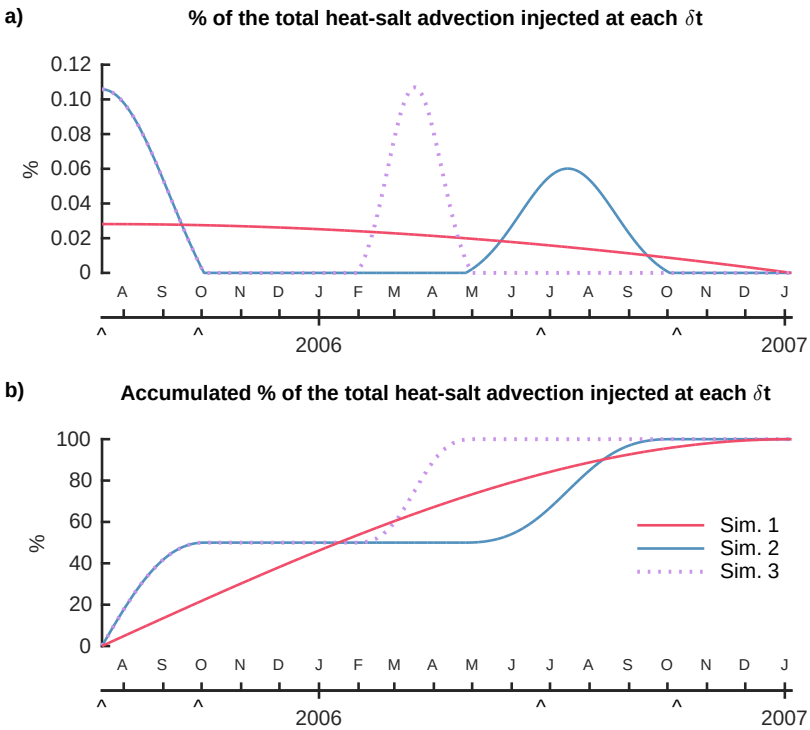

Figure 4.4. (a) Percentage of the total source term included in the simulation in each temporal step. (b) Accumulated percentage of the source term included in the simulation over time. Vertical arrow tips in the time axes of (a) and (b) indicate the dates in which the Minorca deep station was occupied.

4.4.2 Vertical structure of the mixing rate

Figure 4.5 shows the $K^{\infty}(z)$ profiles optimized by the DE algorithm for the 2005-2007 period under the parameterizations used for lateral advection and diffusive mixing in the model. Following the first imposed condition on the advective input rate (i.e. smoothly decreasing over time; Simulation 1) and giving equal weight to both tracers, minimum errors $\mathrm{RMSE}_{\theta} = 0.004$ °C and $\mathrm{RMSE}_{S} = 0.001$ are obtained with $c_1 = 17.84 \times 10^{-4}$ m^2 s^{-1}, $c_2 = 35$ m and $c_3 = 1446$ m after 300 simulations within the evolutionary algorithm. The resulting $K^{\infty}(z)$ profile shows a prominent increase in the mixing coefficient by about five-fold over the background value, not only within the cWMDW-nWMDW portion but over a thick layer that extends 1000 dbar above the bottom, coinciding with the upper limit of the source term at 1400 dbar. The transition between the two layers occurs abruptly in a few tens of meters. Following the advective Gaussian-shaped two-pulse distributions (Simulations 2 and 3) similar minimum errors and hyperbolic function parameters are obtained, replicating the $K^{\infty}(z)$ vertical structure optimized for Simulation 1. Thus, $K^{\infty}(z)$ exhibits little sensitivity to the temporal distribution of the advective pulses. In broad terms, $K^{\infty}(z) \in (19 \times 10^{-4}$ m^2 s$^{-1}, 23 \times 10^{-4}$ m^2 s$^{-1})$ below 1400 dbar is consistent with reasonable variations in the temporal distribution of lateral advection over the 2005-2007 period. The improvement achieved in the simulations including vertical-varying $K^{\infty}(z)$ instead of the constant-K^{∞} profile is described

in the following section.

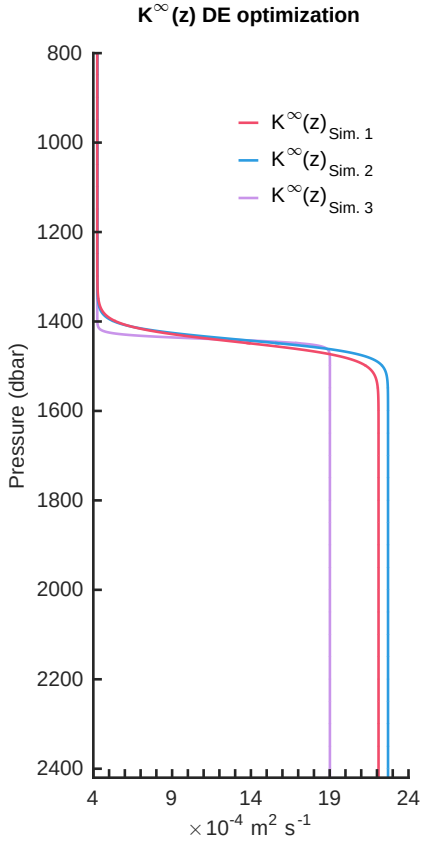

Figure 4.5. Optimized $K^{\infty}(z)$ profiles for Simulation 1 (red line), Simulation 2 (blue line) and Simulation 3 (purple line).

4.5 Results

4.5.1 Simulated 2005-2007 θ-S profile evolution

In order to evaluate the realism of the modeled thermohaline evolution under the different assumptions regarding advection and their corresponding optimized $K^{\infty}(z)$ profiles, the outputs of the 540-day simulations are compared with the fortnightly observational set.

For the Simulation 1 (Figure 4.6 and Movie S1 in supporting information at https://doi.org/10.1029/2020JC016535), advection rate is set to smoothly decrease and the corresponding optimized $K^{\infty}(z)$ profile is used (Simulation 1 in Figure 4.4 and Figure 4.5). The

initial Turner angle profile indicates an intricate succession of mixing regimes in the deep layers (Figure 4.6d). As the lateral advection of dense water progresses, the vertical configuration of the complex deep-water structure that emerged in winter 2005 is maintained throughout the entire simulation, preserving water column segments prone to developing double-diffusive instabilities. The thermo-halocline region exhibits strong salt-fingering activity ($Tu \approx 87°$), resulting in an asymmetric enhancement of the diffusive coefficients ($K_\theta \approx 5.4 \times 10^{-4}$ $\mathrm{m^2\,s^{-1}}$ and $K_S \approx 6 \times 10^{-4}$ $\mathrm{m^2\,s^{-1}}$) and downward heat-salt fluxes (Figure 4.6e). Beneath the base of the thermo-halocline, diffusive layering operates ($Tu \approx -81°$), transporting heat upward more efficiently than salt ($K_\theta \approx 4.4 \times 10^{-4}$ $\mathrm{m^2\,s^{-1}}$ and $K_S \approx 4.3 \times 10^{-4}$ $\mathrm{m^2\,s^{-1}}$). Even though the entire oWMDW-nWMDW portion ($1200 - 1700$ dbar) is prone to moderate-to-strong diffusive layering activity, its effect is barely noticeable due to the background turbulent mixing intensification beneath 1400 dbar. The impact on vertical heat-salt fluxes of moderate salt fingering ($Tu \approx 69°$) operating in the cWMDW-nWMDW portion is likewise negligible for the overall thermohaline evolution in the deepest part of the water column, which is also dominated by background turbulent mixing.

Discrepancies between the observational record and model runs are expected. The observed evolution of the nWMDW core progressively gained heat and salt within the modeled period while preserving a double θ-S maximum, which the model rapidly eroded. Such double maximum was caused by transient structures captured by the raw observational record and that cannot be accounted for in an exercise aiming to understand the general hydrographic evolution of the water column from simple theoretical premises.

Overall, the θ-S profiles evolve similarly to the measured hydrography, and after 540 days model outputs match the observations reasonably with maximum θ (°C) and S differences of $\mathcal{O}(10^{-3})$ below 1210 dbar (the maximum pressure reached by the assimilation term. Figure 4.6a,b,f). The evolution of the density structure is also reproduced satisfactorily (Figure 4.6c). Erosion of the cascading waters is slightly more prominent in the simulation than observed, resulting in a warmer and saltier 29.12 $\mathrm{kg\,m^{-3}}$ isopycnal occupying the bottom of the water column in January 2007.

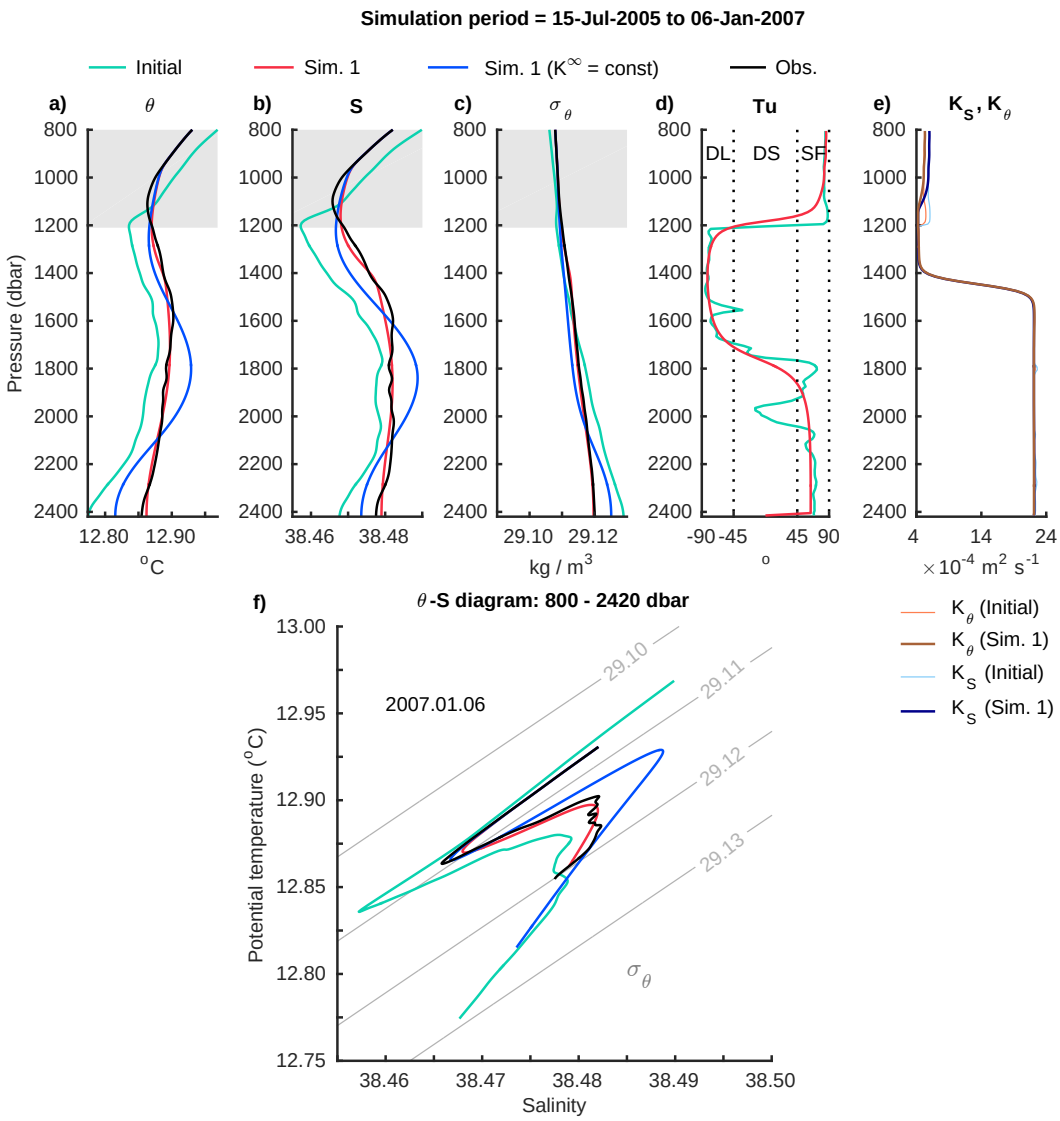

Figure 4.6. (a) θ profile evolution between July 2005 and January 2007 ($800 - 2420$ dbar). The initial profile is shown by the turquoise line. Observed (black line), Simulation 1 (red line) and Simulation 1 with constant $K^{\infty}(z)$ (blue line) profiles in January 2007 are also shown. Shaded areas indicate the maximum assimilation pressure range during the simulations. (b) Same as (a) but for S. (c) Same as (a) and (b) but for potential density anomaly (σ_θ). (d) Turner angle in Simulation 1 in January 2007 (red line) and for the July 2005 initial profile (turquoise line). Dotted vertical lines delimit the three mixing regimes: salt fingers (SF), diffusive layering (DL) and doubly stable (DS). (e) K_θ (brown line) and K_S (dark blue line) profiles in Simulation 1 in January 2007, and initial K_θ (thin orange line) and K_S (thin light blue line) profiles. (f) Same as (a), (b) and (c) but for θ-S. Gray lines denote isopycnal levels (σ_θ). For the complete simulation, the reader is referred to Movie S1 in the supporting information (https://doi.org/10.1029/2020JC016535).

For reference, the modeled evolution of the thermohaline profiles using a constant $K^{\infty}(z) = 4.25 \times 10^{-4}\ \mathrm{m^2\,s^{-1}}$ is also shown in Figure 4.6. Lateral advection of heat and salt during the 2005-2007 period causes a pronounced increase of the nWMDW θ-S relative maxima and a subsequent enhancement of the vertical gradients in the transition regions between water masses. In the absence of vertical structure in the mixing coefficient, the increased heat-salt vertical fluxes are not intense enough to effectively erode the θ-S maxima, ultimately producing a markedly warmer and saltier nWMDW and a weaker erosion of the cWMDW-nWMDW signal at the end of the simulation.

Observations between 2005 and 2007 are therefore compatible with a lateral advection of heat and salt in the nWMDW density levels and a deep intensification of the background mixing coefficient. Using different approaches to represent the evolution of the advection rate, similar optimized $K^{\infty}(z)$ profiles and errors are obtained. Imposing a decreasing advection rate is the most straightforward approach given the impossibility of extracting further information from the temporally sparse observations, but the distribution of the lateral source term into two discrete pulses is conceptually more adequate to realistically represent the arrival of dense water formed in the convection area during winter. The comparisons between simulations, the observations on the dates when the Minorca station was actually occupied (i.e. those underpinning the interpolated dataset; see vertical arrow tips in Figure 4.4) and the observed final θ-S profile on 6 January 2007 are synthesized in Figure 4.7. On the whole, the observed evolution is correctly reproduced using a smooth progression of the input rate (Simulation 1). Giving the same weight to the pulses in 2005 and 2006 (Simulations 2 and 3), θ-S profiles are noticeably mismatched from the observations in September 2005, as they overestimate the remnants of the 2005 injection. By June 2006, Simulation 3 (second pulse centered in March 2006) reproduced more accurately the observations than Simulation 2 (second pulse centered in July 2006), suggesting a rapid arrival of the newly-formed deep water to Minorca. During the closing months of the time series, all simulations evolve according to the observations. In all cases, the optimized $K^{\infty}(z)$ is similar between the three simulations, thus indicating low sensitivity to the temporal evolution of the lateral advection.

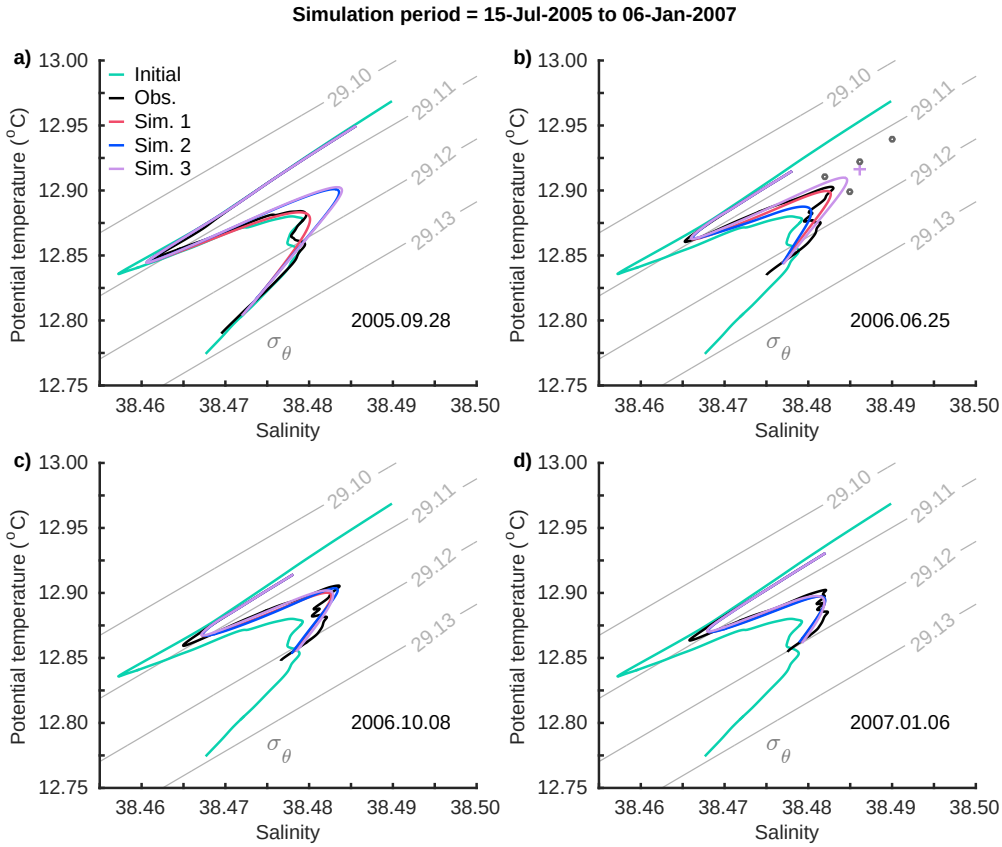

Figure 4.7. (a) θ-S profile evolution between July 2005 and September 2005 (800 – 2420 dbar). The initial profile is shown by the turquoise line. Observed (black line), Simulation 1 (red line), Simulation 2 (blue line) and Simulation 3 (purple line) profiles in September 2005. (b) Same as (a) but in June 2006. Gray dots refer to reported observations of the nWMDW properties in 2006 in the GoL and Ligurian Sea (Smith et al. 2008, Somot et al. 2018, Puig et al. 2013, 2009). Purple cross indicates nWMDW core properties in April 2006 in Simulation 3. (c) Same as (a) and (b) but in October 2006. (d) Same as (a), (b) and (c) but in January 2007. Gray lines in (a), (b), (c) and (d) denote isopycnal levels (σ_θ).

4.5.2 Slope density structure and circulation during winter 2017-2018

Intensive hydrographic and current meter observations in the study area (Figure 4.1b) over the deep convective winter of 2017-2018 offer further insights into regional dynamics associated with the lateral advection of newly-formed dense waters toward the Minorca site.

The θ-S diagram (Figure 4.8a) beneath 1200 dbar in November 2017 shows the presence of much warmer, saltier and lighter deep waters than those occupying the deepest parts of the basin in 2005-2007. The original thermohaline signature of the WMT is no longer present, and only a warm and salty tongue perturbs the bottom of the θ-S profile (see Piñeiro et al. (2019) – Chapter 3 – for the complete description of the thermohaline evolution within the period). Beneath 800 dbar, profiles

along the cross-slope section show a generalized off-shore density reduction over isobaric levels, indicating an on-slope piling of the deep waters (Figure 4.8b). Maximum densities of 29.116 kg m^{-3} were recorded in the outermost stations of the section, in quasi-homogeneous bottom layers that extended 300 dbar above the bottom. Additional homogeneous layers of differentiated density in on-slope profiles indicate the presence of bottom boundary layers (BBLs) more than a hundred meters thick that are distinct from the weakly stratified ambient bottom water mass (Figure 4.8b).

In February 2018, a new deep structure emerged in the θ-S diagram between 1400 – 1800 dbar as a result of the lateral advection of newly-formed dense waters, creating new relative maxima of θ and S in the deep layers (Figure 4.8a). Density profiles along the hydrographic section show significant changes compared to November 2017. The outermost stations recorded density inversions of tens of meters throughout the water column portion where the dense water intrusion occurred, especially notable at station 224. Furthermore, new BBLs in on-slope profiles coinciding with that pressure range were registered, as well as a generalized reduction of density in the BBLs that were observed in 2017 (Figure 4.8c).

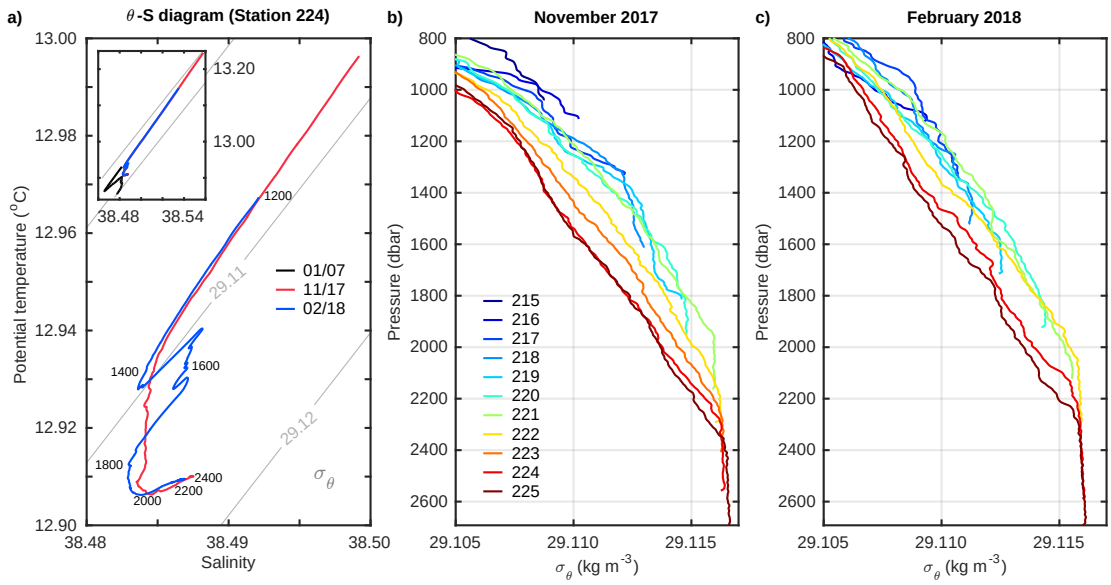

Figure 4.8. (a) θ-S diagram at station 224 beneath 1200 dbar in November 2017 (red line) and in February 2018 (blue line). Gray lines denote isopycnal levels (σ_θ). Pressure levels corresponding to the February 2018 profile are included for reference. Inset diagram in (a) shows a comparison between θ-S profiles beneath 800 dbar in November 2017 (red line) and February 2018 (blue line) at station 224, and January 2007 (black line) at the Minorca deep station. 29.10 kg m^{-3} and 29.12 kg m^{-3} isopycnal levels are included. (b) Potential density anomaly (σ_θ) profiles (800 – 2694 dbar) of the ATHAPOC section in November 2017. (c) Same as (b) but in February 2018. The profile color denote the station number (see locations in Figure 4.1b).

Circulation patterns in the outer continental slope of Minorca were captured by current meter measurements between September 2015 and August 2018 in the ATHAPOC mooring site, which show that the deep boundary circulation is characterized by a predominantly southward flow

(Figure 4.9a). About 75% of all observations were directed toward the S-SE ($\bar{v}$ = 0.07 m / s), following the longitudinal axis of the continental slope. Records at 1000, 1600 and 2500 dbar reveal a depth-intensification of the current, with maximum velocities of 0.3 m / s. Decomposing current time series into cross-slope and along-slope components (38° anticlockwise rotation; see Figure 4.1b) yields Figure 4.9b,c. As expected, along-slope circulation dominates over the cross-slope component, with a stable southward flow of varying intensity that appears to periodically oscillate throughout the 2015-2018 period. Cross-slope velocities exhibited more variability, with recurrent swings between on-slope and off-slope directions. Maximum intensification of the along-slope current occurred during three depth-intensified strong pulses of 2-3 weeks each between February and March 2018, coinciding with the deep-water formation period and the intrusion of dense water detected in station 224 (Figure 4.8). From then until the end of the time series in August 2018, the intensity and variability of both current velocity components increased markedly.

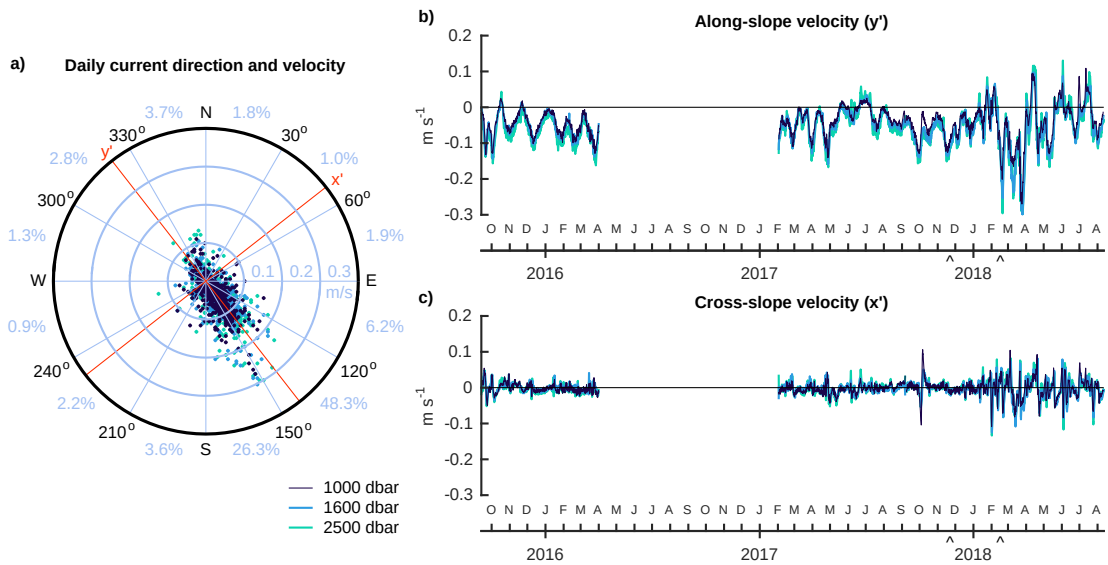

Figure 4.9. (a) 24-hour low-passed daily current direction and velocity at 1000 dbar (dark blue dots), 1600 dbar (light blue dots) and 2500 dbar (turquoise dots) at the ATHAPOC mooring site (see location in Figure 4.1b). Red axes refer to cross-slope (x') and along-slope (y') directions. Percentages of the total observations for each direction range are included for reference. (b) Along-slope component at 1000 dbar (dark blue line), 1600 dbar (light blue line) and 2500 dbar (turquoise line). (c) Same as (b) but for cross-slope component. Vertical arrow tips in the time axes of (b) and (c) indicate the dates on which the ATHAPOC section was occupied.

4.6 Discussion

The evolution of the complex hydrographic structure emerging after the WMT onset in the deep waters off Minorca Island is consistent with a rather simple conceptual study, explored through a numerical model in which a source term modulates nWMDW heat-salt advective gains and the

background mixing coefficient is enhanced near the bottom. In this section, we will discuss the robustness of the assumptions behind the 1-D simulation that supports this study, the discrepancies between the observed and simulated evolution and their possible causes, and the insights that can be drawn on deep-ocean mixing dynamics over the continental slope of Minorca during the post-convective periods.

4.6.1 Simulation of the 2005-2007 θ-S evolution in the deep waters

4.6.1.1 Source term properties

Propagation of newly-formed dense waters from the convection area toward Minorca implies the advection of vertically heterogeneous water columns that evolve by mixing with the surrounding waters as they spread throughout the basin. Since the simulation of the thermohaline evolution of the deep layers over 2005-2007 depends on an *ad hoc* heat-salt source conveniently injected into the July 2005 initial profile, a first question that should be addressed is whether the idealized source term reasonably represents known properties of the dense-water formation in 2005-2006.

The heat and salt lateral advection source term was concentrated around the nWMDW core, i.e. beneath the thermo-halocline and above the cWMDW-nWMDW class. The rationale of this choice is that the observed evolution of the θ-S diagram indicates a strong pull from warmer and saltier water at around the 29.115 $\mathrm{kg\,m^{-3}}$ isopycnal, in accordance with the observed 2006 nWMDW characteristics in the Ligurian Sea and the GoL area (Figure 4.3d; Smith et al. 2008, Somot et al. 2018, Puig et al. 2013, 2009). Likewise, it is known that dense shelf waters barely modified the background characteristics of the deep water in winter 2006 (Fuda et al. 2009, Puig et al. 2013, Schroeder et al. 2013). Dedicated simulations revealed that the newly-formed dense waters in winter 2005 reached densities of $29.10 - 29.13\ \mathrm{kg\,m^{-3}}$ and a formation density threshold of 29.12 $\mathrm{kg\,m^{-3}}$ the following winter (Beuvier et al. 2012, Somot et al. 2018), not inconsistent with our choice of density classes in which the source term adds heat and salt in the simulation, i.e. $29.110 - 29.124\ \mathrm{kg\,m^{-3}}$ (Figure 4.3).

4.6.1.2 Biases associated with cascading water sources

As outlined above, the intensity of the cascading water signal is maximum at the start of the record (lowest θ and S at the bottom of the water column) and the 2006 cascading event was not reported to generate a conspicuous dense water mass as in 2005, so we assume no further specific cascading water sources at these levels in our simple model. Nevertheless, a careful look at the evolution of the cWMDW-nWMDW water column segment shows a subtle deviation from the straight mixing line that would be expected from diffusion (Figure 4.2). The actual evolution of heat and salt in the deepest part of the water column simulated by the model is slightly warmer and saltier on the near-bottom isopycnal levels in 2007 than observed (Figure 4.7); thus, a modest contribution of cascading waters in 2006 may be an explanation for this mismatch.

It is important to emphasize that, although the observations are *consistent with* the model constraints that we have defined (advection at nWMDW and enhanced deep mixing), this is not the only possible explanation of the observations. In particular, we are not considering the possible

drainage (via advection) of deep cascading waters within the simulation period. If such a drainage was considered, the mixing coefficient required to match the observations would depend on the magnitude of the cascading water source/sink. This possibility cannot be explored without a 3D model and precise knowledge of horizontal property distributions. However, a simulation of the spatio-temporal evolution of the deep waters formed in the winter of 2005 by Beuvier et al. (2012) suggests that dense cascading waters were effectively eroded while circulating off Minorca in less than a year. While those authors argue that the waters' spreading velocities may be underestimated in their model, observations of the anomalous WMT structure in the central abyssal plain between Minorca and Sardinia in April-May 2005 (Schroeder et al. 2006) and in the Algerian sub-basin in the subsequent early-summer (López-Jurado et al. 2005, Schroeder et al. 2008) do not exhibit bottom waters denser than 29.125 $\mathrm{kg\,m^{-3}}$, thus endorsing the notion of a strong local consumption of the dense cascading waters off the continental slope of Minorca. In any case, the erosion of cWMDW at our observation site may be explained exclusively by mixing with overlying waters.

4.6.1.3 The post-convective third year: the heave issue

By construction, the model constrains the hydrographic evolution to arise from a combination of diapycnal mixing and a localized source term that simulates the advective arrival of distinct water masses. Therefore, our scheme does not account for hydrographic changes due to the vertical displacement of isopycnals, known as heave (Bindoff & McDougall 1994). Heave-induced changes preserve the θ-S diagram while altering the volumetric expression of different water masses, and are commonly caused by dynamical factors (e.g., perturbed currents driving a shift of isopycnal levels, or the lateral translation of a large-scale gyre).

Heave is thus an issue that must be considered in our attempts to isolate the hydrographic signatures of diffusive processes in a single hydrographic station. Piñeiro et al. (2019) (Chapter 3) used the constant K^{∞}-only version of the present model to analyze the long-term evolution of the deep waters over 2005-2017, seeking to disentangle advective vs diffusive contributions. Advective effects due to the formation of new water types clearly emerged in years when deep convection occurred, but other years (like 2007) when no deep-water formation was identified also exhibited heat-salt content changes of advective origin in the deep layers, mostly linked to the vertical displacement of the overall water column structure (i.e. heave).

In 2007, strong heave pushed downward the oWMDW-nWMDW interface, as well as the underlying water masses. The overall deepening of isopycnals that year was interpreted as a large-scale dynamical effect, related to post-convective rearrangement of water masses following major deep-water formation events. The isopycnal deepening was associated with a reduction in near-bottom density, suggesting to stem from a leakage of the densest resident waters toward the deepest parts of the basin (Chapter 3; Piñeiro et al. 2019). At any rate, from early 2007 onward the strong heave present in the record invalidates our modeling premises. Indeed, attempts to simulate this period with the adopted model setup and $K^{\infty}(z)$ optimization were fruitless. $K^{\infty}(z)$ estimated under strong heave is not only meaningless, but it is also not possible to satisfactorily reproduce the observed hydrographic evolution.

4.6.1.4 Bulk heat and salt content: advection vs diffusion

The net lateral advection of heat and salt into the deep layers was estimated from the bulk differences between the observed profiles in July 2005 and January 2007 beneath 1300 dbar. This direct calculation is likely to underestimate the advective terms, since it doest not take into account the upward diffusion of heat and salt out of this domain. Simulated profiles in January 2007 display a heat and salt content deficit of 4×10^6 J m^{-2} and 0.6711 kg m^{-2} when compared to the observations (Figure 4.7). Therefore, the advective term should have been 2.4% and 8.9% warmer and saltier to balance such a heat and salt leakage.

Piñeiro et al. (2019) (Chapter 3) estimated the advective contributions to the evolution of the deep layers' heat and salt content between 2005 and 2017 off Minorca, by calculating the differences between the observed profiles (i.e. those underpinning the interpolated dataset) and the evolution that each profile would have followed up to the next profile if only diffusion was operating. Accounting for the diffusive leakage of heat and salt toward the oWMDW-nWMDW interface, computed in this way, yields a mismatch error reduced to about 0.6%.

A more rigorous approach would thus be to re-run the model with slightly enhanced advective sources and apply further corrections recursively, since the transfer of heat and salt depends on the simulated evolution of the hydrographic profiles. This further tuning has no significant impact on either the simulated evolution of the thermohaline structure or the estimated $K^{\infty}(z)$. Accordingly, no further corrections were implemented, in order to avoid adding unnecessary complexity.

4.6.1.5 Advective inputs of newly-formed convective waters

The evolution of source water inputs to the sampling site is not well captured by the relatively sparse hydrographic record, so up to three plausible distinct temporal distributions of the source water injection were defined in order to test the robustness of the K^{∞} profile optimization (Figure 4.4). The model's final outcome is rather insensitive to source water function choice , i.e. all the distributions provide similar vertical profiles of the mixing coefficient. However, the modeled intermediate stage deserves further analysis (Figure 4.7). Simulations using two equally weighted advective pulses in 2005 and 2006 overemphasize the remnants of the 2005 injection, which are nearly fully integrated into the initial profile of July 2005. The θ-S profile in July 2006 is well reproduced when the 2006 injection is centered in March (Simulation 3) and not in April-October (Simulation 2), once the deep-water formation period in the GoL is concluded (Somot et al. 2018). Further, nWMDW-core θ and S in late winter of 2006 in Simulation 3 are in close agreement with reported observations of the nWMDW characteristics in the convection area (see purple cross and gray dots in Figure 4.7b), suggesting that the source term is representative and that newly-formed deep waters spread rapidly toward our site.

Schroeder et al. (2008) documented the spreading of the 2005-2006 anomaly from repeated CTD stations throughout the basin. By April-May 2005, the deep structure of the WMT was apparent in the θ-S diagrams to the east and south of the Balearic Islands and traceable in the Algerian basin, reaching the entrance of the Alboran Sea in less than 6 months. By late 2006, the anomaly was detectable all over the basin. Estimates from CTD and current meter data in 2018 off Minorca show the same rapid spread of newly-formed deep waters. Persistent near-bottom peak velocities of $0.15-0.40$ m / s are commonly reported on the Catalan continental slope and in the GoL abyssal

plain (e.g. Durrieu de Madron et al. 2013, 2017, Houpert et al. 2016, Salat et al. 2010) during the post-convective stages, as deep waters leave the convection area with the along-slope boundary current and are transported into the basin interior by submesoscale eddies (Send et al. 1996, Send & Testor 2017, Testor & Gascard 2003, 2006). These velocities are similar to those recorded off Minorca in winter 2018 in association with dense waters flowing south-eastward into the Algerian sub-basin. Assuming a sustained propagation at $0.15 - 0.30$ m / s between the formation area and our site, newly-formed dense waters would arrive at the continental slope off Minorca in less than one month. Therefore, signatures of distinct newly-formed dense waters quickly arriving at our sampling site within each deep convective year should be noticeable in the hydrographic profiles. A higher sampling rate is required to confirm this in future deep-water formation events.

4.6.2 Bottom-enhanced mixing during the post-convective stages

From consecutive observations with a marked diffusive behaviour, Piñeiro et al. (2019) (Chapter 3) estimated a depth-independent coefficient for the entire water column of $K^{\infty} = 4.25 \times 10^{-4}$ m^2 s^{-1}, which was considered representative of the mean level of mechanical mixing in the region. In this study, we find the evolution of the hydrographic structure during the convective and post-convective stages of the 2005-2007 period to be best described by a $K^{\infty}(z)$ profile with a sharp increase from ~ 1400 dbar to the bottom, where the mixing rate is five times larger than the previously estimated local background diffusivity (Figure 4.5).

Since the present study was motivated by the rapid erosion of the cascading water properties, it is somewhat surprising that the observed thermohaline evolution cannot be satisfactorily reproduced with a mixing intensification restricted to near the bottom, where the cascading waters lie. Instead, the layer of elevated turbulence extends 1000 dbar above the bottom, coinciding with the upper limit of the source term beneath the base of the thermo-halocline. Thus, enhanced diapycnal fluxes of heat and salt in the deep layers effect a more efficient transfer of the laterally advected properties throughout the water column, leading to a rapid erosion of the intruding signals (see red and blue lines in Figure 4.6).

While the representativeness of the imposed temporal distributions of lateral advective sources and the suitability of a temporally invariable $K^{\infty}(z)$ profile may be debated, our results robustly indicate that the dense waters injected in 2005-2006 experienced persistent, intense diapycnal mixing. Evidence of such strong mixing has not been reported so far in observations or estimates from previous ocean mixing studies in the WMED basin interior. Our estimated $K^{\infty} \sim 22 \times 10^{-4}$ m^2 s^{-1} in the deep layer greatly exceeds the upper limit of reported values in the deep WMED interior, which are in the range $0.1 - 10 \times 10^{-4}$ m^2 s^{-1} (Cuypers et al. 2012, Ferron et al. 2017), as well as characteristic mixing rates beneath the permanent thermocline of the global ocean (Waterhouse et al. 2014). Thus, the occurrence of this intense deep mixing calls for further discussion.

Local intensification of turbulent mixing is commonly observed in association with shear stresses at the seabed, and results in well-mixed bottom boundary layers (BBLs) that can extend tens of meters above the bottom (Lueck 2001). The deep amplification of $K^{\infty}(z)$ in our model spans well above the vertical range where intense mixing might be expected to be sustained by locally generated near-bottom turbulence. Indeed, the presence of BBLs in the four actual observations that underpin our interpolated record is intermittent and detectable at most up to 60 m above

the bottom. This suggests that the intense mixing required to explain the observed hydrographic evolution off Minorca during 2005-2007 does not reflect an *in situ* mixing process, but may be the signature of well-mixed waters being laterally advected toward our site.

The continental slope of Minorca is regarded as a plausible source of the mixing necessary to reproduce the 2005-2007 observations. Topographic stress generated by a steady flow along a sloping boundary produces an associated downwelling Ekman transport if the background flow is in the direction of Kelvin wave propagation (Benthuysen & Thomas 2012). The bottom Ekman transport across isobaths advects relatively light water beneath denser waters, rendering stratification unstable and triggering convective instabilities. The ensuing mixing over the sloping bottom induces a tilt of isopycnals and a thickening of the BBLs, which have been suggested to act as hotspots for water mass transformation in the abyssal ocean (Ferrari et al. 2016). Recently, boundary-interior communication of the effects of such topographically localized turbulence associated with a Southern Ocean deep current flowing along a sloping bottom was thoroughly documented by Naveira-Garabato et al. (2019) (Figure 4.10), who reported large K^{∞} values in the near-boundary region comparable to those estimated with our optimization-based approach. The occurrence of such a deep boundary mixing in the continental slope of Minorca is explored by means of the ATHAPOC CTD cross-slope high-resolution section and mooring, which captured the arrival of newly-formed dense waters in winter 2018, over a decade after the WMT onset.

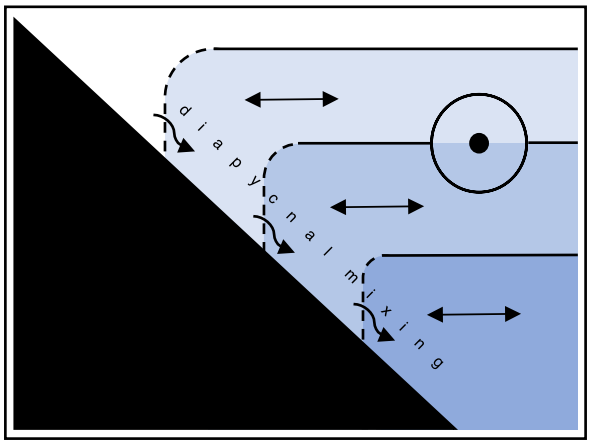

Figure 4.10. Schematic of the deep boundary mixing mechanism developing over a linear topographic slope. Solid contours indicate density surfaces and dashed lines indicate the weakly stratified BBL. The direction of the background flow is denoted by the circled dot. Topographic stress induced by the boundary current triggers a downwelling Ekman transport of relatively light waters across the BBL, enhancing diapycnal mixing. Lateral exchange between well-mixed near-boundary layers and the stratified interior advects away the effects of the topographically localized water transformations.

Hydrographic and current data gathered above the continental slope of Minorca during 2017-2018 exhibit a range of features indicative of the deep-ocean mixing mechanism documented in the Southern Ocean. Current meter data during 2015-2018 show that the general circulation pattern over the continental slope is characterized by a depth-intensified, predominantly southeastward flow that follows the longitudinal axis of the continental slope (Figure 4.9a), in line with the deep

cyclonic circulation of the WMED basin (Send & Testor 2017). In February-March 2018, the along-slope velocity intensified to values of 0.3 m / s in three distinct episodes (Figure 4.9b), and lateral advection of newly-formed dense waters is evident at the outer continental slope (Figure 4.8). The expected response in the density structure due to the topographic stress associated with the intensified along-slope flow may be registered in the on-shore stations in February 2018, which show the occurrence of new thick BBLs (not present in the November 2017 profiles) coinciding with the isobaric range where the intrusion's core was detected in the off-shore station (Figure 4.8). Interestingly, cross-slope velocity variability and intensity increased markedly following the along-slope transport of the newly-formed dense waters until the end of the time series in August 2018 (Figure 4.9c). This is compatible with the lateral exchange of well-mixed boundary layers that effectively propagates the effect of the BBL turbulence away from the sloping boundary (Naveira-Garabato et al. 2019). The overall sequence observed in winter of 2018 is, thus, plausibly consistent with intensified bottom boundary mixing over the continental slope induced by the enhanced along-slope circulation that follows deep-water formation in the GoL area. This deep-ocean mixing mechanism is expected to have been operating after the much more dramatic deep-water formation events in 2005 and 2006, and could explain the strong deep mixing diagnosed by our optimization procedure in the outer continental slope off Minorca during the WMT initial stages. A future targeted study of boundary mixing in this region is called for to corroborate and develop the indicative evidence presented here.

4.7 Conclusions

Hydrographic time series from a regularly occupied deep station in the outer continental slope off Minorca enables to trace the changes in the WMED deep layers following the appearance of the WMT thermohaline structure in the winter 2005, up to the present day. The rapid erosion of the original WMT near-bottom hydrographic structure, observed during the first two years of the record, is shown to provide evidence of regional bottom-intensified mixing. The local evolution of the WMT hydrographic structure during 2005-2007 was reproduced through a combination of lateral advection of dense waters and diapycnal mixing, using a 1-D diffusion model with a source water term that encapsulates our current knowledge of dense-water renewal in the area. An optimization algorithm was adopted to infer a depth-dependent turbulent mixing rate.

We find that almost the entire water column influenced by the WMT experienced persistent, intense mixing greatly exceeding previous rates estimated for the region, and not only in the densest waters. As no indication of such a vertically extensive, local depth-intensified mixing can be obtained from the observations, *ex situ* mixing of the deep waters and subsequent transport toward our site was considered. New hydrographic and current measurements above the continental slope off Minorca in the winter of 2018 show evidence of mixing intensification near sloping topography as along-slope flow of newly-formed dense waters occurs. This suggests that strong boundary mixing and lateral export is a plausible source of the remarkably intense and extensive deep-water transformation inferred during the 2005-2007 period offshore Minorca Island.

This study advances our knowledge of the WMT evolution during its initial stages, and points to a boundary mixing mechanism not previously described in the WMED. A dedicated investigation of this mechanism will be the subject of future work.

Acknowledgments

The authors are very grateful to H. L. Bryden for reviewing the original manuscript and stimulating future research. Authors also appreciate the constructive comments and suggestions from two anonymous reviewers that helped to improve this manuscript. S. Piñeiro acknowledges the pre-doctoral FPI Fellowship (BES-2015-074316) support from the Spanish Ministry of Science and Innovation (MICINN), co-funded by the European Social Fund. The authors would also like to thank the fieldwork and effort made by all the personnel involved in the RADMED and ATHAPOC surveys. This work was supported by the ATHAPOC project (CTM2014-54374-R), funded by *'Plan Nacional I+D+I'* and by the RADMED project, funded by the IEO. Some of the instruments were made available by the Balearic Islands Coastal Observing and Forecasting System (ICTS-SOCIB), the Mediterranean Institute for Advanced Studies (IMEDEA CSIC-UIB), and the University of the Balearic Islands (UIB). All CTD casts and current meter data used in this work can be accessed upon request at the SeaDataNet repository (www.seadatanet.org).

Chapter 5

Boundary mixing of the Western Mediterranean deep waters

This chapter is in preparation for publication as:

Piñeiro, S., Naveira-Garabato, A. C., González-Pola, C., Sánchez-Leal, R., Puig, P., and Balbin, R. Boundary mixing of the Western Mediterranean deep waters.

Keypoints

- Occurrence of conditions conducive of small-scale turbulent mixing over the continental slope of Minorca is explored
- Evidence of bottom-generated mixing and lateral exchange of boundary-interior waters was found
- Bottom boundary mixing is promoted by submesoscale instabilities of the intense background boundary flow

Abstract

The continental slope of Minorca Island has been suggested to be a region were persistent, intensified diapycnal mixing may occur in the deep waters during certain periods of enhanced dynamics. Strong boundary mixing has been indicated to be a plausible source of this mechanical mixing intensification. In this study, we analyze the variability and stability of the deep boundary flow off Minorca by means of available current and hydrographic data gathered along a high-resolution cross-slope oceanographic section, visited between summer 2018 and winter 2020, and explore the occurrence of conditions conducive of small-scale turbulent mixing enhancement. Observations provide evidence of near-boundary turbulent mixing intensification over the continental slope of Minorca concurrent with the activation of the deep boundary circulation. Boundary mixing documented in the observations is triggered by submesoscale instabilities of the deep boundary flow due to frictional stresses over the sloping boundary, which promote topography-localized turbulent mixing and lateral exchange between well-mixed near-boundary waters and stratified interior waters. These observations are consistent with a deep-ocean boundary mixing mechanism that has been reported to be associated with large diapycnal mixing rates near the boundary region above common background levels of the ocean interior, and indicate that regional deep mixing intensification can occur in the continental slope of Minorca during certain periods of intensified dynamics. Observations during early post-convective stages in 2018 are indicative of near-boundary mixing enhancement following the intensification of the along-slope transport of newly-formed dense waters, consistent with the development of the boundary mixing mechanism. Circumstantial evidence compatible with the lateral export of deep waters away from the topographic boundary was also found and is discussed in regard to other plausible explanations.

5.1 Introduction

Deep waters produced in the GoL region during certain winters exit the formation area integrated in the general cyclonic boundary circulation, skirting the Catalan and Balearic continental slope on their way toward the Algerian sub-basin (Figure 5.1a); and transported away into the basin interior by mesoscale and submesoscale structures (Herrmann et al. 2008, Send et al. 1996, Send & Testor 2017, Testor & Gascard 2003, 2006).

Laterally spreading newly-ventilated deep waters replenish the basin with new density classes

or increase the volume of existing levels. This generates an uplift of lighter vintages of resident deep waters after deep-water production (Schroeder et al. 2008). Ultimately, deep waters may become available to overflow the Strait of Gibraltar (García-Lafuente et al. 2009) by a such a long-term uplifting and by diabatic upwelling due to geothermal heating and downward buoyancy diffusion by diapycnal mixing (Bryden 2009, Ferron et al. 2017). Estimations from microstructure observations reveal that the overall turbulent diapycnal mixing levels of the deep waters in WMED interior are relatively weak and play a minor role in this balance (Ferron et al. 2017). However, mixing intensification in the deep layers is expected in the vicinity of topographic boundaries such as continental margins and during certain periods of enhanced dynamics.

The northern continental slope of the Balearic Archipelago has been suggested to be a region where remarkably intense, depth-intensified mixing may occur during post-convective stages after major deep-water formation events (Piñeiro et al. 2021, Chapter 4). Hydrographic and current observations over the continental slope of Minorca Island during winter of 2018 presented in Piñeiro et al. (2021) (Chapter 4) show indicative evidence of turbulent mixing intensification over topography concurrent with the impinging of newly-formed dense waters on their way toward the Algerian sub-basin. Also, it was highlighted that the near-boundary mixing intensification observed in winter 2018 resembles a deep boundary mixing mechanism recently documented by Naveira-Garabato et al. (2019) in the Southern Ocean. This mechanism, associated with topography-flow interactions induced by an abyssal boundary current navigating along sloping topography, concurrently generates intense mixing and lateral export of mixed waters away from bathymetry.

In this chapter, we explore the occurrence of such a boundary mixing mechanism over the continental slope of Minorca. We first analyze available ship-based current and hydrographic data gathered along the ATHAPOC high-resolution cross-slope transect, occupied four times between August 2018 and January 2020, in order to characterize the spatial structure variability of the deep boundary circulation and the development of conditions prone to small-scale turbulence production. Then, we expand the observational dataset of winter 2017-2018 presented in Piñeiro et al. (2021) (Chapter 4) and further analyze the indicative evidence shown by those authors of deep boundary mixing over the continental slope of Minorca during the post-convective stages of 2018. The complete observational record comprises novel extensive hydrographic, current and turbidity measurements obtained through the ATHAPOC cross-slope oceanographic section, regularly visited between 2017-2020, and by means of the two deep moorings deployed during 2015-2019 in the outer continental slope.

This chapter is organized as follows. Section 5.2 presents the observational record and data processing. The procedure used to evaluate the occurrence of conditions prone to small-scale turbulent mixing generation along the cross-slope section off Minorca is described in Section 5.3. Results are presented in Section 5.4 and are subsequently discussed in Section 5.5. Lastly, conclusions and final remarks are gathered in Section 5.6.

5.2 Dataset

The hydrographic properties of the deep waters off Minorca Island have been continuously documented by the IEO for almost two decades through the Minorca deep station. This deep-water observatory provides valuable information on the long-term variability of the deep waters prop-

erties midway from its formation area and the southernmost parts of the basin (see for instance Piñeiro et al. (2019); Chapter 3). However, relying on this single station we lack information to properly characterize the local deep boundary circulation and dynamic processes occurring at shorter time scales, which may be paramount to better understand the observed regional evolution of the deep waters on the large scale. In order to increase the spatio-temporal resolution of the observations and fill this gap, under the auspices of the ATHAPOC and RADMED projects (see Section 2.2 and 2.3), two deep moorings were deployed (each one at different times) in the outer continental slope of Minorca between 2015-2018 (ATHAPOC mooring) and 2018-2019 (HC-IEO-M mooring), and a high-resolution oceanographic section was repeatedly conducted twice a year in winter-spring and summer-autumn between 2017-2020.

5.2.1 The ATHAPOC and HC-IEO-M moorings

The fully instrumented ATHAPOC mooring line (red vertical line in Figure 5.1a,c) was active in the water between September 2015-April 2016 and February 2017-August 2018 (Figure 5.1b). In this study, we use the instrumentation located on its deepest part: (i) three single-point Nortek Aquadopp current meters at nominal depths of 1000, 1600 and 2500 meters, (ii) four SeaBird MicroCats SBE37 at 1600, 1900, 2250 (this one is discarded due to unreliable signal drifts) and 2500 meters, and (iii) the Seapoint turbidimeter that was included at 2500 meters in the second period (February 2017-August 2018). Instruments included in the HC-IEO-M mooring (Figure 5.1b), the much shorter and simpler moored line that replaced the ATHAPOC mooring in August 2018, are also used in this chapter: a single-point Nortek Aquadopp current meter (which unfortunately stopped functioning a few weeks after deployment), a SeaBird MicroCat SBE37 and a Seapoint turbidimeter located at 2500 meters depth.

The moored instrumentation was regularly calibrated by means of shipborne CTD casts encompassing the deployment periods (Figure 5.1b,c. Station 224). When the ATHAPOC mooring was not installed (April 2016-February 2017), the calibration station continued to be regularly visited to obtain reference values to ensure continuity of the hydrographic time series.

Turbidity measurements recorded by the moored turbidimeter were processed as follows. First, to the Formazin Turbidity Units (FTU) time series, the lowest value throughout each period was extracted. Then, FTU values were converted to estimated suspended sediment concentration (SSC) following calibration curves described in Guillén et al. (2000) for the WMED, specifically for the North Balearic region ($\mathrm{SSC} = 0.79\mathrm{FTU} + 0.18\ (\mathrm{mg\,l^{-1}})$).

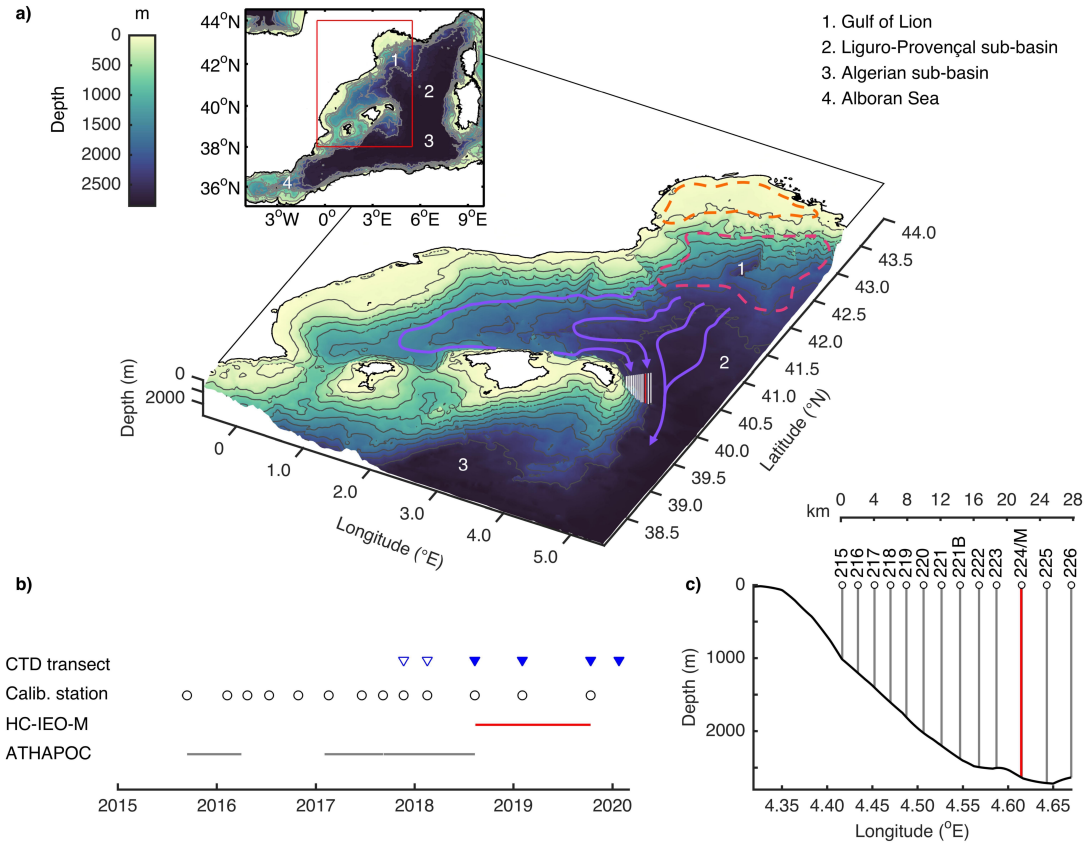

Figure 5.1. (a) Regional domain of the study area (red square). White vertical lines indicate the location of the stations that constitute the cross-slope oceanographic section. Red vertical line in the outer continental slope indicates the position of the ATHAPOC and HC-IEO-M moorings. Red dashed line and orange dashed line delineate the open-ocean deep convection area and the dense shelf-waters formation area, respectively, as stated in Houpert et al. (2016). Purple arrows outline the general boundary circulation of the deep waters north of the Balearic Archipelago following Send & Testor (2017). (b) Temporal distribution of the different elements comprising the observational dataset. Blue triangles indicate when the hydrographic section was occupied. Solid blue triangles denote when current observations from LADCP measurements were available. Black circles indicate when the mooring's calibration station (station 224) was visited. Gray and red lines show the temporal coverage of the ATHAPOC and the HC-IEO-M moorings, respectively. (c) Schematic of the cross-slope oceanographic section and nomenclature of the stations. Red vertical line indicates the location of the ATHAPOC and HC-IEO-M moored lines (M) and the nearby hydrographic calibration station (224). The upper axis indicates the horizontal spatial scale.

5.2.2 The ATHAPOC oceanographic section

In order to complement the ATHAPOC/HC-IEO-M mooring time series and provide insight into the hydrographic and circulation structure of the deep waters over the northeastern continental margin of Minorca, we use oceanographic data gathered through the ATHAPOC high-resolution

cross-slope oceanographic section (Figure 5.1a,c), visited in November 2017, February 2018, August 2018, February 2019, October 2019, and January 2020 (Figure 5.1b); aiming to obtain observations during winter-spring and summer-autumn periods. The first four occupations involved 11 oceanographic stations that spanned 25 km off-shore. From October 2019 onward, two additional stations were included (Figure 5.1c. Stations 221B and 226), increasing the spatial resolution of the section and extending the observations to more than 28 km off-shore up to the abyssal plain. In addition to hydrographic measurements, current velocities throughout the water column were obtained during August 2018-January 2020 surveys (blue solid triangles in Figure 5.1b) by means of a LADCP mounted in the CTD carousel. LADCP profiles were processed following the inversion method described in Visbeck (2002), limited by bottom-tracked and vessel-mounted Acoustic Doppler Current Profiler (VMADCP) velocity data. VMADCP data were processed using the Common Ocean Data Access System (Firing & Hummon 2010).

As the reader will notice, the oceanographic section could not be completed during certain surveys, especially in February 2019 due to rough weather conditions.

5.3 Methodology

5.3.1 Diagnosis of potential flow instabilities of the boundary current

From occupations between August 2018 and January 2020 of the cross-slope oceanographic section (in which LADCP measurements were available), we use current velocity and hydrographic data to analyze the variability of the deep boundary circulation off Minorca Island and to explore evidence of topography-generated turbulent mixing over the continental slope.

Following Naveira-Garabato et al. (2019), we use the Ertel potential vorticity, q (Hoskins 1974), to identify portions of the water column susceptible to submesoscale flow instabilities along the cross-slope transect:

$$q = (f\hat{k} + \nabla \times \boldsymbol{u}) \cdot \nabla b, \tag{5.1}$$

where f is the Coriolis parameter, $\hat{k}$ is the vertical unitary vector, $\boldsymbol{u}$ refers to the three-dimensional velocity vector, and $b = -g\rho/\rho_o$ is the buoyancy, where g corresponds to the gravitational acceleration, ρ is density and ρ_o is a reference density. Ertel potential vorticity can be used as an indicator of flow stability in a geophysical fluid. When q takes the opposite sign of f (positive in the Northern Hemisphere), a variety of overturning instabilities can arise, resulting in small-scale turbulence and mixing which tends to restore q toward marginal stability.

To calculate q field along the cross-slope section, we assume that the main flow of the boundary current is associated with the along-slope axis and that the predominant buoyancy gradient occurs perpendicular to the predominant flow direction, such that the local vertical component of the relative vorticity $\zeta = \partial v/\partial x - \partial u/\partial y$ can be approximated by its first term and $|(\partial v/\partial z)(\partial b/\partial x)| \gg |(\partial u/\partial z)(\partial b/\partial y)|$. These approximations yield

$$q \approx \left(f + \frac{\partial v}{\partial x}\right) N^2 - \frac{\partial v}{\partial z}\frac{\partial b}{\partial x}, \tag{5.2}$$

where x, y and z refer to the cross-slope, along-slope and vertical distances, respectively; (u, v) is the horizontal velocity vector referenced to the cross-slope and along-slope directions and N is the Brunt-Väisälä frequency.

The overturning instabilities that may develop when $fq < 0$ are termed centrifugal, gravitational or symmetrical depending on whether the instability criterion is achieved due to the fluid's large anticyclonic vertical relative vorticity, unstable stratification or strong baroclinicity, respectively. The instability criterion can be similarly expressed as $\phi_{Ri_B} < \phi_c$ (Hamlington et al. 2014, Naveira-Garabato et al. 2019, Thomas et al. 2013), where

$$\phi_{Ri_B} = \tan^{-1}\left(-N^{-2}\left|\frac{\partial v}{\partial z}\right|^2\right), \tag{5.3}$$

is the balanced Richardson number angle and

$$\phi_c = \tan^{-1}(-1 - f^{-1}\nabla \times \boldsymbol{u} \cdot \hat{k}) \approx \tan^{-1}\left(-1 - f^{-1}\left(\frac{\partial v}{\partial x}\right)\right), \tag{5.4}$$

is the critical angle. The type of overturning instability is determined by ϕ_{Ri_B}. Gravitational instability is associated with

$$-\pi < \phi_{Ri_B} < -3\pi/4 \qquad \text{with} \qquad N^2 < 0.$$

An hybrid gravitational-symmetric instability may occur when

$$-3\pi/4 < \phi_{Ri_B} < -\pi/2 \qquad \text{with} \qquad N^2 < 0.$$

Symmetric instability is defined by

$$-\pi/2 < \phi_{Ri_B} < -\pi/4 \qquad \text{with} \qquad N^2 > 0 \qquad \text{and} \qquad f^{-1}\nabla \times \boldsymbol{u} \cdot \hat{k} \leq 0;$$

or

$$-\pi/2 < \phi_{Ri_B} < \phi_c \qquad \text{with} \qquad N^2 > 0 \qquad \text{and} \qquad f^{-1}\nabla \times \boldsymbol{u} \cdot \hat{k} > 0.$$

Finally, hybrid symmetric-centrifugal instability mode is related to

$$-\pi/4 < \phi_{Ri_B} < \phi_c \qquad \text{with} \qquad N^2 > 0 \qquad \text{and} \qquad f^{-1}\nabla \times \boldsymbol{u} \cdot \hat{k} < 0.$$

5.4 Results

5.4.1 Spatio-temporal variability and stability of the deep boundary flow

Occupations of the cross-slope hydrographic section in Minorca between August 2018 and January 2020 reveal a generalized piling of the deep waters over the continental slope and the presence of thick, weakly stratified BBLs that extended hundreds of meters above the seafloor in the off-shore stations, developing over the continental slope up to the 1800 meters isobath in January 2020 (Figure 5.2 and Figure 5.3).

Local circulation of the deep waters off Minorca was characterised by a predominantly southward flow following the longitudinal axis of the topographic slope (Figure 5.2a), with mean velocities ranging between $0.02 - 0.07$ m s^{-1}. Two distinct circulation patterns readily emerge by visually inspecting the along-slope (Figure 5.2a) and cross-slope (Figure 5.2b) components of the velocity field during summer-autumn and winter-spring occupations of the hydrographic section.

In the latter (February 2019 and January 2020), the core of the boundary current is located off-shore, well defined by along-slope peak velocities of $0.16 - 0.24$ m s^{-1} (Figure 5.2a). The cross-slope component shows an overturning circulation associated with the high-velocity core of the boundary current which extends more than 10 km horizontally (Figure 5.2b). Above the core, the upper limb of the cross-slope overturning circulation is characterized by on-slope velocities of $0.07 - 0.12$ m s^{-1}, while the lower limb entails an off-slope flow of similar magnitude. BBLs were integrated within the deep off-slope flow observed beneath the core of the boundary current, while the on-shore edge of the cross-slope overturning circulation was associated with a conspicuous tilting of isopycnals toward the topographic slope. The overall features of the circulation pattern were present in both winter-spring surveys; still, since the hydrographic section could not be fully visited in February 2019, the structure was not comprehensively characterized (especially the lower limb of the overturning circulation).

During summer-autumn occupations (August 2018 and October 2019), the circulation pattern observed in winter-spring vanished. In contrast, circulation over the continental slope exhibited a weaker predominant southward flow with maximum velocities of $0.08 - 0.10$ m s^{-1}, and a prevailing off-slope circulation with maximum velocities of $0.04 - 0.09$ m s^{-1}. During these surveys, enhanced fine-scale density structure and the presence of recurrent density inversions of tens of meters were observed.

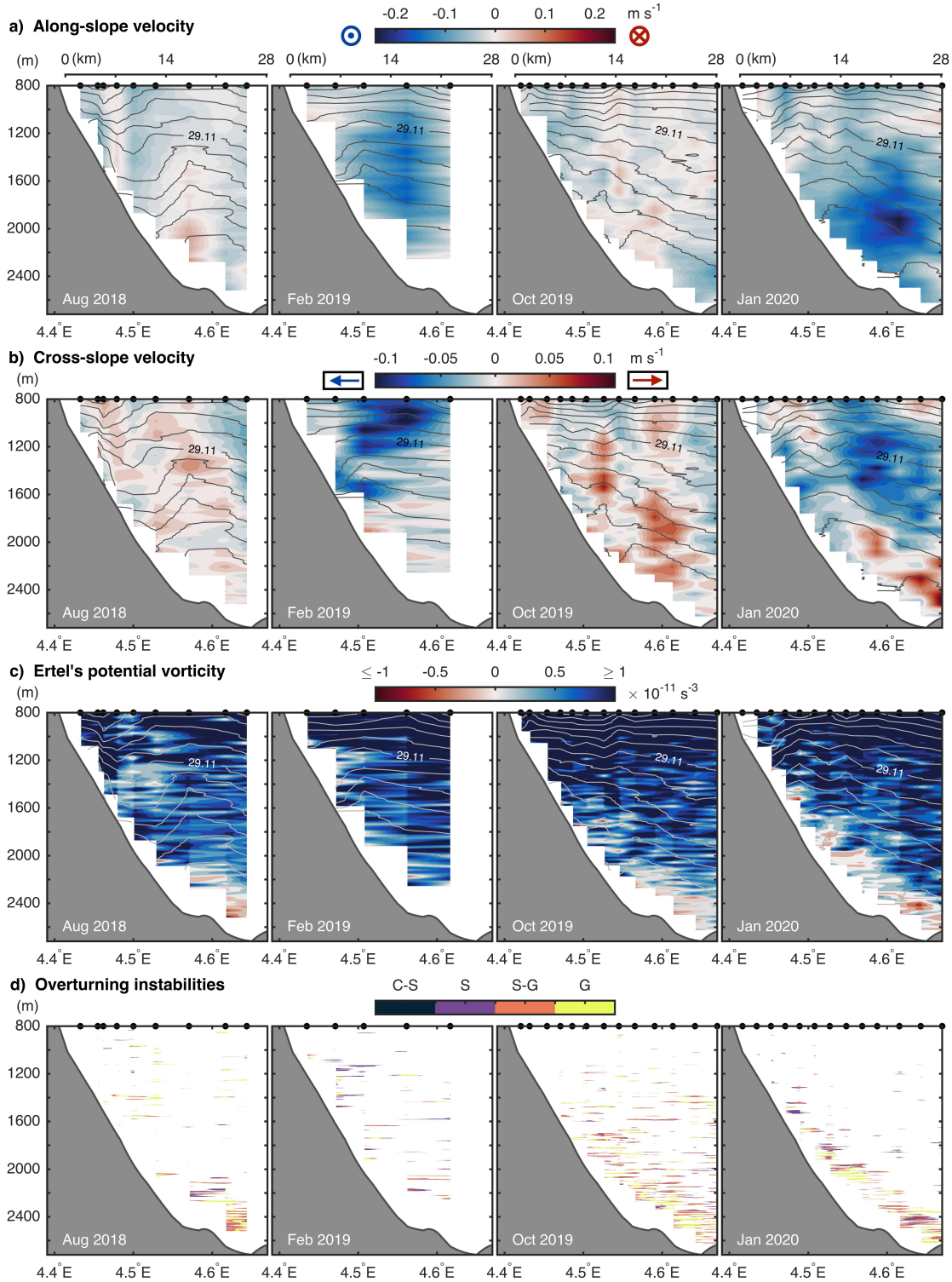
a) Along-slope velocity
-0.2 -0.1 0 0.1 0.2 m s-1
b) Cross-slope velocity
-0.1 -0.05 0 0.05 0.1 m s-1
c) Ertel's potential vorticity
≤ -1 -0.5 0 0.5 ≥ 1
× 10-11 s-3
d) Overturning instabilities
C-S S S-G G
(m)
0 (km) 14 28
800 1200 1600 2000 2400
29.11
Aug 2018
Feb 2019
Oct 2019
Jan 2020
4.4°E 4.5°E 4.6°E

Figure 5.2. (a) Along-slope component of the horizontal velocity field beneath 800 meters in August 2018, February 2019, October 2019 and January 2020. (b) Same as (a) but for the cross-slope component. Reference axes in (a) and (b) are rotated 38° anticlockwise. (c) Same as (a) and (b) but for Ertel potential vorticity field. (d) Same as (a), (b) and (c) but for overturning instability types (C-S: centrifugal-symmetrical. S: symmetric. S-G: symmetric-gravitational. G: gravitational). Flow direction in (a) and (b) is indicated above the colorbar. Solid lines in (a), (b) and (c) denote isopycnal levels (σ_θ) every 0.001 kg m^{-3}. 29.11 kg m^{-3} isopycnal is indicated for reference. Cross-slope distances are shown in the upper axes in (a). Dates are indicated in the bottom left corner of each subfigure for clarity.

Evaluation of the q field in the four occupations of the cross-slope section shows a bulk stability of the boundary flow ($q \approx 2 \times 10^{-11}$ s^{-3}; Figure 5.2c) with disperse small-scale patches of negative values due to vertical shear and fine-scale perturbations of the density field (Figure 5.2d). Nevertheless, a systematic reversal of q sign is consistently observed near the topographic boundary, primarily associated with the weakly stratified waters of the thick BBLs (Figure 5.2c and Figure 5.3). This indicates that submesoscale overturning instabilities may occur within this region, promoting turbulent mixing. The most notable case is January 2020, in which thick patches of negative q are found across a wide bathymetric range over the continental slope, coinciding with the intensification of the along-slope boundary current and the up-slope progression of BBLs up to 1800 dbar. Such near-boundary waters were embedded within the lower branch of the cross-slope overturning circulation. Diagnosis of the nature of the submesocale instabilities over the four transects reveals that the observed BBLs are fundamentally subjected to a combination of symmetric and gravitational instabilities, produced by the unstable stratification and strong vertical shear triggered by the horizontal buoyancy gradients between the well-mixed layer and the more stratified interior waters, respectively (Figure 5.2d). Centrifugal mode is found to be a minority. This may be caused by an underestimation of the horizontal shear of the background flow as a consequence of the spatial resolution of the hydrographic section.

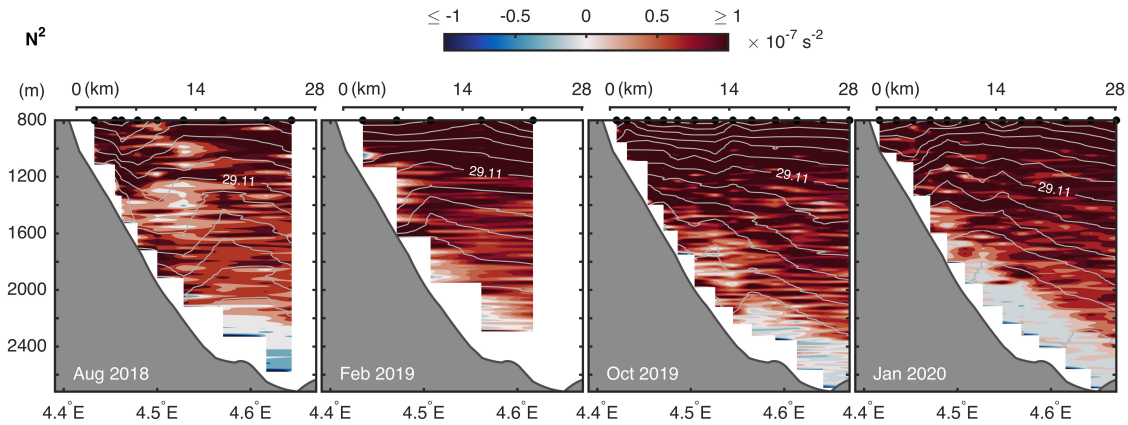

Figure 5.3. Brunt-Väisälä frequency squared (N^2) beneath 800 meters in August 2018, February 2019, October 2019 and January 2020. N^2 field has been smoothed in order to avoid small-scale variability for clarity. Solid lines denote isopycnal levels (σ_θ) every 0.001 kg m^{-3}. 29.11 kg m^{-3} isopycnal is indicated for reference. Cross-slope distances are shown in the upper axes.

5.4.2 Observations over the continental slope during 2018 post-convective stages

The ATHAPOC and HC-IEO-M moorings provide continuous hydrographic and current data at discrete locations of the water column in the outer continental slope northeast of Minorca, hence adding further insight into regional dynamics of the deep boundary circulation and the variability of the deep water properties and transport.

Long-term current velocity observations between September 2015 and August 2018 at the ATHAPOC/HC-IEO-M mooring site show a predominant southward flow of the deep waters following the isobaths of the continental slope (75% of the observations were S-SE directed; $\bar{v} = 0.07\ \mathrm{m\,s^{-1}}$. Figure 5.4), as suggested by the ship-based observations gathered between August 2018 and January 2020 (Figure 5.2). Current meter records at 1000, 1600 and 2500 dbar indicate a slight depth intensification of the boundary current. Intensity of the stable southward flow regularly oscillates during 2015-2018 with a periodicity between $\sim 20 - 60$ days, reaching along-slope peak velocities in excess of $0.10\ \mathrm{m\,s^{-1}}$ (Figure 5.4b). Cross-slope velocities were less intense but rather more variable, with constant swings between the on-slope and off-slope directions (Figure 5.4a). Maximum along-slope velocities of $0.30\ \mathrm{m\,s^{-1}}$ were observed in winter 2018 during three distinct intensification pulses of the southward circulation which lasted 2-3 weeks each, coinciding with the deep-water production period in the formation area. From then until the end of the record, variability and intensity of both current velocity components increased.

Occupations of the cross-slope section between November 2017 and January 2020 show newly-formed deep waters intruding in February 2018 between $1400 - 1800$ dbar in the outermost stations (Figure 5.5), concomitant with the intensification of the boundary circulation recorded by the moored current meters. The new deep-water hydrographic structure was found at shallower and deeper levels later that year as lateral advection of newly-formed dense waters occurred, incorporating heat and salt into the deep layers between $\sim 1200 - 2200$ dbar. Beneath 2200 dbar, weakly stratified bottom waters experienced a slight density reduction during the period. From 2018 onward, no emergence of additional, sharp hydrographic structures can be identified at our site, suggesting that new deep waters with differentiated thermohaline properties were not produced in the subsequent winters, at least in the required amounts.

Following the intensification of the deep along-slope transport in winter 2018, potential density time series from the moored CTD at 2500 dbar (Figure 5.4c) shows that waters within the BBL in the external continental slope underwent a series of abrupt density reductions between February and May 2018 above the intrinsic variability of the record (shaded periods in Figure 5.4c). In early July 2018, a remarkable SSC peak of $4.75\ \mathrm{mg\,l^{-1}}$ was recorded at 2500 dbar. Such a peak is well-above the fairly constant background levels ($\approx 0.22\ \mathrm{mg\,l^{-1}}$) of the bottom waters in the outer continental slope during the 2017-2019 period (Figure 5.4c) and does not seem to be related to local dynamics. After the event, SSC levels in the BBL decreased smoothly toward background values in less than a month.

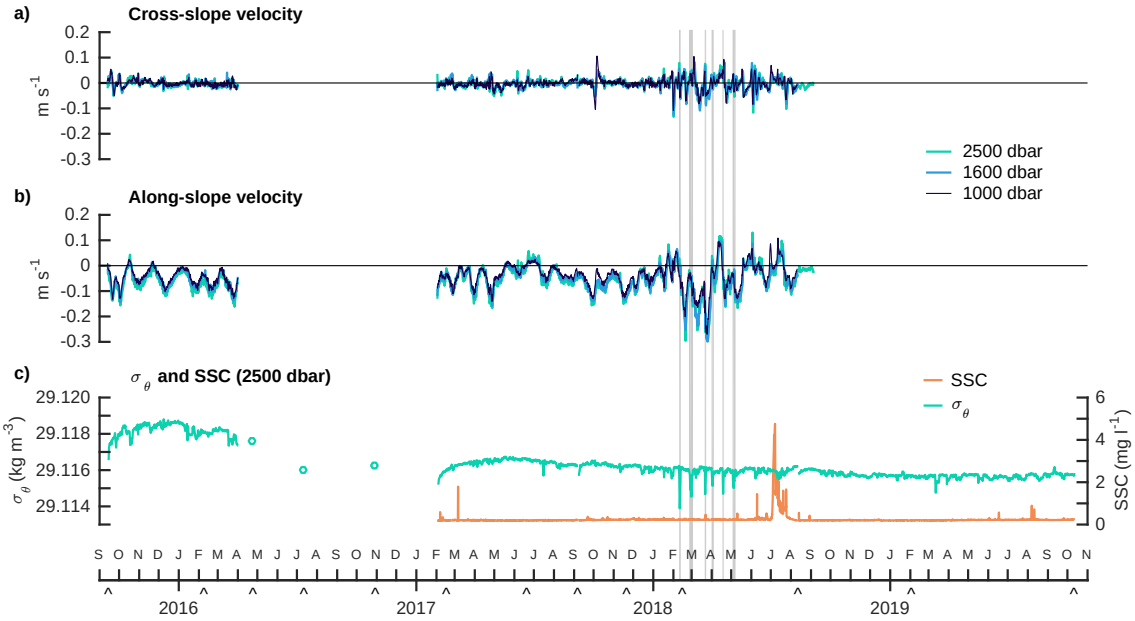

Figure 5.4. (a) 24-hour low-passed cross-slope component of the horizontal velocity at 1000 dbar (dark blue line), 1600 dbar (light blue line) and 2500 dbar (turquoise line) at the ATHAPOC/HC-IEO-M mooring site (see Figure 5.1a,c). (b) Same as (a) but for the along-slope component. (c) 24-hour low-passed potential density anomaly (σ_θ; turquoise line) and smoothed (daily running-mean) estimated SSC (orange line) time series at 2500 dbar. Turquoise circles indicate σ_θ values obtained from CTD casts in the nearby calibration station (see Section 5.2.1). Vertical shaded areas indicate the abrupt density reduction events recorded at 2500 dbar. Vertical arrow tips in the temporal axis refer to the occupations of the mooring calibration station (station 224. Figure 5.1).

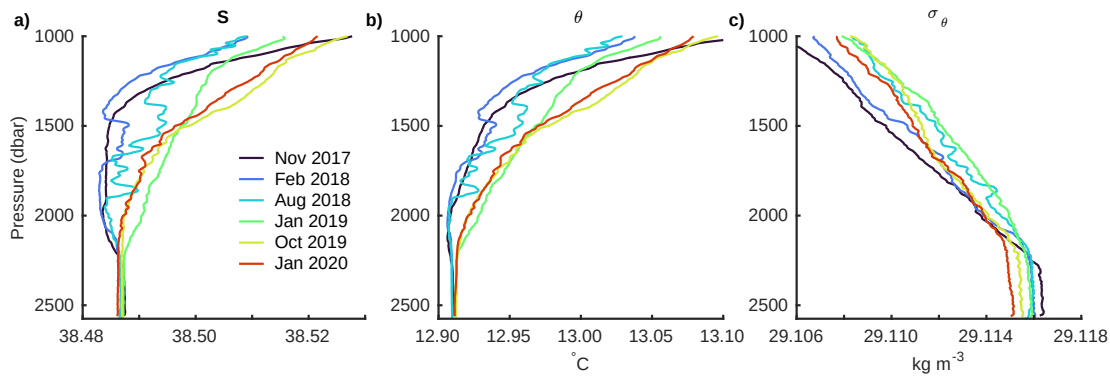

Figure 5.5. (a) Salinity profiles between November 2017 and January 2020 at station 224 beneath 1000 dbar. (b) Same as (a) but for potential temperature (θ). (c) Same as (a) and (b) but for potential density anomaly (σ_θ).

A more detailed inspection of the sharp bottom density reduction events in winter-spring 2018 unveils an interesting connection between density, current velocity and SSC time series variability at 2500 dbar (Figure 5.6). During this period, near-bottom waters were characterized by a background potential density around 29.116 kg m^{-3}. Between February and early-May, six distinct events were recorded in which density abruptly decreased 0.001 – 0.002 kg m^{-3} in 1-3 days (Figure 5.6a). No density abrupt reductions were detected at 1600 dbar and 1900 dbar (Figure 5.7). The onset of these events was robustly associated with off-slope and low along-slope velocities. Density minima were inhibited either by a reversal of the cross-slope flow from off-slope to on-slope direction or an intensification of the along-slope circulation (Figure 5.6b), entailing a similar rapid increase of the bottom waters density toward the initial background value. Increments of SSC over background levels were also linked to off-slope velocities and, consequently, to the occurrence of the density reduction events (Figure 5.6a). However, such a response of the SSC signal to off-slope flows was not constrained by the intensity of the along-slope component (as density reductions) but the direction. The few observed northward along-slope circulation stages did not present enhancement of the turbidity levels of the bottom waters.

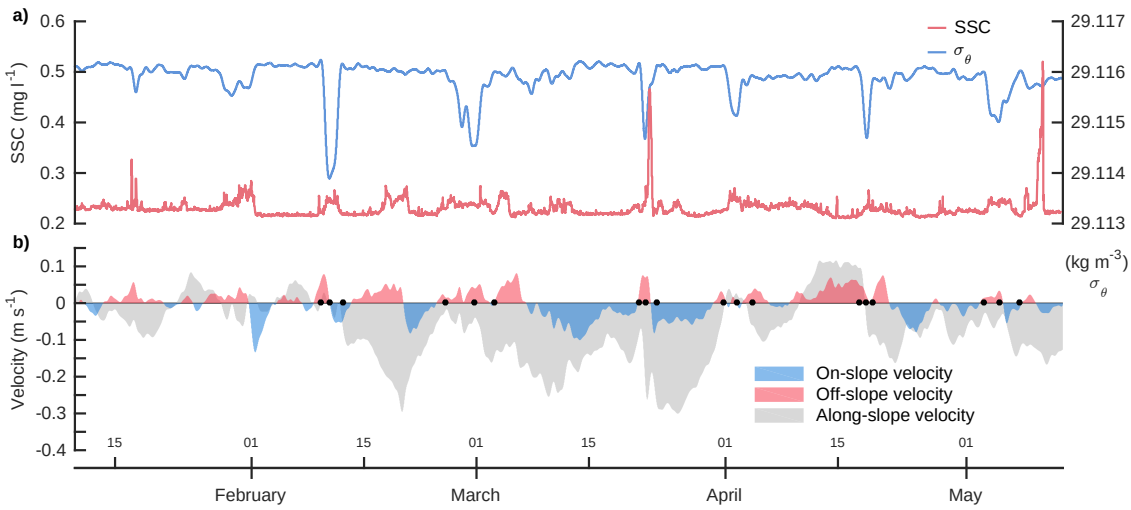

Figure 5.6. (a) 24-hour low-passed potential density anomaly (σ_θ. Blue line) and smoothed (daily running-mean) SSC (red line) at 2500 dbar in the ATHAPOC mooring site. (b) Along-slope component (gray area. Positive northward, negative southward) and cross-slope component (red areas indicate off-slope direction and blue areas refer to the on-slope direction) of the 24-hour low-passed horizontal current velocity at 2500 dbar. Black dots in (b) indicate the start, the density minimum and the end dates of the six abrupt density reduction events (> 0.001 kg m^{-3}).

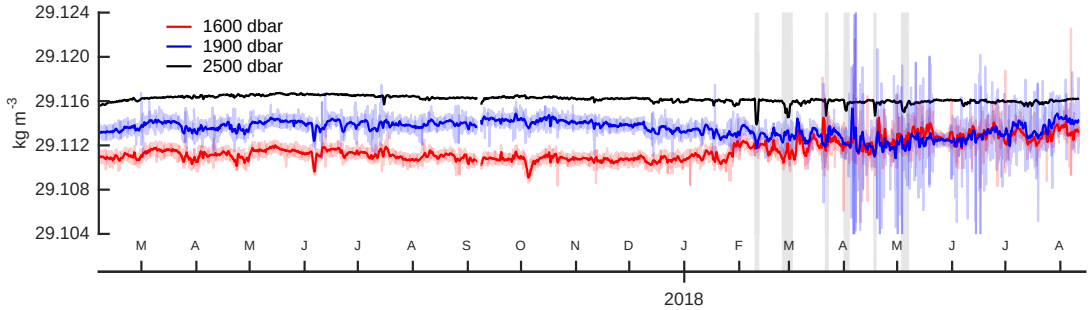

Figure 5.7. (a) 24-hour low-passed potential density anomaly (σ_θ) at 1600 (solid red line), 1900 (solid blue line), and 2500 dbar (solid black line) between February 2017 and August 2018. Light red line and light blue line refer to the raw σ_θ time series at 1600 and 1900 dbar, respectively. Shaded areas indicate the abrupt density reduction events recorded at 2500 dbar.

Hydrographic structure of the deep waters between November 2017 and August 2018 along the high-resolution section (Figure 5.8) enable us to have a broader view of the changes induced by the intensification of the along-slope transport of the deep waters during post-convective stages in 2018, and complement the observations from the moored instrumentation in the outer continental slope.

Density structure in November 2017 (Figure 5.8a) shows the already described on-slope piling of deep waters toward the continental slope (Figure 5.2), indicated by the off-shore density reduction over isobaric levels. Thick BBLs were observed beneath 1800 dbar (Figure 5.8a). In February 2018, concurrent with the first pulse of the along-slope deep-water transport, density profiles in the outer continental slope registered density inversions as a result of the newly-formed dense waters intruding between $\sim 1400 - 1800$ dbar (Figure 5.8b). The BBL in the outermost stations thickened notably and the on-shore profiles show the appearance of new BBLs of distinct density not previously recorded in November 2017 and unrelated to the off-shore ambient bottom water, coinciding with the isobaric range in which the dense-water intrusion was clearly detected off-shore. In August 2018, the horizontal density gradient along the transect was drastically reduced and density inversions of tens of meters were widely observed, even within the BBL in the outermost stations (Figure 5.8c). Density time series at 1600 dbar and 1900 dbar at the mooring site (Figure 5.7) show the persistent occurrence of vertically unstable conditions that followed the arrival of the newly-formed dense waters and endorse the complex evolution suggested by the ship-based observations.

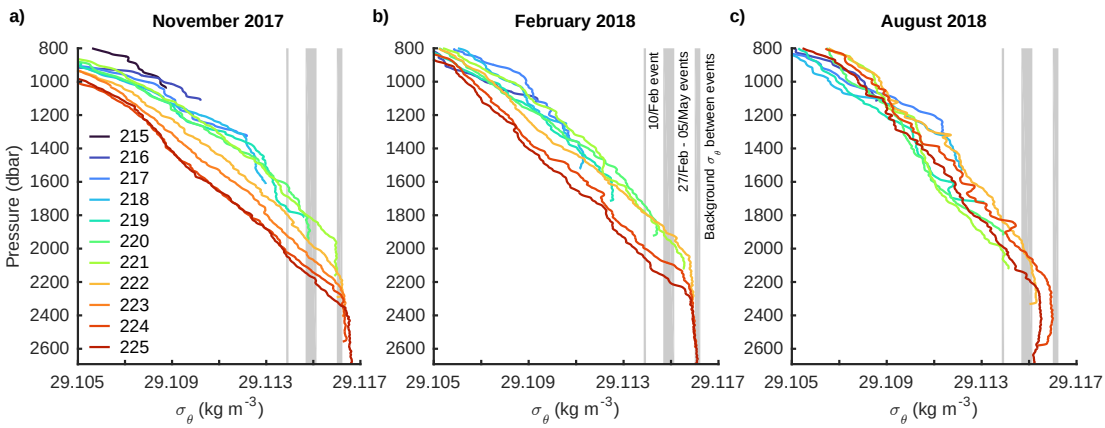

Figure 5.8. Potential density anomaly (σ_θ) profiles of the ATHAPOC cross-slope section in (a) November 2017, (b) February 2018 and (c) August 2018. Colours refer to the station number (see Figure 5.1). Shaded areas in (a) refer to the σ_θ minimum reached on the first density reduction event (10 February 2018) at 2500 dbar in the mooring site and during the following density reduction events (27 February-5 May 2018). Background σ_θ observed between events is also indicated.

5.5 Discussion

Ship-based and mooring observations between 2015 and 2020 provide a comprehensive view of the hydrographic structure variability of the deep waters flowing over the continental slope of Minorca and provide insight into deep regional mixing dynamics. Unfortunately, mooring observations and occupations of the oceanographic transect that include LADCP data do not overlap in time. Thus, in this section we first discuss the observed variability of the deep boundary circulation spatial pattern and the occurrence of submesoscale overturning instabilities over the continental slope of Minorca between August 2018 and January 2020. Then, we address the observed evolution following the arrival of newly-formed dense waters in winter 2018.

5.5.1 Near-boundary mixing during intensification periods of the boundary circulation

Current observations across the continental slope of Minorca and in its outer part indicate that the local deep circulation is predominantly oriented toward the S-SE, parallel to the longitudinal axis of the bathymetry (Figure 5.2a,b; Figure 5.4a,b); in agreement with the general deep cyclonic circulation of the basin (Send & Testor 2017). However, two distinct circulation patterns are registered in the winter-spring and summer-autumn surveys in which LADCP data are available, suggesting that regional deep-water transport along the continental slope might present a seasonal character.

During summer-autumn surveys, intensity of the boundary circulation off Minorca is low and its structure is unsettled (Figure 5.2a,b). Modest along-slope transport is likewise observed in the

mooring site during 2017 summer months (Figure 5.4b). Conditions prone to small-scale turbulence production were primarily found over the deepest part of the continental slope ($\gtrsim$ 2200 dbar) within the BBL related to the weakly stratified bottom ambient water.

During winter-spring surveys, almost all deep waters flow strongly toward the Algerian sub-basin along the continental slope and the core of the deep boundary current is well defined off-shore, $\sim$ 500 meters above the seafloor. The intense deep boundary current off Minorca flows in the direction of the Kelvin wave propagation, i.e. with the coastline to the right in the Northern Hemisphere. Such steady flows along a topographic slope force an associated downwelling bottom Ekman transport, which advects relative light water across isobaths toward deeper-denser layers. Near-boundary buoyancy advection renders stratification unstable, triggering convective instabilities and turbulent mixing (see Chapter 4; Figure 4.10; Benthuysen & Thomas 2012, Wenegrat & Thomas 2020). This eventually results in tilting of isopycnals toward the topographic boundary and thickening of BBLs. The hydrographic expression of such a stress-induced mixing over the sloping topography may be documented in the observations gathered during winter-spring surveys, in which up-slope progression of thick quasi-homogeneous BBLs up to $\sim$ 1800 dbar is observed (Figure 5.3), linked to substantial patches of negative q (specially notable in the well-sampled transect of January 2020; Figure 5.2c). Within this zone, background flow was found to be unstable due to symmetric and gravitational submesoscale instabilities modes (Figure 5.2d), arising from the enlarged horizontal buoyancy gradients and statically unstable conditions across the BBLs. This indicates that near-bottom intensified turbulent mixing can occur in the deep waters across a wide bathymetric range of the continental slope of Minorca during periods of enhanced along-slope deep-water transport.

Naveira-Garabato et al. (2019) documented the development of such a boundary mixing mechanism in the Southern Ocean, induced by an abyssal boundary current flowing along sloping topography. These authors found that the stress-induced flow instabilities near the boundary force a cross-slope overturning circulation around the current's core that promotes rapid lateral exchange of boundary and interior waters, propagating the effects of topography-localized small-scale turbulence away from the boundary. A similar cross-slope circulation pattern emerges from the winter-spring observations off Minorca enclosing the on-shore edge of the intense along-slope boundary current (Figure 5.2b), which conveys stratified interior waters toward the continental slope and advects well-mixed near-bottom waters off-slope. Naveira-Garabato et al. (2019) showed that waters being laterally exchanged were subjected to enhanced levels of small-scale turbulence characterized by large diapycnal mixing rates of $\kappa \sim 10^{-4} - 10^{-2}$ m^2 s^{-1}, well-above typical background values. Following a simple modeling approach, Piñeiro et al. (2021) (Chapter 4) diagnosed comparable ($\kappa \sim 10^{-3}$ m^2 s^{-1}) background turbulent mixing rates in order to reproduce the local, vertical thermohaline evolution off-shore Minorca that followed the major 2005 and 2006 deep-water formation events. These authors argued that intense deep water-mass transformations may have occurred over the regional continental slope during that period due to intense boundary mixing. The present analysis supports this hypothesis and identify the deep continental slope of Minorca as a source of intensified deep turbulent mixing during periods of enhanced along-slope deep-water transport.

It is important to emphasize that no microstructure observations were available and small-scale turbulence levels could not be explicitly evaluated. Therefore, our observations must be understood as indicative of a deep-ocean boundary mixing mechanism associated with vigorous diapycnal mixing levels, larger than the deep western basin-averaged estimations in the WMED

(Ferron et al. 2017) and compatible with previous regional estimations during particular periods (Piñeiro et al. 2021, Chapter 4). The temporal recurrence of such a boundary mixing mechanism is also uncertain. Available observations across the continental slope of Minorca between August 2018 and January 2020 suggest a seasonal pattern. Nevertheless, enhancement of the along-slope deep interior flow favourable to the mixing mechanism is shown to occur frequently at a sub-seasonal scale (Figure 5.4b). The periodic oscillatory pattern ($\sim 20 - 60$ days) of the along-slope circulation observed in the mooring site between 2015-2018 is comparable to the ~1-month time scale of topographic Rossby waves suggested to develop north of the Balearic Archipelago in Testor & Gascard (2006). This mesoscale process may play an important role in setting the recurrence and intensity of the boundary mixing mechanism. This should be clarified in the future and further investigations are called for to explore the potential connection between both processes.

5.5.2 Winter 2018: evidence of intensified boundary mixing and plausible lateral export of near-bottom waters from the continental slope

In winter of 2018, a pronounced intensification of the southward along-slope deep circulation was observed in the outer continental slope in three distinct long-lasting pulses between February and March (Figure 5.4b). Lateral advection of newly-formed deep waters (Margirier et al. 2020) was evident at mid-depths in the deep hydrographic profiles off Minorca (Figure 5.5).

Observations across the oceanographic section in February 2018 indicate the emergence of BBLs across the continental slope in the isobaric range in which the dense-water intrusion was recorded in the outer stations (Figure 5.8), compatible with the expected response to the frictional stress induced by the intensified along-slope flow as documented in February 2019 and January 2020 surveys (Figure 5.2 and Figure 5.3).

As newly-formed dense waters flowed toward the Algerian sub-basin, continuous observations in the deepest part of the ATHAPOC mooring – within the thick BBL in the outer continental slope – recorded relatively light waters flowing off-slope in a series of events between February and May with associated SSC above the stable near-bottom background levels (Figure 5.6). During the events, near-bottom density was rapidly reduced to $29.114 - 29.115$ kg m^{-3}. In February 2018, such isopycnal levels were located above the BBL at our mooring site ($\sim$ 2000 dbar) and matching the topography at $\sim 1700 - 1900$ dbar, within the new BBLs that emerged over the continental slope (Figure 5.8b). This suggests that these waters were exported from shallower parts of the continental slope, in consistency with the near-bottom, off-slope transport promoted by the circulation pattern recorded in February 2019 and January 2020 off Minorca (Figure 5.2b).

The off-slope flow of relative light waters observed at the mooring site (external BBL) was related to modest along-slope velocities and a SSC increment (Figure 5.6). Nevertheless, SSC increments were observed not only associated with the density reductions, but constantly linked to bottom waters flowing off-slope and southward regardless of the intensity of the along-slope component. This is precisely the along-slope direction of the interior flow favourable to the deep boundary mixing mechanism over the continental slope (Naveira-Garabato et al. 2019). Indeed, in the few intervals that northward circulation dominates, off-slope flows were observed to not entail an increase of SSC in the outer BBL (note mid-April observations in Figure 5.6). Since

SSC enhancements are robustly associated with off-slope flows during the period (as density reduction events), such signals are consistent with near-bottom up-slope waters transported across the topographic slope.

However, caution must be taken with the interpretation of this observations, since other processes may produce a similar signal and must be considered. Abrupt density reductions were not clearly registered at 1600 dbar and 1900 dbar (Figure 5.7), but oscillatory patterns of the density field were also recorded by the instrumentation in the upper levels of the ATHAPOC mooring (not shown) during the period, although within the intrinsic variability of those levels. Such bottom density anomalies may be produced by the downward displacement of isopycnals associated with the arrival of mesoscale and submesoscale eddies advected away from the deep-water formation area, such as highly energetic submesoscale coherent vortices (SCVs; Testor & Gascard 2003, 2006, Damien et al. 2017). SCVs play an important role in the basin-scale spreading of the newly-formed dense waters since they transport large columns of dense waters embedded within and isolated from the surrounding waters. SCVs have been identified circulating along the continental slope of the Balearic Archipelago (Bosse et al. 2016, Durrieu de Madron et al. 2017) and Testor & Gascard (2006) estimated that SCVs propagating throughout the basin can generate anomalies in the mooring records on the order of a few days, compatible with our observed density evolution at the bottom of the ATHAPOC mooring. Abrupt density reduction events occurred with a temporal lag between $10-24$ days and other modest near-bottom density reductions events (< 0.001 kg m^{-3}) were recorded by the ATHAPOC mooring before the abrupt events following February 2018 with similar recurrence, associated with low southward off-slope flows and increased SSC above ambient levels (note the two events in late January 2018 in Figure 5.6). Since horizontal current directions throughout the water column at the external continental slope of Minorca varied quasi-synchronically, a plausible large-scale response of the density structure over the continental slope to an oscillatory mesoscale process may also be also considered, such as the dynamic oscillation recorded between 2015-2018 by the moored current meters, presumably associated with topographic Rossby waves.

No additional abrupt, remarkable density reductions in the external BBL were recorded in 2018 from May onward. Until the end of the time series in August 2018, along-slope deep boundary circulation reduced its intensity and the stable flow toward the Algerian sub-basin was recurrently reversed to the north, while cross-slope velocities remained intense and constantly changing direction (Figure 5.4). A numerical study of the major deep convection event in winter of 1987 by Herrmann et al. (2008) showed that newly-formed deep waters were evacuated from the formation area mainly incorporated in the large-scale cyclonic boundary circulation during the formation period, and primarily advected southeastward by mesoscale structures during more advanced post-convective stages. The overall sequence over the continental slope of Minorca in 2018 is likely indicative of the existence of two local distinct dynamical regimes following deep-water production in the formation area and resembles the results reported by Herrmann et al. (2008). During early stages, boundary circulation is activated and newly-formed dense waters flow intensively along the continental slope of Minorca. Intense deep boundary mixing and lateral exchange of near-boundary and interior waters is expected during this stages. During late-spring and summer, deep-water transport shifts toward a less defined pattern, suggesting weaker and highly variable boundary circulation affected by eddy activity. This regime is expected to favour further lateral transport of deep waters mixed over the continental slope toward the basin interior. Reduction of the cross-slope density gradient and the presence of frequent, notable density inversions across the high resolution section in August 2018 (Figure 5.8c) suggest that the deep waters over the continental slope were subjected

to recurrent elevated mixing following the impinging of the newly-formed dense waters in winter 2018. Direct evidence of conditions conducive of mixing was recorded systematically from April 2018 onward by the moored instrumentation at 1600 dbar and 1900 dbar (Figure 5.7). The prominent peak of suspended particulate matter in the deepest part of the ATHAPOC mooring in July 2018, which is well-above the near-bottom ambient SSC in the mooring site, presumably results from the propagation of transient turbidity anomalies throughout the basin, induced by sediment resuspension due to enhanced stresses over the seabed during convective events in the formation area and effectively transported away by the eddy field (Durrieu de Madron et al. 2017, Palanques & Puig 2018).

5.6 Conclusions

Extensive oceanographic observations gathered over the continental slope of Minorca in recent years enabled us to gain insight into regional deep circulation patterns and mixing dynamics.

We find indicative evidence of elevated turbulent mixing over the continental slope of Minorca and lateral exchange of near-boundary, well-mixed layers and stratified interior waters during intensification periods of the along-slope boundary circulation, associated with the development of submesoscale overturning instabilities of the background boundary flow due to frictional stresses. Our observations capture a wide range of features of a deep-ocean boundary mixing mechanism described in the Southern Ocean, reported to be related to prominent diapycnal mixing rates above typical levels of the ocean interior and comparable to previous regional estimates during certain periods of enhanced dynamics. Observations during early post-convective stages in winter of 2018 suggest intensified bottom mixing over the topography compatible with the development of the boundary mixing mechanism. Circumstantial evidence of off-slope export of near-boundary waters might have been recorded in the outer continental slope during this period.

The documented deep boundary mixing mechanism is expected to be specially intense during early stages following deep-water formation events, as newly-formed dense waters flow strongly along-slope toward the Algerian sub-basin, but also during activations of the regional boundary circulation not related to deep-water production events. Consequently, the continental slope of Minorca is suggested to be an adequate and easily accessible site to conduct further research on the dynamics of this deep-ocean boundary mixing mechanism.

Acknowledgments

The authors are grateful to P. Vélez-Belchí and J. Salat for the fruitful comments and discussions during the development of this study and the writing of the manuscript. The authors would like to thank the fieldwork and effort made by all the personnel involved in the RADMED and ATHAPOC surveys. This work was supported by the ATHAPOC project (CTM2014-54374-R), funded by *'Plan Nacional I+D+I'* from the Spanish Ministry of Economy and Competitiveness, and by the RADMED project, funded by the IEO. S. Piñeiro acknowledges the pre-doctoral FPI Fellowship (BES-2015-074316) support from the Spanish Ministry of Science, Innovation and Universities (MICINN), co-funded by the European Social Fund. Some of the instruments were provided by

the Balearic Islands Coastal Observing and Forecasting System (ICTS-SOCIB), the Mediterranean Institute for Advanced Studies (IMEDEA CSIC-UIB) and the University of the Balearic Islands (UIB).

Chapter 6

Summary and final remarks

This section aims to summarize the main achievements and results of this doctoral thesis and provide an integrated view of this work. Additional questions emanating from the research conducted throughout this thesis and future research directions are also discussed.

Since the onset of the WMT in winter of 2005, a wide variety of authors and research groups have studied different aspects of the thermohaline anomaly: its formation event in the northwestern part of the basin (e.g. Grignon et al. 2010, Herrmann et al. 2010) and further deep-water production events in subsequent years (e.g. Durrieu de Madron et al. 2013, Houpert et al. 2016, Somot et al. 2018, Testor et al. 2018), the factors that contributed to its emergence (e.g. Herrmann et al. 2010, Schroeder et al. 2010), its spreading and progression throughout the WMED basin (Beuvier et al. 2012, Schroeder et al. 2008, 2016), its impact on the historic thermohaline structure (e.g. Borghini et al. 2014, Schroeder et al. 2016, Zunino et al. 2012) or its influence on the bulk properties of the Mediterranean waters that overflow the Strait of Gibraltar into de Atlantic (e.g. Naranjo et al. 2017). In this doctoral thesis, the thermohaline variability of the deep layers within the WMT period was analyzed in detail, by means of comprehensive oceanographic datasets gathered and maintained by the IEO off Minorca Island in the last two decades, midway between the deep-water formation area and the Alboran Sea. The results of this doctoral thesis complement the current knowledge generated over the last 16 years on the WMT climatic event and provide new insights into the deep-ocean mixing dynamics of the WMED interior.

One of the main achievements of this work is the development of a 1-D diffusion numerical model that includes double-diffusive mixing parameterizations, a data assimilation scheme, and permits vertical variation of the background vertical mixing coefficient and the inclusion of a source water term. By means of this tool, the large-scale hydrographic evolution of the deep waters off Minorca Island within the WMT period was analyze as a combination of lateral advection of dense waters and continuous vertical diffusion. Our approach enabled us to estimate a regional mean background diffusive mixing coefficient, to assess the relative contribution to the bulk heat and salt content of the deep layers off Minorca of lateral advection versus downward diffusive transfer from the intermediate layers, and to study the large-scale specificities and converging effects of the distinct mixing regimes operating throughout the multi-layered vertical structure of the WMT. Furthermore, this approach made it possible to optimize a vertically varying background turbulent diffusion coefficient profile for the initial stages of the WMT and reproduce the temporal evolution of the deep hydrographic structure off Minorca between 2005-2007 as a combination of localized lateral advection of distinct newly-formed waters and strong depth-intensified mixing. Our findings prompted subsequent investigations in order to explore evidence of deep boundary turbulent mixing intensification over the continental slope of Minorca by means of an extensive oceanographic dataset gathered in recent years.

In concrete terms, the analysis of the long-term thermohaline variability of the deep layers during the first 12 years of the WMT (2005-2017) off Minorca reveals that the overall implication of this climatic event to the regional characteristics of the deep waters is remarkable. Long-term smooth salinification and warming trends estimated for the twentieth century were abruptly disrupted in 2005. A large step-like increment of temperature and salinity was observed in the deep layers off Minorca during the first two years of the anomaly, comparable to the previous reported decadal increments. Throughout the analyzed period, the deep waters underwent significant heat and salt gains, largely dominated by the injection of dense waters between the 2005-2006 and 2011-2013 periods. Heat uptake rate in the deep layers during the period exceeds that estimated for the intermediate layers of the global ocean in recent decades, highlighting the relevance of the

WMT in terms of heat transfer to the deep ocean interior. Continuous downward heat-salt diffusive transfer from the intermediate layers was estimated to have played a minor role in the overall local heat and salt content evolution during the period. Nevertheless, its relative importance in this balance is larger during particular periods and of course, ultimately depends on the magnitude of the advective inputs in the deep layers. At any rate, large-scale downward diffusion of heat and salt from the intermediate layers via salt-finger instabilities is a continuous process that may be of greater importance in other regions of the WMED and its intensity largely depends on the thermohaline variability of the intermediate waters present in the WMED, which have been reported to be increasingly gaining heat and salt during the last decade (Margirier et al. 2020, Schroeder et al. 2017).

The WMT also disrupted the classic smooth stratification observed in the deep layers due to the emergence of the thick multi-layered hydrographic structure in winter of 2005, which vertically displaced the resident deep waters. The evolution of such a deep structure was mainly modulated by continuous diapycnal mixing – which eroded the stratification and was the main driver of the thermohaline configuration evolution in the absence of deep water production – and the subsequent injections of dense waters, which added further complexity to the deep stratification. After 12 years of evolution, deep waters off Minorca Island were denser and more stratified than those in 2004, prior to the onset of the WMT. This may have important implications for the deep-water renewal rate future evolution, since bottom density and deep stratification establish the threshold that newly-formed dense waters must overcome in the formation area to reach the deep and bottom layers and ventilate the deep WMED. Model projections suggest a reduction of deep-water formation rates in the future (Somot et al. 2006). Ultimately, the future evolution of deep-water production rate in the basin will depend on the complex interaction of diverse factors: (i) the efficiency of diapycnal mixing in eroding the deep stratification and lightening the deep waters, (ii) the intensity of the downward bouyancy inputs from the intermediate waters – which will be determined by the changes in thermohaline properties of the intermediate layers that, in turn, affect the preconditioning for new deep-water formation events in the northwestern part of the basin –, (iii) changes in the large-scale atmospheric forcing, (iv) and the recurrence of anomalous atmospheric patterns such as that of the winter of 2005. Therefore, it is consequently expected that the enhanced thermohaline variability observed in the deep waters since 2005 may be reinforced in the coming years and that the future evolution of the deep waters will be likely driven by abrupt shifts like the event that initiated the WMT.

In this context of basin-wide change, it is paramount to maintain and expand the observational systems that monitor the thermohaline properties of the WMED, such as the RADMED monitoring program, in order to be able to track the long-term spatio-temporal evolution of such changes and advance our understanding of the associated oceanographic processes that modulate the future of the deep-water renewal rate in the basin. Our analysis in the Minorca deep station should be extended to the present day – incorporating new observations obtained since 2017 – and even expanded to other deep stations of the RADMED program located along the Spanish Mediterranean continental margin. Routine implementation of such an approach may be a useful tool to study the evolution of vertical diffusive and lateral advective transports of heat and salt in the deep layers in the future in a much broader spatial context.

The analysis of the long-term thermohaline variability of the deep waters off Minorca between 2005-2017 also highlighted the rapid consumption of bottom waters signatures during the first two years of the WMT (2005-2007), plausibly indicative of intensified deep mixing. The same approach

and conceptual premises followed to study the long-term evolution of the WMT were adopted and, by means of the 1-D numerical model and an global optimization algorithm, the local hydrographic evolution was reproduced. The results robustly indicate that the observed evolution is compatible with strong depth-intensified mixing during the analyzed period and stress that, besides being the main driver of the long-term thermohaline evolution in the absence of deep water renewals, background diapycnal mixing is a rather important agent during deep-convective periods in the region, since it rapidly propagates the lateral advective inputs of heat and salt throughout the deep water column and erodes the increased deep stratification imposed by the intruding dense waters. Our approach diagnosed that almost the whole water column disrupted by the WMT structure off Minorca underwent persistent, intensified vertical mixing during the 2005-2007 period, at a rate five-fold over the previous mean background diapycnal mixing rates estimated for the region.

The regional continental slope was suggested to be a plausible source of the deep mixing necessary to reproduce the observations during the 2005-2007 period, and the occurrence of small-scale turbulence production over the local deep topography was explored. Extensive hydrographic and current observations over the continental slope of Minorca during post-convective stages in winter 2018 are compatible with a stress-induced deep boundary mixing mechanism associated with the development of instabilities of the boundary flow, which promote large diapycnal mixing rates over the sloping boundary and lateral exchange of well-mixed near-boundary waters and stratified interior waters. Observations gathered across the northeastern continental slope of Minorca in 2019 and 2020 show a wide range of features indicative of this boundary mixing mechanism not previously described in the WMED, and suggest its development during intensification periods of the along-slope deep boundary circulation. This mechanism is expected to operate particularly intensively in the region during post-convective periods, as newly-formed deep waters flow strongly along the continental slope toward the southern parts of the WMED basin. Lateral export of near-boundary waters associated with the development of the boundary mixing mechanism may have been captured by moored records in the outer continental slope during the convective winter of 2018, which show the off-slope transport of relative light-turbid waters in a series of events following the intensification of the along-slope transport of newly-formed dense waters. Besides being consistent with the arrival of up-slope deep waters signatures, this interesting record motivates additional questions about the large-scale post-convective dynamical response in the region. The occurrence of other plausible processes and even their potential coupling must be appraised in the future.

In conclusion, large-scale estimates and observational evidence shown throughout this thesis indicate that the northern continental slope of the Balearic Archipelago may be a region of particularly active deep-ocean mixing, where strong regional deep water-mass transformations can occur. Our findings suggest a rich deep mixing environment in the region and encourage further research in order to evaluate the overall background turbulent mixing levels in the area, explore the variability and dynamics of the regional deep boundary circulation, the recurrence and magnitude of the deep boundary mixing intensification over the continental slope, and its potential interactions with other processes occurring at larger spatio-temporal scales. Exploring such deep dynamics will drastically improve our understanding of the transport and transformations of the deep waters and consequently, the analysis of the regional large-scale thermohaline evolution of the water column.

To address such questions, a future observational effort should be focus on increasing the resolution of the ATHAPOC transect across the continental slope of Minorca, extending further off-shore its spatial domain, and conducting similar oceanographic sections along the northern continental

slope of the Balearic Archipelago in order to obtain a broader view of the deep boundary circulation and its spatial variability. The development of the deep Argo array in the Mediterranean (Euro-Argo-ERIC 2017) will drastically enhance our observational capabilities. Likewise, it would be necessary to include microstructure profiles in the sampling strategy in order to assess the turbulent mixing levels in the region. This would not only improve our knowledge of the overall local deep mixing environment, but also the understanding of diapycnal transports and its spatio-temporal variability in the WMED basin, where microstructure measurements are sparse. Besides the aforementioned necessity of long-term monitoring, it is important to develop ambitious processes' studies including mooring arrays and synchronous in-situ sampling. Indeed, LADCP sections used in this thesis to explore the local variability of the deep boundary circulation and the occurrence of conditions conducive of small-scale turbulence production, and the only available mooring did not overlap in the critical periods. Deployment of a moored profiler (e.g. McLane) would really improve our understanding of the deep-ocean structure erosion.

Chapter 7

Conclusions

- A 1-D diffusion numerical model was set up in order to analyze in detail the long-term thermohaline evolution of the WMT since its formation in 2005, as observed in the outer continental slope of Minorca Island. Such a model has proven to be a useful tool to study several aspects of the anomaly under simple conceptual premises.
- Since the onset of the WMT, the evolution of the deep waters off Minorca Island shows several stages, driven by diapycnal mixing and interannual deep-water renewals. After 12 years of evolution, its original interleaved structure had been effectively eroded.
- The deep waters off Minorca underwent substantial warming (0.059 °C) and salt increase (0.021) between 2004 and 2017. In 2017, deep waters were notably denser and more stratified than those prior to 2005, potentially with important implications for the future deep-ventilation rate in the basin. Heat uptake rate of the deep layers within the WMT exceeds that estimated for the upper 2000 dbar in the global ocean during the same period.
- Two intense deep-convective periods, 2005-2006 and 2011-2013, account for most of the heat and salt gains. Continuous downward diffusion from the intermediate layers played a modest role in the overall evolution of the heat and salt content of the deep waters.
- Background diapycnal mixing, the driver of the regional deep thermohaline evolution during non-deep-convective periods, is also an important agent during deep-convective ones, since it promotes rapid vertical propagation of the intruding thermohaline signatures and erosion of the deep stratification.
- Analysis of the local evolution of the WMT hydrographic structure during its initial stages was satisfactorily reproduced through a combination of localized lateral advection of heat and salt and a depth-dependent background turbulent mixing coefficient. Results indicate that almost the whole deep water column disrupted by the WMT structure underwent persistent, intensified turbulent mixing during the 2005-2007 period at a rate exceeding previous regional estimates.
- Strong deep boundary mixing over the regional continental slope and subsequent lateral transport of deep waters toward the Minorca deep station was considered as a plausible source of the local, intense deep-water transformations inferred for the 2005-2007 period.
- Hydrographic and current measurements across the Minorca oceanographic section evidence the development of bottom-generated turbulent mixing over the deep topographic slope, concurrent with the intensification of the along-slope deep boundary transport. The observations present a wide range of features of a deep-ocean boundary mixing mechanism not previously described in the WMED, which generates stress-induced, intense near-boundary turbulent mixing, and lateral exchange of well-mixed waters and stratified interior waters.

Appendix

A Data assimilation in the model upper boundary

Data assimilation from the observed profiles in the upper boundary of the model is performed up to a pressure determined by an isopycnal depth that always remains above the oWMDW-nWMDW interface. Before estimating K_θ and K_S profiles, at each δt:

$$c(z,t) = c_{assi}(z,t) \cdot \gamma(z,t)^n + c_{model}(z,t) \cdot (1 - \gamma(z,t)^n), \qquad z_{min} \leq z \leq z_{max}(t), \tag{A.1}$$

where c is the thermohaline tracer, z is the vertical coordinate, t is time, z_{max} is isopycnal pressure and the maximum pressure to assimilate, z_{min} is the minimum pressure of the simulation, c_{model} is the thermohaline tracer in the model and n controls the smoothness of the tracer assimilation in z_{max} ($n = 4$ was used in this study but since the diffusion equation (3.1) – Section 3.3.2 – is solved by a second-order approximation, any correction above that order would be suitable). γ is defined as follows:

$$\gamma(z,t) = \frac{z_{max}(t) - z}{z_{max}(t) - z_{min}}, \tag{A.2}$$

z_{max} is obtained from the observed profiles, for each δt:

$$z_{max}(t) = (1 - \epsilon(t)) \cdot \sigma_i + \epsilon(t) \cdot \sigma_{i+1} \tag{A.3}$$

$$\epsilon(t) = \frac{t - i(t) \cdot \delta t - t_0}{\delta t} \tag{A.4}$$

$$i(t) = \left\lfloor \frac{t - t_0}{\delta t} \right\rfloor \tag{A.5}$$

where t_0 corresponds to the initial time ($t = 0$), i indexes the position of the first observed profile of the 15-day time window in which assimilation is taking place and σ is the isopycnal pressure in the observed profile indexed by i.

The c_{assi} term in equation (A.1) is the thermohaline tracer profile to be assimilated obtained from the fortnightly time series (c_{obs}) indexed by i. It is obtained as follows:

$$c_{assi}(z,t) = (1 - \epsilon(t)) \cdot c_{obs_i}(z) + \epsilon(t) \cdot c_{obs_{i+1}}(z). \tag{A.6}$$

B Differential Evolution global optimization algorithm

The best guess of the $K^\infty(z)$ profile is obtained by means of a DE global optimization algorithm which finds the parameters of (4.1) (Section 4.3.3) that minimize errors between the observed θ

and S profiles and the simulation. DE is an iterative method, not derivate-based, which use a population of individuals, here representing the parameters of (4.1) (Section 4.3.3), that evolves generation by generation toward the solution that minimises the objetive function. The algorithm operates as follows:

Initially, a random population of size m, is generated in the search space. Every individual, $j \in [1, m]$, is defined by a vector $v_j = [c_{j1}, c_{j2}, c_{j3}]$ which contains a value for each parameter of (4.1) (Section 4.3.3). For every j, a fit value is also defined, g_j, in our case the error computed by means of (4.2) (Section 4.3.3). At every generation, the best individual (b) in the population that satisfies $g_b = \min(g_j)$ for all j is identified. The initial values for v are taken from a uniform distribution between two limits for each parameter:

$$v_j = L_j^{\min} + (L_j^{\max} - L_j^{\min})U[0, 1). \tag{B.1}$$

In our case, appropriate values for theses limits were: $c_1 \in [0.0010, 0.0040]$ $\mathrm{m^2\,s^{-1}}$, $c_2 \in [10, 100]$ m and $c_3 \in [z_{\min}, z_{\max}]$, where $z_{\min}$ and $z_{\max}$ correspond to the upper and lower limit of the vertical domain of the simulation.

There are several variants of DE. In this study, DE/current-to-best/1 scheme was used. The evolution process at each generation, $ig \in [1, ng]$, follows the algorithm:

1. ig is increased in 1. The fit, g_j, of every individual, j, is then calculated, and the best one, b, is detected.

2. For each individual, j, two individuals are randomly selected k_1, k_2, $j \neq k_1 \neq k_2$, and the following calculation is performed:

$$u_{jl} = (1 - \mu)v_{jl} + \mu v_{bl} + F(v_{k_1 l} - v_{k_2 l}), \tag{B.2}$$

   where F is a mutation factor and μ is the weight of the best individual in the mixing (B.2). $l \in [1, 3]$ refers to each parameter of function (4.1) defining v_j.

3. A crossover is carried out, depending on a probability, CR, by:

$$w_{jl} = \begin{cases} u_{jl}, & \text{if} \quad x_{jl} < CR, \\ v_{jl}, & \text{otherwise}, \end{cases} \tag{B.3}$$

   where x_{jl} is a randomly selected number that satisfies $x_{jl} = U[0, 1)$.

4. If some of parameters w_{jl} violate the constraints, they are returned into the feasible area:

$$v_{jl} = \max(\min(w_{jl}, L_j^{\max}), L_j^{\min}). \tag{B.4}$$

   Then v_{jl}, $j \in [1, m]$, $l \in [1, 3]$, is the population for the next generation.

5. If ig reaches ng or the population has little dispersion, due to $\bar{g} < tol \cdot s_g$, being $\bar{g}$ the mean and s_g the standard deviation of g_j, $j \in [1, m]$, then the iteration is halted, with the best individual as the solution. Otherwise step 1 follows.

Numerical parameters adopted in this study were: $m = 15$, $ng = 60$, $tol = 0.0025$, $F = 0.5671$, $CR = 0.5$. Weight of the best individual in the mixing, $\mu = 0.2 + 0.8(ig/ng)^2$, changes at every generation, ig. This enables the optimization algorithm to first widely explore the search space, but afterward it focuses on the exploitation of the most promising area. For further information on DE, the reader is referred to Chakraborty (2008) and Feoktistov (2006).

Bibliography

Aparicio-González, A., López-Jurado, J. L., Balbín, R., Alonso, J. C., Amengual, B., Jansá, J., García, M. C., Moyá, F., Santiago, R., Serra, M. & Vargas-Yáñez, M. (2015), 'Ibamar database: Four decades of sampling on the Western Mediterranean Sea', *Data Science Journal* **13**(January), 172–191.

Balbín, R., López-Jurado, J. L., Aparicio-González, A. & Serra, M. (2014), 'Seasonal and interannual variability of dissolved oxygen around the Balearic Islands from hydrographic data', *Journal of Marine Systems* **138**, 51–62.

Barker, P. M. & McDougall, T. J. (2017), 'Stabilizing hydrographic profiles with minimal change to the water masses', *Journal of Atmospheric and Oceanic Technology* **34**(9), 1935–1945.

Benthuysen, J. & Thomas, L. N. (2012), 'Friction and diapycnal mixing at a slope: Boundary control of potential vorticity', *Journal of Physical Oceanography* **42**(9), 1509–1523.

Bergamasco, A. & Malanotte-Rizzoli, P. (2010), 'The circulation of the Mediterranean Sea: a historical review of experimental investigations', *Advances in Oceanography and Limnology* **1**(1), 11–28.

Bethoux, J. P. (1979), 'Budgets of the Mediterranean Sea. Their dependance on the local climate and on the characteristics of the Atlantic waters', *Oceanologica acta* **2**(2), 157–163.

Bethoux, J. P., Durrieu de Madron, X., Nyffeler, F. & Tailliez, D. (2002), 'Deep water in the western Mediterranean: Peculiar 1999 and 2000 characteristics, shelf formation hypothesis, variability since 1970 and geochemical inferences', *Journal of Marine Systems* **33-34**, 117–131.

Bethoux, J. P., Gentili, B., Morin, P., Nicolas, E., Pierre, C. & Ruiz-Pino, D. (1999), 'The Mediterranean Sea: A miniature ocean for climatic and environmental studies and a key for the climatic functioning of the North Atlantic', *Progress in Oceanography* **44**(1-3), 131–146.

Bethoux, J. P. & Tailliez, D. (1994), Deep-Water in the Western Mediterranean Sea, Yearly Climatic Signature and Enigmatic Spreading, *in* P. Malanotte-Rizzoli & A. R. Robinson, eds, 'Ocean Processes in Climate Dynamics: Global and Mediterranean Examples', 1 edn, Springer Netherlands, Dordrecht, pp. 355–369.

Beuvier, J., Béranger, K., Brossier, C. L., Somot, S., Sevault, F., Drillet, Y., Bourdallé-Badie, R., Ferry, N. & Lyard, F. (2012), 'Spreading of the Western Mediterranean Deep Water after winter 2005: Time scales and deep cyclone transport', *Journal of Geophysical Research: Oceans* **117**(7), 1–26.

Bindoff, N. L. & McDougall, T. J. (1994), 'Diagnosing Climate Change and Ocean Ventilation Using Hydrographic Data', *Journal of Physical Oceanography* **24**(6), 1137–1152.

Borghini, M., Bryden, H., Schroeder, K., Sparnocchia, S. & Vetrano, A. (2014), 'The Mediterranean is becoming saltier', *Ocean Science* **10**(4), 693–700.

Bosse, A., Testor, P., Houpert, L., Damien, P., Prieur, L., Hayes, D., Taillandier, V., Durrieu de Madron, X., D'Ortenzio, F., Coppola, L., Karstensen, J. & Mortier, L. (2016), 'Scales and dynamics of Submesoscale Coherent Vortices formed by deep convection in the northwestern Mediterranean Sea', *Journal of Geophysical Research: Oceans* **121**(10), 7716–7742.

Bryden, H. L. (2009), Where does the new Mediterranean deep water go, *in* F. Briand, ed., 'CIESM Workshop Monographs', Vol. 38, CIESM, Monaco, pp. 67–70.

Bryden, H. L., Candela, J. & Kinder, T. H. (1994), 'Exchange through the Strait of Gibraltar', *Progress in Oceanography* **33**(3), 201–248.

Bryden, H. L., Schroeder, K., Borghini, M., Vetrano, A. & Sparnocchia, S. (2014), Mixing in the deep waters of the Western Mediterranean, *in* G. L. E. Borzelli, M. Gacic, P. Lionello & P. Malanotte-Rizzoli, eds, 'The Mediterranean Sea: temporal variability and spatial patterns', John Wiley and Sons Inc, Oxford, chapter 4, pp. 51–58.

Bryden, H. L., Schroeder, K., Sparnocchia, S., Borghini, M. & Vetrano, A. (2014), 'Thermohaline staircases in the western Mediterranean Sea', *Journal of Marine Research* **72**(1), 1–18.

Canals, M., Puig, P., Durrieu de Madron, X., Heussner, S., Palanques, A. & Fabres, J. (2006), 'Flushing submarine canyons', *Nature* **444**(7117), 354–357.

Chakraborty, U. K. (2008), *Advances in Differential Evolution*, Vol. 143 of *Studies in Computational Intelligence*, Springer Berlin Heidelberg, Berlin, Heidelberg.

Cheng, L., Abraham, J., Hausfather, Z. & Trenberth, K. E. (2019), 'How fast are the oceans warming?', *Science* **363**(6423), 128–129.

Chiggiato, J., Schroeder, K. & Trincardi, F. (2016), 'Cascading dense shelf-water during the extremely cold winter of 2012 in the Adriatic, Mediterranean Sea: Formation, flow, and seafloor impact', *Marine Geology* **375**, 1–4.

Conan, P., Testor, P., Estournel, C., D'Ortenzio, F., Pujo-Pay, M. & Durrieu de Madron, X. (2018), 'Preface to the Special Section: Dense Water Formations in the Northwestern Mediterranean: From the Physical Forcings to the Biogeochemical Consequences', *Journal of Geophysical Research: Oceans* **123**(10), 6983–6995.

Coppola, L., Raimbault, P., Mortier, L. & Testor, P. (2019), 'Monitoring the Environment in the Northwestern Mediterranean Sea', *Eos* **100**.

Crank, J. & Nicolson, P. (1947), 'A practical method for numerical evaluation of solutions of partial differential equations of the heat-conduction type', *Mathematical Proceedings of the Cambridge Philosophical Society* **43**(1), 50–67.

Cuypers, Y., Bouruet-Aubertot, P., Marec, C. & Fuda, J. L. (2012), 'Characterization of turbulence from a fine-scale parameterization and microstructure measurements in the Mediterranean Sea during the BOUM experiment', *Biogeosciences* **9**(8), 3131–3149.

Damien, P., Bosse, A., Testor, P., Marsaleix, P. & Estournel, C. (2017), 'Modeling Postconvective Submesoscale Coherent Vortices in the Northwestern Mediterranean Sea', *Journal of Geophysical Research: Oceans* **122**(12), 9937–9961.

Davies, J. H. & Davies, D. R. (2010), 'Earth's surface heat flux', *Solid Earth* **1**(1), 5–24.

de Boer, G. J., Pietrzak, J. D. & Winterwerp, J. C. (2008), 'Using the potential energy anomaly equation to investigate tidal straining and advection of stratification in a region of freshwater influence', *Ocean Modelling* **22**, 1–11.

Durante, S., Schroeder, K., Mazzei, L., Pierini, S., Borghini, M. & Sparnocchia, S. (2019), 'Permanent Thermohaline Staircases in the Tyrrhenian Sea', *Geophysical Research Letters* **46**, 1562–1570.

Durrieu de Madron, X., Houpert, L., Puig, P., Sanchez-Vidal, A., Testor, P., Bosse, A., Estournel, C., Somot, S., Bourrin, F., Bouin, M. N., Beauverger, M., Beguery, L., Calafat, A., Canals, M., Cassou, C., Coppola, L., Dausse, D., D'Ortenzio, F., Font, J., Heussner, S., Kunesch, S., Lefevre, D., Le Goff, H., Martín, J., Mortier, L., Palanques, A. & Raimbault, P. (2013), 'Interaction of dense shelf water cascading and open-sea convection in the northwestern Mediterranean during winter 2012', *Geophysical Research Letters* **40**(7), 1379–1385.

Durrieu de Madron, X., Ramondenc, S., Berline, L., Houpert, L., Bosse, A., Martini, S., Guidi, L., Conan, P., Curtil, C., Delsaut, N., Kunesch, S., Ghiglione, J. F., Marsaleix, P., Pujo-Pay, M., Séverin, T., Testor, P., Tamburini, C. & ANTARES (2017), 'Deep sediment resuspension and thick nepheloid layer generation by open-ocean convection', *Journal of Geophysical Research: Oceans* **122**, 2291–2318.

Durrieu De Madron, X., Zervakis, V., Theocharis, A. & Georgopoulos, D. (2005), 'Comments on "cascades of dense water around the world ocean"', *Progress in Oceanography* **64**(1), 83–90.

Emery, W. J. & Thomson, R. E. (2001), *Data Analysis Methods in Physical Oceanography*, revised edn, Elsevier Science & Technology, Oxford.

Euro-Argo-ERIC (2017), Strategy for evolution of Argo in Europe, Technical report, EA-2016-ERIC-STRAT.

Feoktistov, V. (2006), *Differential Evolution*, Vol. 5 of *Springer Optimization and Its Applications*, Springer US, Boston, MA.

Ferrari, R., Mashayek, A., McDougall, T. J., Nikurashin, M. & Campin, J. M. (2016), 'Turning ocean mixing upside down', *Journal of Physical Oceanography* **46**(7), 2239–2261.

Ferron, B., Bouruet-Aubertot, P., Cuypers, Y., Schroeder, K. & Borghini, M. (2017), 'How important are diapycnal mixing and geothermal heating for the deep circulation of the Western Mediterranean?', *Geophysical Research Letters* **44**, 7845–7854.

Firing, E. & Hummon, J. M. (2010), Shipboard ADCP Measurements, *in* E. M. Hood, C. L. Sabine & B. M. Sloyan, eds, 'The GO-SHIP repeat hydrograpy manual: a collection of expert reports and guidelines', IOCCP Report No. 14; ICPO Publication Series No. 134.

Font, J., Béranger, K., Bryden, H., Budillon, G., Fuda, J. L., Gačić, M., Gascard, J. C., Packard, T., Puig, P., Roether, W., Salat, J., Salusti, E., Schroeder, K., Theocharis, A. & Van Haren, H. (2009), Executive summary of CIESM workshop 38 "Dynamics of Mediterranean deep waters", *in* F. Briand, ed., 'CIESM Workshop Monographs', Vol. 38, CIESM, Monaco, pp. 5–17.

Font, J., Puig, P., Salat, J. & Palanques, A. (2007), 'Sequence of hydrographic changes in NW Mediterranean deep water due to the exceptional winter of 2005', *Scientia Marina* **71**(2), 339–346.

Fuda, J. L., Bengara, L., Ismail, S. B., Curtil, C., Moumni, B. E., Font, J., Lefevre, D., Millot, C., Taupier-Letage, I., Raimbault, P., Rougier, G., Sammari, C. & Tamburini, C. (2009), Recent dense water formation in the Med western basin, as observed by HYDROCHANGES, *in* F. Briand, ed., 'CIESM Workshop Monographs', number 38, CIESM, Monaco, pp. 29–33.

Fuda, J. L., Etiope, G., Millot, C., Favali, P., Calcara, M., Smriglio, G. & Boschi, E. (2002), 'Warming, salting and origin of the Tyrrhenian Deep Water', *Geophysical Research Letters* **29**(19), 17–20.

García-Lafuente, J., Delgado, J., Sánchez Román, A., Soto, J., Carracedo, L. & Díaz del Río, G. (2009), 'Interannual variability of the Mediterranean outflow observed in Espartel sill, western Strait of Gibraltar', *Journal of Geophysical Research* **114**(C10), C10018.

Gasparini, G. P., Ortona, A., Budillon, G., Astraldi, M. & Sansone, E. (2005), 'The effect of the Eastern Mediterranean Transient on the hydrographic characteristics in the Strait of Sicily and in the Tyrrhenian Sea', *Deep-Sea Research Part I: Oceanographic Research Papers* **52**(6), 915–935.

Grignon, L., Smeed, D. A., Bryden, H. L. & Schroeder, K. (2010), 'Importance of the variability of hydrographic preconditioning for deep convection in the Gulf of Lion, NW Mediterranean', *Ocean Science* **6**(2), 573–586.

Guillén, J., Palanques, A., Puig, P., Durrieu de Madron, X. & Nyffeler, F. (2000), 'Field calibration of optical sensors for measuring suspended sediment concentration in the western Mediterranean', *Scientia Marina* **64**(4), 427–435.

Hamlington, P. E., Van Roekel, L. P., Fox-Kemper, B., Julien, K. & Chini, G. P. (2014), 'Langmuir-submesoscale interactions: Descriptive analysis of multiscale frontal spindown simulations', *Journal of Physical Oceanography* **44**(9), 2249–2272.

Herrmann, M., Sevault, F., Beuvier, J. & Somot, S. (2010), 'What induced the exceptional 2005 convection event in the northwestern Mediterranean basin? Answers from a modeling study', *Journal of Geophysical Research* **115**(C12), C12051.

Herrmann, M., Somot, S., Sevault, F., Estournel, C. & Déqué, M. (2008), 'Modeling the deep convection in the northwestern Mediterranean Sea using an eddy-permitting and an eddy-resolving model: Case study of winter 1986-1987', *Journal of Geophysical Research* **113**(C4), C04011.

Hofmann, M. & Morales Maqueda, M. A. (2009), 'Geothermal heat flux and its influence on the oceanic abyssal circulation and radiocarbon distribution', *Geophysical Research Letters* **36**(3), 2–5.

Hoskins, B. J. (1974), 'The role of potential vorticity in symmetric stability and instability', *Quarterly Journal of the Royal Meteorological Society* **100**(425), 480–482.

Houpert, L., Durrieu de Madron, X., Testor, P., Bosse, A., D'Ortenzio, F., Bouin, M. N., Dausse, D., Le Goff, H., Kunesch, S., Labaste, M., Coppola, L., Mortier, L. & Raimbault, P. (2016), 'Observations of open-ocean deep convection in the northwestern Mediterranean Sea: Seasonal and interrannual variability of mixing and deep water masses for the 2007-2013 period', *Journal of Geophysical Research: Oceans* **121**, 8139–8171.

IOC, SCOR & IAPSO (2010), *The international thermodynamic equation of seawater – 2010: Calculation and use of thermodynamic properties*, number June, UNESCO.

Ivanovic, R. F., Valdes, P. J., Gregoire, L., Flecker, R. & Gutjahr, M. (2014), 'Sensitivity of modern climate to the presence, strength and salinity of Mediterranean-Atlantic exchange in a global general circulation model', *Climate Dynamics* **42**(3-4), 859–877.

Jayne, S. R. (2009), 'The Impact of Abyssal Mixing Parameterizations in an Ocean General Circulation Model', *Journal of Physical Oceanography* **39**(7), 1756–1775.

Johannessen, O. M. & Lee, O. S. (1974), 'A deep stepped thermo-haline structure in the Mediterranean', *Deep-Sea Research and Oceanographic Abstracts* **21**(8), 629–639.

Juza, M., Escudier, R., Vargas-Yáñez, M., Mourre, B., Heslop, E., Allen, J. & Tintoré, J. (2019), 'Characterization of changes in Western Intermediate Water properties enabled by an innovative geometry-based detection approach', *Journal of Marine Systems* **191**, 1–12.

Juza, M., Renault, L., Ruiz, S. & Tintoré, J. (2013), 'Origin and pathways of winter intermediate water in the northwestern mediterranean sea using observations and numerical simulation', *Journal of Geophysical Research: Oceans* **118**(12), 6621–6633.

Kelley, D. E. (1984), 'Effective diffusivities within oceanic thermohaline staircases', *Journal of Geophysical Research* **89**(11), 484–488.

Kelley, D. E. (1990), 'Fluxes Through Diffusive Staircases: A New Formulation', *J. Geophys. Res.* **95**(C3), 3365–3371.

Kelley, D. E., Fernando, H. J. S., Gargett, A. E., Tanny, J. & Özsoy, E. (2003), 'The diffusive regime of double-diffusive convection', *Progress in Oceanography* **56**(3-4), 461–481.

Kinder, T. H. & Bryden, H. L. (1990), Aspiration of deep waters through straits, *in* L. J. Pratt, ed., 'The Physical Oceanography of Sea Straits', Springer Netherlands, Dordrecht, pp. 295–319.

Klymak, J. & Nash, J. D. (2009), Estimates of Mixing, *in* H. J. Steele, S. A. Thorpe & K. K. Turekian, eds, 'Encyclopedia of Ocean Sciences', 2nd edn, Vol. 2, Elsevier Ltd, London, pp. 288–298.

Kubin, E., Poulain, P.-M., Mauri, E., Menna, M. & Notarstefano, G. (2019), 'Levantine Intermediate and Levantine Deep Water Formation: An Argo Float Study from 2001 to 2017', *Water* **11**(9), 1781.

Kunze, E. & Toole, J. M. (1997), 'Tidally Driven Vorticity, Diurnal Shear, and Turbulence atop Fieberling Seamount', *Journal of Physical Oceanography* **27**(12), 2663–2693.

Lacombe, H., Tchernia, P. & Gamberoni, L. (1985), 'Variable bottom water in the Western Mediterranean basin', *Progress in Oceanography* **14**(C), 319–338.

Lascaratos, A., Roether, W., Nittis, K. & Klein, B. (1999), 'Recent changes in deep water formation and spreading in the Eastern Mediterranean Sea: A review', *Progress in Oceanography* **44**(1-3), 5–36.

Ledwell, J. R., Montgomery, E. T., Polzin, K. L., St. Laurent, L. C., Schmitt, R. W. & Toole, J. M. (2000), 'Evidence for enhanced mixing over rough topography in the abyssal ocean', *Nature* **403**(6766), 179–182.

Ledwell, J. R., Watson, A. J. & Law, C. S. (1993), 'Evidence for slow mixing across the pycnocline from an open-ocean tracer-release experiment', *Nature* **364**(6439), 701–703.

Ledwell, J. R., Watson, A. J. & Law, C. S. (1998), 'Mixing of a tracer in the pycnocline', *Journal of Geophysical Research: Oceans* **103**(C10), 21499–21529.

López-Jurado, J. L., Balbín, R., Alemany, F., Amengual, B., Aparicio-González, A., Fernandez de Puelles, M. L., García-Martínez, M. C., Gazá, M., Jansá, J., Morillas-Kieffer, A., Moya, F., Santiago, R., Serra, M. & Vargas-Yáñez, M. (2015), 'The RADMED monitoring programme as a tool for MSFD implementation : towards an ecosystem-based approach', *Ocean Science* **11**, 897–908.

López-Jurado, J. L., González-Pola, C. & Vélez-Belchí, P. (2005), 'Observation of an abrupt disruption of the long-term warming trend at the Balearic Sea, western Mediterranean Sea, in summer 2005', *Geophysical Research Letters* **32**(24), L24606.

Lozier, M. S. & Stewart, N. M. (2008), 'On the temporally varying northward penetration of mediterranean overflow water and eastward penetration of Labrador sea water', *Journal of Physical Oceanography* **38**(9), 2097–2103.

Lueck, R. (2001), Turbulence in the benthic boundary layer, *in* J. H. Steele, S. A. Thorpe & K. K. Turekian, eds, 'Elements of Physical Oceanography', 2nd edn, Elsevier, London, pp. 311–316.

Malanotte-Rizzoli, P., Artale, V., Borzelli-Eusebi, G. L., Brenner, S., Crise, A., Gacic, M., Kress, N., Marullo, S., Ribera D'Alcalà, M., Sofianos, S., Tanhua, T., Theocharis, A., Alvarez, M., Ashkenazy, Y., Bergamasco, A., Cardin, V., Carniel, S., Civitarese, G., D'Ortenzio, F., Font, J., Garcia-Ladona, E., Garcia-Lafuente, J. M., Gogou, A., Gregoire, M., Hainbucher, D., Kontoyannis, H., Kovacevic, V., Kraskapoulou, E., Kroskos, G., Incarbona, A., Mazzocchi, M. G., Orlic, M., Ozsoy, E., Pascual, A., Poulain, P. M., Roether, W., Rubino, A., Schroeder, K., Siokou-Frangou, J., Souvermezoglou, E., Sprovieri, M., Tintoré, J. & Triantafyllou, G. (2014), 'Physical forcing and physical/biochemical variability of the Mediterranean Sea: A review of unresolved issues and directions for future research', *Ocean Science* **10**(3), 281–322.

Malanotte-Rizzoli, P., Manca, B. B., D'Alcala, M. R., Theocharis, A., Brenner, S., Budillon, G. & Ozsoy, E. (1999), 'The Eastern Mediterranean in the 80s and in the 90s: The big transition in the intermediate and deep circulations', *Dynamics of Atmospheres and Oceans* **29**(2-4), 365–395.

Manca, B., Burca, M., Giorgetti, A., Coatanoan, C., Garcia, M. J. & Iona, A. (2004), 'Physical and biochemical averaged vertical profiles in the Mediterranean regions: An important tool to trace the climatology of water masses and to validate incoming data from operational oceanography', *Journal of Marine Systems* **48**(1-4), 83–116.

Margirier, F., Testor, P., Heslop, E., Mallil, K., Bosse, A., Houpert, L., Mortier, L., Bouin, M.-N., Coppola, L., D'Ortenzio, F., Durrieu de Madron, X., Mourre, B., Prieur, L., Raimbault, P. & Taillandier, V. (2020), 'Abrupt warming and salinification of intermediate waters interplays with decline of deep convection in the Northwestern Mediterranean Sea', *Scientific Reports* **10**(1), 20923.

Marshall, J. & Schott, F. (1999), 'Open-ocean convection: Observations, theory, and models', *Reviews of Geophysics* **37**(1), 1–64.

Marty, J. C. (2002), 'The DYFAMED time-series program (French-JGOFS)', *Deep-Sea Research Part II: Topical Studies in Oceanography* **49**(11), 1963–1964.

Meccia, V., Simoncelli, S. & Sparnocchia, S. (2016), 'Decadal variability of the Turner Angle in the Mediterranean Sea and its implications for double diffusion', *Deep-Sea Research Part I: Oceanographic Research Papers* **114**, 64–77.

MEDOC Group (1970), 'Observation of formation of deep water in the Mediterranean Sea', *Nature* **227**, 1037–1040.

Millot, C. (1999), 'Circulation in the Western Mediterranean Sea', *Journal of Marine Systems* **20**(1-4), 423–442.

Millot, C. (2007), 'Interannual salinification of the Mediterranean inflow', *Geophysical Research Letters* **34**(21), L21609.

Millot, C. & Taupier-Letage, I. (2005), Circulation in the Mediterranean Sea, *in* 'The Handbook of Enviromental Chemistry', Vol. 5, Springer-Verlag Berlin Heidelberg, Berlin, pp. 29–66.

Naranjo, C., García-Lafuente, J., Sammartino, S., Sánchez-Garrido, J. C., Sánchez-Leal, R. & Jesús Bellanco, M. (2017), 'Recent changes (2004-2016) of temperature and salinity in the Mediterranean outflow', *Geophysical Research Letters* **44**(11), 5665–5672.

Naveira-Garabato, A. C., Frajka-Williams, E. E., Spingys, C. P., Legg, S., Polzin, K. L., Forryan, A., Abrahamsen, E. P., Buckingham, C. E., Griffies, S. M., McPhail, S. D., Nicholls, K. W., Thomas, L. N. & Meredith, M. P. (2019), 'Rapid mixing and exchange of deep-ocean waters in an abyssal boundary current', *Proceedings of the National Academy of Sciences* **116**(27), 13233–13238.

Onken, R. (2003), 'Double diffusion in the Mediterranean Sea: Observation and parameterization of salt finger convection', *Journal of Geophysical Research* **108**(C9), 8124.

Palanques, A. & Puig, P. (2018), 'Particle fluxes induced by benthic storms during the 2012 dense shelf water cascading and open sea convection period in the northwestern Mediterranean basin', *Marine Geology* **406**(April), 119–131.

Piñeiro, S., González-Pola, C., Fernández-Díaz, J. M. & Balbin, R. (2019), 'Thermohaline Evolution of the Western Mediterranean Deep Waters Since 2005: Diffusive Stages and Interannual Renewal Injections', *Journal of Geophysical Research: Oceans* **124**(12), 8747–8766.

Piñeiro, S., González-Pola, C., Fernández-Díaz, J. M., Naveira-Garabato, A. C., Sánchez-Leal, R., Puig, P., Salat, J. & Balbin, R. (2021), 'Persistent, depth-intensified mixing during the Western Mediterranean Transition's initial stages', *Journal of Geophysical Research: Oceans* **126**(2), e2020JC016535.

Planque, B., Lazure, P. & Jegou, A. (2006), 'Typology of hydrological structures modelled and observed over the Bay of Biscay shelf', *Scientia Marina* **70**(June), 43–50.

Polzin, K. L. (1997), 'Spatial Variability of Turbulent Mixing in the Abyssal Ocean', *Science* **276**(5309), 93–96.

Puig, P., Durrieu de Madron, X., Salat, J., Schroeder, K., Martín, J., Karageorgis, A. P., Palanques, A., Roullier, F., López-Jurado, J. L., Emelianov, M., Moutin, T. & Houpert, L. (2013), 'Thick bottom nepheloid layers in the western Mediterranean generated by deep dense shelf water cascading', *Progress in Oceanography* **111**, 1–23.

Puig, P., Palanques, A., Font, J., Salat, J., Latasa, M. & Scharek, R. (2009), Interactions between open-sea convection and shelf cascading dense waters in the formation of the Western Mediterranean Deep Water, *in* F. Briand, ed., 'CIESM Workshop Monographs', number 38, CIESM, Monaco, pp. 81–89.

Puig, P., Palanques, A., Orange, D. L., Lastras, G. & Canals, M. (2008), 'Dense shelf water cascades and sedimentary furrow formation in the Cap de Creus Canyon, northwestern Mediterranean Sea', *Continental Shelf Research* **28**(15), 2017–2030.

Radko, T. (2013), *Double-diffusive convection*, first edn, Cambridge University Press, New York.

Reid, J. L. (1979), 'On the contribution of the Mediterranean Sea outflow to the Norwegian-Greenland Sea', *Deep Sea Research Part A, Oceanographic Research Papers* **26**(11), 1199–1223.

Rixen, M., Beckers, J. M., Levitus, S., Antonov, J., Boyer, T., Maillard, C., Fichaut, M., Balopoulos, E., Iona, S., Dooley, H., Garcia, M. J., Manca, B., Giorgetti, A., Manzella, G., Mikhailov, N., Pinardi, N. & Zavatarelli, M. (2005), 'The Western Mediterranean Deep Water: A proxy for climate change', *Geophysical Research Letters* **32**(12), 1–4.

Rohling, E. J. & Bryden, H. L. (1992), 'Man-Induced Salinity and Temperature Increases in Western Mediterranean Deep Water', *Journal of Geophysical Research* **97**(C7), 11191–11198.

Ruddick, B. (1983), 'A practical indicator of the stability of the water column to double-diffusive activity', *Deep Sea Research Part A, Oceanographic Research Papers* **30**(10), 1105–1107.

Salat, J., Emelianov, M. & López-Jurado, J. L. (2006), Unusual extension of Western Mediterranean deep water formation during winter 2005, *in* '5ª Asamblea Hispano-Portuguesa de Geodesia y Geofísica', Seville, pp. 1–4.

Salat, J., Emelianov, M. & López-Jurado, J. L. (2007), Atypical Western Mediterranean Deep Water formation during winter 2005, *in* F. Briand, ed., 'Rapport du Commission International de la Mer Medittanee, 38', CIESM, Istanbul, p. 197.

Salat, J., Emelianov, M. & Puig, P. (2009), From Bottom Water (Lacombe , 1985) to New-WMDW since 2005 . Possible shifts on Open Sea Deep Convection, *in* F. Briand, ed., 'CIESM Workshop Monographs', number 38, CIESM, Monaco, pp. 41–49.

Salat, J. & Font, J. (1987), 'Water mass structure near and offshore the Catalan coast during the winters of 1982 and 1983', *Annales Geophysicae* **5B**(1), 49–54.

Salat, J., Puig, P. & Latasa, M. (2010), 'Violent storms within the Sea: dense water formation episodes in the NW Mediterranean', *Advances in Geosciences* **26**, 53–59.

Sammartino, S., García-Lafuente, J., Naranjo, C. & Simoncelli, S. (2018), Ventilation of the western Mediterranean deep water through the strait of Gibraltar, *in* 'Copernicus Service Ocean State Report, 2', Journal of Operational Oceanography, 11, pp. s101–s103.

Schmitt, R. W. (1981), 'Form of the Temperature-Salinity Relationship in the Central Water: Evidence for Double-Diffusive Mixing', *Journal of Physical Oceanography* **11**(7), 1015–1026.

Schmitt, R. W. (1994), 'Double diffusion in oceanography', *Annual Review of Fluid Mechanics* **26**, 255–285.

Schmitt, R. W. (2009), Double-diffusive convection, *in* H. J. Steele, S. A. Thorpe & K. K. Turekian, eds, 'Encyclopedia of Ocean Sciences', 2nd edn, Vol. 2, Elsevier Ltd, London, pp. 162–170.

Schmitt, R. W. & Ledwell, J. R. (2001), Dispersion and difussion in the deep ocean, *in* J. H. Steele, S. A. Thorpe & K. K. Turekian, eds, 'Encyclopedia of Ocean Sciences', 1st edn, Vol. 2, Elsevier Ltd, London, pp. 726–733.

Schmitt, R. W., Ledwell, J. R., Montgomery, E. T., Polzin, K. L. & Toole, J. M. (2005), 'Enhanced diapycnal mixing by salt fingers in the thermocline of the tropical atlantic', *Science* **308**(5722), 685–688.

Schroeder, K., Chiggiato, J., Bryden, H. L., Borghini, M. & Ben Ismail, S. (2016), 'Abrupt climate shift in the Western Mediterranean Sea', *Scientific Reports* **6**(1), 23009.

Schroeder, K., Chiggiato, J., Josey, S. A., Borghini, M., Aracri, S. & Sparnocchia, S. (2017), 'Rapid response to climate change in a marginal sea', *Scientific Reports* **7**(1), 4065.

Schroeder, K., Garcia-Lafuente, J., Josey, S. A., Artale, V., Nardelli, B. B., Carrillo, A., Gacic, M., Gasparini, G. P., Herrmann, M., Lionello, P., Ludwig, W., Millot, C., Ozsoy, E., Pisacane, G., Sanchez-Garrido, J. C., Sannino, G., Santoleri, R., Somot, S., Struglia, M., Stanev, E., Taupier-Letage, I., Tsimplis, M. N., Vargas-Yañez, M., Zervakis, V. & Zodiatis, G. (2012), Circulation of the mediterranean sea and its variability, *in* P. Lionello, ed., 'The Climate of the Mediterranean Region', Elsevier, London, chapter 4, pp. 187–256.

Schroeder, K., Gasparini, G. P., Borghini, M. & Ribotti, A. (2009), Experimental evidence of recent abrupt changes in the deep Western Mediterranean Sea, *in* F. Briand, ed., 'CIESM Workshop Monographs', number 38, CIESM, Monaco, pp. 51–56.

Schroeder, K., Gasparini, G. P., Tangherlini, M. & Astraldi, M. (2006), 'Deep and intermediate water in the western Mediterranean under the influence of the Eastern Mediterranean Transient', *Geophysical Research Letters* **33**(21), L21607.

Schroeder, K., Josey, S. A., Herrmann, M., Grignon, L., Gasparini, G. P. & Bryden, H. L. (2010), 'Abrupt warming and salting of the Western Mediterranean Deep Water after 2005: Atmospheric forcings and lateral advection', *Journal of Geophysical Research* **115**(C8), C08029.

Schroeder, K., Millot, C., Bengara, L., Ben Ismail, S., Bensi, M., Borghini, M., Budillon, G., Cardin, V., Coppola, L., Curtil, C., Drago, A., El Moumni, B., Font, J., Fuda, J. L., García-Lafuente, J., Gasparini, G. P., Kontoyiannis, H., Lefevre, D., Puig, P., Raimbault, P., Rougier, G., Salat, J., Sammari, C., Sánchez-Garrido, J. C., Sanchez-Roman, A., Sparnocchia, S., Tamburini, C., Taupier-Letage, I., Theocharis, A., Vargas-Yáñez, M. & Vetrano, A. (2013), 'Long-term monitoring programme of the hydrological variability in the Mediterranean Sea: A first overview of the HYDROCHANGES network', *Ocean Science* **9**(2), 301–324.

Schroeder, K., Ribotti, A., Borghini, M., Sorgente, R., Perilli, A. & Gasparini, G. P. (2008), 'An extensive western Mediterranean deep water renewal between 2004 and 2006', *Geophysical Research Letters* **35**(18), L18605.

Schroeder, K., Tanhua, T., Bryden, H. L., Álvarez, M., Chiggiato, J. & Aracri, S. (2015), 'Mediterranean sea ship-based hydrographic investigations program (Med-SHIP)', *Oceanography* **28**(3), 12–15.

Seifert, B. & Gasser, T. (2004), Local Polynomial Smoothing, *in* S. Kotz, N. Balakrishnan, C. B. Read, B. Vidakovic & N. L. Johnson, eds, 'Encyclopedia of Statistical Sciences, 7', 2nd edn, John Wiley and Sons Inc, Hoboken, New Jersey, pp. 4334–4339.

Send, U., Font, J., Krahmann, G., Millot, C., Rhein, M. & Tintoré, J. (1999), 'Recent advances in observing the physical oceanography of the Western Mediterranean Sea', *Progress in Oceanography* **44**(1-3), 37–64.

Send, U., Font, J. & Mertens, C. (1996), 'Recent observation indicates convection's role in deep water circulation', *EOS Transactions AGU* **77**(7), 61–65.

Send, U. & Testor, P. (2017), 'Direct Observations Reveal the Deep Circulation of the Western Mediterranean Sea', *Journal of Geophysical Research: Oceans* **122**(12), 10091–10098.

Smith, R. O., Bryden, H. L. & Stansfield, K. (2008), 'Observations of new western Mediterranean deep water formation using Argo floats 2004-2006', *Ocean Sciences* **4**, 133–149.

Somavilla, R., González-Pola, C., Schauer, U. & Budéus, G. (2016), 'Mid-2000s North Atlantic shift: Heat budget and circulation changes', *Geophysical Research Letters* **43**(5), 2059–2068.

Somot, S., Houpert, L., Sevault, F., Testor, P., Bosse, A., Taupier-Letage, I., Bouin, M. N., Waldman, R., Cassou, C., Sanchez-Gomez, E., Durrieu de Madron, X., Adloff, F., Nabat, P. & Herrmann, M. (2018), 'Characterizing, modelling and understanding the climate variability of the deep water formation in the North-Western Mediterranean Sea', *Climate Dynamics* **51**(3), 1179–1210.

Somot, S., Sevault, F. & Déqué, M. (2006), 'Transient climate change scenario simulation of the Mediterranean Sea for the twenty-first century using a high-resolution ocean circulation model', *Climate Dynamics* **27**(7-8), 851–879.

St. Laurent, L. C. & Schmitt, R. W. (1999), 'The Contribution of Salt Fingers to Vertical Mixing in the North Atlantic Tracer Release Experiment*', *Journal of Physical Oceanography* **29**(7), 1404–1424.

St. Laurent, L. C., Toole, J. M. & Schmitt, R. W. (2001), 'Buoyancy Forcing by Turbulence above Rough Topography in the Abyssal Brazil Basin', *Journal of Physical Oceanography* **31**(12), 3476–3495.

Stommel, H., Bryden, H. L. & Mangelsdorf, P. (1973), 'Does some of the Mediterranean outflow come from great depth?', *Pure and Applied Geophysics* **105**(1), 879–889.

Tel, E., Balbin, R., Cabanas, J. M., Garcia, M. J., Carmen Garcia-Martinez, M., Gonzalez-Pola, C., Lavin, A., Lopez-Jurado, J. L., Rodriguez, C., Ruiz-Villarreal, M., Sánchez-Leal, R. F., Vargas-Yáñez, M. & Vélez-Belchí, P. (2016), 'IEOOS: The Spanish Institute of Oceanography Observing System', *Ocean Science* **12**(2), 345–353.

Testor, P., Bosse, A., Houpert, L., Margirier, F., Mortier, L., Legoff, H., Dausse, D., Labaste, M., Karstensen, J., Hayes, D., Olita, A., Ribotti, A., Schroeder, K., Chiggiato, J., Onken, R., Heslop, E., Mourre, B., D'ortenzio, F., Mayot, N., Lavigne, H., de Fommervault, O., Coppola, L., Prieur, L., Taillandier, V., Durrieu de Madron, X., Bourrin, F., Many, G., Damien, P., Estournel, C., Marsaleix, P., Taupier-Letage, I., Raimbault, P., Waldman, R., Bouin, M. N., Giordani, H., Caniaux, G., Somot, S., Ducrocq, V. & Conan, P. (2018), 'Multiscale Observations of Deep Convection in the Northwestern Mediterranean Sea During Winter 2012–2013 Using Multiple Platforms', *Journal of Geophysical Research: Oceans* **123**(3), 1745–1776.

Testor, P. & Gascard, J. C. (2003), 'Large-scale spreading of deep waters in the Western Mediterranean Sea by submesoscale coherent eddies', *Journal of Physical Oceanography* **33**(1), 75–87.

Testor, P. & Gascard, J. C. (2006), 'Post-convection spreading phase in the Northwestern Mediterranean Sea', *Deep-Sea Research Part I: Oceanographic Research Papers* **53**(5), 869–893.

Testor, P., Send, U., Gascard, J.-C., Millot, C., Taupier-Letage, I. & Béranger, K. (2005), 'The mean circulation of the southwestern Mediterranean Sea: Algerian Gyres', *Journal of Geophysical Research* **110**(C11), C11017.

Thomas, L. N., Taylor, J. R., Ferrari, R. & Joyce, T. M. (2013), 'Symmetric instability in the Gulf Stream', *Deep-Sea Research Part II: Topical Studies in Oceanography* **91**, 96–110.

Thorpe, S. A. (2007), *An introduction to ocean turbulence*, 1st edn, Cambridge University Press, Cambridge.

Tintoré, J., Pinardi, N., Álvarez-Fanjul, E., Aguiar, E., Álvarez-Berastegui, D., Bajo, M., Balbin, R., Bozzano, R., Nardelli, B. B., Cardin, V., Casas, B., Charcos-Llorens, M., Chiggiato, J., Clementi, E., Coppini, G., Coppola, L., Cossarini, G., Deidun, A., Deudero, S., D'Ortenzio, F., Drago, A., Drudi, M., El Serafy, G., Escudier, R., Farcy, P., Federico, I., Fernández, J. G., Ferrarin, C., Fossi, C., Frangoulis, C., Galgani, F., Gana, S., García Lafuente, J., Sotillo, M. G., Garreau, P., Gertman, I., Gómez-Pujol, L., Grandi, A., Hayes, D., Hernández-Lasheras, J., Herut, B., Heslop, E., Hilmi, K., Juza, M., Kallos, G., Korres, G., Lecci, R., Lazzari, P., Lorente, P., Liubartseva, S., Louanchi, F., Malacic, V., Mannarini, G., March, D., Marullo, S., Mauri, E., Meszaros, L., Mourre, B., Mortier, L., Muñoz-Mas, C., Novellino, A., Obaton, D., Orfila, A., Pascual, A., Pensieri, S., Pérez Gómez, B., Pérez Rubio, S., Perivoliotis, L., Petihakis, G., de la Villéon, L. P., Pistoia, J., Poulain, P.-M., Pouliquen, S., Prieto, L., Raimbault, P., Reglero, P., Reyes, E., Rotllan, P., Ruiz, S., Ruiz, J., Ruiz, I., Ruiz-Orejón, L. F., Salihoglu, B., Salon, S., Sammartino, S., Sánchez Arcilla, A., Sánchez-Román, A., Sannino, G., Santoleri, R., Sardá, R., Schroeder, K., Simoncelli, S., Sofianos, S., Sylaios, G., Tanhua, T., Teruzzi, A., Testor, P., Tezcan, D., Torner, M., Trotta, F., Umgiesser, G., von Schuckmann, K., Verri, G., Vilibic, I., Yucel, M., Zavatarelli, M. & Zodiatis, G. (2019), 'Challenges for Sustained Observing and Forecasting Systems in the Mediterranean Sea', *Frontiers in Marine Science* **6**(September).

Tintoré, J., Vizoso, G., Casas, B., Heslop, E., Pascual, A., Orfila, A., Ruiz, S., Martínez-Ledesma, M., Torner, M., Cusí, S., Diedrich, A., Balaguer, P., Gómez-Pujol, L., Álvarez-Ellacuria, A., Gómara, S., Sebastian, K., Lora, S., Beltrán, J. P., Renault, L., Juzà, M., Álvarez, D., March, D., Garau, B., Castilla, C., Cañellas, T., Roque, D., Lizarán, I., Pitarch, S., Carrasco, M. A., Lana, A., Mason, E., Escudier, R., Conti, D., Sayol, J. M., Barceló, B., Alemany, F., Reglero, P., Massuti, E., Vélez-Belchí, P., Ruiz, J., Oguz, T., Gómez, M., Álvarez, E., Ansorena, L. & Manriquez, M. (2013), 'SOCIB: The Balearic Islands Coastal Ocean Observing and Forecasting System Responding to Science, Technology and Society Needs', *Marine Technology Society Journal* **47**(1), 101–117.

Toole, J. M., Polzin, K. L. & Schmitt, R. W. (1994), 'Estimates of diapycnal mixing in the abyssal ocean', *Science* **264**, 1120–1123.

Tsimplis, M. N. & Bryden, H. L. (2000), 'Estimation of the transports through the Strait of Gibraltar', *Deep Sea Research Part I: Oceanographic Research Papers* **47**(12), 2219–2242.

Tsimplis, M. N., Zervakis, V., Josey, S. A., Peneva, E. L., Struglia, M. V., Stanev, E. V., Theocharis, A., Lionello, P., Malanotte-Rizzoli, P., Artale, V., Tragou, E. & Oguz, T. (2006), Changes in the oceanography of the Mediterranean Sea and their link to climate variability, *in* 'Developments in Earth and Environmental Sciences', Vol. 4, pp. 227–282.

Turner, J. S. (1973), *Buoyancy effects in fluids*, Cambridge University Press, London.

Valdés, L., Lavín, A., Fernández de Puelles, M. L., Varela, M., Anadon, R., Miranda, A., Camiñas, J. & Mas, J. (2002), Spanish Ocean Observation System, IEO core project: studies on time series of oceanographic data, *in* N. Flemming, S. Vallerga, N. Pinardi, H. W. A. Behrens, G. Manzella, D. Prandle & J. H. Stel, eds, 'Elsevier Oceanography Series, volume 66', 1st edn, Elsevier, pp. 99–105.

Vargas-Yáñez, M., García-Martínez, M. C., Moya, F., Balbín, R., López-Jurado, J. L., Serra, M., Zunino, P., Pascual, J. & Salat, J. (2017), 'Updating temperature and salinity mean values and trends in the Western Mediterranean: The RADMED project', *Progress in Oceanography* **157**(August), 27–46.

Vargas-Yáñez, M., Juza, M., Balbín, R., Velez-Belchí, P., García-Martínez, M. C., Moya, F. & Hernández-Guerra, A. (2020), 'Climatological Hydrographic Properties and Water Mass Transports in the Balearic Channels From Repeated Observations Over 1996–2019', *Frontiers in Marine Science* **7**(September).

Vargas-Yáñez, M., Moya, F., García-Martínez, M. C., Tel, E., Zunino, P., Plaza, F., Salat, J., Pascual, J., López-Jurado, J. L. & Serra, M. (2010), 'Climate change in the Western Mediterranean Sea 1900-2008', *Journal of Marine Systems* **82**(3), 171–176.

Vargas-Yáñez, M., Moya, F., Tel, E., García-Martínez, M. C., Guerber, E. & Bourgeon, M. (2009), 'Warming and salting in the western Mediterranean during the second half of the 20th century: inconsistencies, unknowns and the effect of data processing', *Scientia Marina* **73**(1), 7–28.

Vargas-Yáñez, M., Zunino, P., Schroeder, K., López-Jurado, J. L., Plaza, F., Serra, M., Castro, C., García-Martínez, M. C., Moya, F. & Salat, J. (2012), 'Extreme Western Intermediate Water formation in winter 2010', *Journal of Marine Systems* **105-108**, 52–59.

Visbeck, M. (2002), 'Deep velocity profiling using lowered acoustic Doppler current profilers: Bottom track and inverse solutions', *Journal of Atmospheric and Oceanic Technology* **19**(5), 794–807.

Von Schuckmann, K., Storto, A., Simoncelli, S., Roshin P, R., Samuelsen, A., de Pascual Collar, A., Garcia Sotillo, M. & Szerkely, T. (2018), Ocean heat content, *in* 'Copernicus Service Ocean State Report, 2', Journal of Operational Oceanography, 11, pp. s41–s45.

Waldman, R., Somot, S., Herrmann, M., Testor, P., Estournel, C., Sevault, F., Prieur, L., Mortier, L., Coppola, L., Taillandier, V., Conan, P. & Dausse, D. (2016), 'Estimating dense water volume and its evolution for the year 2012-2013 in the Northwestern Mediterranean Sea: An observing system simnulation experiment approach', *Journal of Geophysical Research: Oceans* **121**, 6696–6716.

Waterhouse, A. F., MacKinnon, J. A., Nash, J. D., Alford, M. H., Kunze, E., Simmons, H. L., Polzin, K. L., St. Laurent, L. C., Sun, O. M., Pinkel, R., Talley, L. D., Whalen, C. B., Huussen, T. N., Carter, G. S., Fer, I., Waterman, S., Naveira Garabato, A. C., Sanford, T. B. & Lee, C. M.

(2014), 'Global Patterns of Diapycnal Mixing from Measurements of the Turbulent Dissipation Rate', *Journal of Physical Oceanography* **44**(7), 1854–1872.

Wenegrat, J. O. & Thomas, L. N. (2020), 'Centrifugal and Symmetric Instability during Ekman Adjustment of the Bottom Boundary Layer', *Journal of Physical Oceanography* **50**(6), 1793–1812.

Winton, M., Griffies, S. M., Samuels, B. L., Sarmiento, J. L. & Frölicher, T. L. (2013), 'Connecting Changing Ocean Circulation with Changing Climate', *Journal of Climate* **26**(7), 2268–2278.

Wu, P. & Haines, K. (1996), 'Modeling the dispersal of Levantine Intermediate Water and its role in Mediterranean deep water formation', *Journal of Geophysical Research C: Oceans* **101**(C3), 6591–6607.

Zhang, J. & Schmitt, R. W. (2000), 'The Impact of Salt Fingering on the Thermohaline Circulation under Mixed Boundary Conditions', *Journal of Physical Oceanography* **30**(6), 1223–1231.

Zhang, J., Schmitt, R. W. & Huang, R. X. (1998), 'Sensitivity of the GFDL Modular Ocean Model to Parameterization of Double-Diffusive Processes', *Journal of Physical Oceanography* **28**(4), 589–605.

Zodiatis, G. & Gasparini, G. P. (1996), 'Thermohaline staircase formations in the Tyrrhenian Sea', *Deep-Sea Research Part I: Oceanographic Research Papers* **43**(5), 655–678.

Zunino, P., Schroeder, K., Vargas-Yáñez, M., Gasparini, G. P. & Coppola, L. (2012), 'Effects of the Western Mediterranean Transition on the resident water masses: Pure warming, pure freshening and pure heaving', *Journal of Marine Systems* **96-97**, 15–23.

Terms and Abbreviations

ATHAPOC *'estudio de la Anomalía TermoHalina en las Aguas Profundas del mediterráneo occidental y su relación con las Oscilaciones Climáticas'*

AW Atlantic Water

BBL Bottom Boundary Layer

CIW Cretan Intermediate Water

CTD Conductivity-Temperature-Depth

cWMDW Cascading-origin Western Mediterranean Deep Water

DE Differential Evolution

DYFAMED Dynamics of Atmospheric Fluxes in the Mediterranean Sea

EMDW Eastern Mediterranean Deep Water

EMED Eastern Mediterranean

EMT Eastern Mediterranean Transient

FTU Formazin Turbidity Units

GoL Gulf of Lion

IEO *'Instituto Español de Oceanografía'* (Spanish Institute of Oceanography)

IEOOS Spanish Institute of Oceanography Observing System

LADCP Lowered Acoustic Doppler Current Profiler

LIW Levantine Intermediate Water

LOESS Locally Estimated Scatterplot Smoothing

MOW Mediterranean Outflow Water

nWMDW New Western Mediterranean Deep Water

oWMDW Old Western Mediterranean Deep Water

QC Heat Content

RADMED *'series tempoRAles de Datos oceanográficos del MEDiterráneo'*

SC Salt Content

SCV Submesoscale Coherent Vortex

SSC Suspended Sediment Concentration

TDW Tyrrhenian Deep Water

VMADCP Vessel-mounted Acoustic Doppler Current Profiler

WIW Western Intermediate Water

WMDW Western Mediterranean Deep Water

WMED Western Mediterranean

WMT Western Mediterranean Transition